To the Graduate Council:

I am submitting herewith a thesis written by Harry Diament entitled "A Transient Two-Dimensional Mathematical Model for Simulating the Transport of Radionuclide Effluents from Nuclear Powered Electric Generating Stations." I recommend that it be accepted in partial fulfillment of the requirements for the degree of Master of Science, with a major in Engineering Science.

Kun H. Kim, Major Professor

We have read this thesis
and recommend its acceptance:

Accepted for the Council:

Vice Chancellor
Graduate Studies and Research

X

A TRANSIENT TWO-DIMENSIONAL MATHEMATICAL MODEL FOR SIMULATING THE TRANSPORT OF RADIONUCLIDE EFFLUENTS FROM NUCLEAR POWERED ELECTRIC GENERATING STATIONS

A Thesis

Presented for the

Master of Science

Degree

The University of Tennessee, Knoxville

Harry Diament

August 1980

3044942

ACKNOWLEDGEMENTS

The author is grateful for the assistance and guidance provided by the members of my committee and the financial assistance obtained through contracts with the Nuclear Regulatory Commission. Appreciation is also expressed to Pam Lampe who typed this thesis, and my wife, Mindy Diament, whose handwriting graces the pages of this thesis. Finally, I would like to express a deep appreciation to my parents, Stefan and Henrietta Diament, who have supported me throughout my educational endeavors.

ABSTRACT

A transient two-dimensional mathematical model for simulating the transport of radionuclide effluents from nuclear powered electric generating stations is presented.

The Eulerian fluid in discrete element (FLIDE) formulation employs the integral forms of the conservation principles of water mass and radionuclide mass in variable sized discrete elements that span the flow region. The transport of the radionuclide effluents are modeled in the water layer as suspended sediment and in the bottom layer as stationary resident sediment.

The contributions of vertical variations of the velocity components and radionuclide concentrations in the water layer are rigorously incorporated in the development of depth-averaged, two-dimensional transport fluxes by spatially integrating the conservation equations over the enclosure surfaces of the discrete elements. Horizontal transport of radionuclides in the bottom layer is not presented. A simple exchange model is used to approximate the formulation of mass transport of radionuclides between the dissolved/adsorbed state in the water layer and the dissolved/adsorbed state in the bottom resident sediment layer.

The resulting mathematical system is a system of weakly coupled, nonlinear, ordinary differential equations that are numerically integrated from arbitrarily specified initial conditions, by the Runge-Kutta-Gill method with a time step based on a stability criterion for explicit methods.

The mathematical model is applied to a hypothetical accidental release of radionuclide effluents at the San Onofre Nuclear Generating Station (SONGS). Flow conditions in the region are modeled using field data, and the released radionuclide is Cesium 132.

During the simulation of a hypothetical accident condition at the San Onofre Generating Station the model showed that it readily takes into account the interaction of dissolved and adsorbed suspended sediment in the water layer and the dissolved and adsorbed resident sediment in the stationary bottom layer. Under high flow conditions, it showed the phenomena of the dissolved and adsorbed resident sediment in the stationary bottom layer being resuspended into the water layer, presenting a realistic simulation of natural conditions. At low flow conditions the settling of the dissolved and adsorbed suspended sediment in the water layer into the stationary bottom layer was modeled, thus giving an effective simulation of the vertical exchange between the two layers. Decay of the radionuclide contaminant is effectively modeled using the basic exponential decay form based on the radionuclides' half-life.

TABLE OF CONTENTS

SECTION		PAGE
1.	INTRODUCTION	1
2.	MATHEMATICAL FORMULATION OF THE GOVERNING EQUATIONS	6
	2.1 General Discussion of Numerical Simulation Model	6
	2.2 Integral Forms of Conservation Principles	8
	2.3 Formulation of the Discrete-Element Equation for Conservation of Water Mass	16
	2.4 Formulation of the Discrete-Element Equation for Conservation of Radionuclide Mass in Water	22
3.	CLOSURE OF MATHEMATICAL SYSTEM OF EQUATIONS	40
	3.1 Formulation of Half-Point Values on Discrete-Element Surfaces	40
	3.2 Initial and Boundary Half-Point Conditions	43
	3.3 Formulation of Intake and Discharge Conditions	52
	3.4 Formulation of Radionuclide Flux Terms	54
	3.5 Approximate Formulation of the Exchange of Radionuclides Between the Water and Bottom Layers	73
4.	APPLICATION OF THE MATHEMATICAL RADIONUCLIDE TRANSPORT MODEL TO A SITE SPECIFIC CASE	79
	4.1 Description of the Coastal Region and San Onofre Nuclear Generating Station	79
	4.2 Description of the Accident	82
	4.3 Application of the Computer Model to the Accident Scenario at San Onofre	84
	4.4 Discussion of Computer Simulation Results	86
5.	CONCLUSIONS AND RECOMMENDATIONS	119
	5.1 Conclusions	119
	5.2 Recommendations	120

SECTION PAGE

LIST OF REFERENCES 122

VITA 126

LIST OF FIGURES

FIGURE		PAGE
1.	Schematic Representation of the Parts of the Flow Variables in the X Direction	12
2.	Geometrical Configuration of Discrete Elements for the FLIDE Method	17
3.	Schematic Representation of the Open-End Boundary Conditions	49
4.	Discrete Element Geometry Representation of the San Onofre Coastal Region	81
5.	Depth Geometry of the San Onofre Coastal Region as Modeled in the RADTWO Computer Code, All Depths are in Feet	83
6.	Velocity Vector Representation of the Flowfield 1 Hour After the Start of the Accidental Release	88
7.	Logarithmic Iso-Concentration Contours of the Dissolved and Adsorbed Sediment in the Water and Bottom Layers 1 Hour After the Start of the Accidental Release	89
8.	Velocity Vector Representation of the Flowfield 3 Hours After the Start of the Accidental Release	90
9.	Logarithmic Iso-Concentration Contours of the Dissolved and Adsorbed Sediment in the Water and Bottom Layers 3 Hours After the Start of the Accidental Release	91
10.	Velocity Vector Representation of the Flowfield 5 Hours After the Start of the Accidental Release	93
11.	Logarithmic Iso-Concentration Contours of the Dissolved and Adsorbed Sediment in the Water and Bottom Layers 5 Hours After the Start of the Accidental Release	94
12.	Velocity Vector Representation of the Flowfield 7 Hours After the Start of the Accidental Release	95
13.	Logarithmic Iso-Concentration Contours of the Dissolved and Adsorbed Sediment in the Water and Bottom Layers 7 Hours After the Start of the Accidental Release	97
14.	Velocity Vector Representation of the Flowfield 12 Hours After the Start of the Accidental Release	98

FIGURE PAGE

15. Logarithmic Iso-Concentration Contours of the Dissolved and Adsorbed Sediment in the Water and Bottom Layers 12 Hours After the Start of the Accidental Release 99

16. Velocity Vector Representation of the Flowfield 24 Hours After the Start of the Accidental Release 101

17. Logarithmic Iso-Concentration Contours of the Dissolved and Adsorbed Sediment in the Water and Bottom Layers 24 Hours After the Start of the Accidental Release 102

18. Velocity Vector Representation of the Flowfield 30 Hours After the Start of the Accidental Release 103

19. Logarithmic Iso-Concentration Contours of the Dissolved and Adsorbed Sediment in the Water and Bottom Layers 30 Hours After the Start of the Accidental Release 104

20. Velocity Vector Representation of the Flowfield 42 Hours After the Start of the Accidental Release 105

21. Logarithmic Iso-Concentration Contours of the Dissolved and Adsorbed Sediment in the Water and Bottom Layers 42 Hours After the Start of the Accidental Release 106

22. Velocity Vector Representation of the Flowfield 48 Hours After the Start of the Accidental Release 108

23. Logarithmic Iso-Concentration Contours of the Dissolved and Adsorbed Sediment in the Water and Bottom Layers 48 Hours After the Start of the Accidental Release 109

24. Velocity Vector Representation of the Flowfield 54 Hours After the Start of the Accidental Release 110

25. Logarithmic Iso-Concentration Contours of the Dissolved and Adsorbed Sediment in the Water and Bottom Layers 54 Hours After the Start of the Accidental Release 111

26. Velocity Vector Representation of the Flowfield 60 Hours After the Start of the Accidental Release 112

27. Logarithmic Iso-Concentration Contours of the Dissolved and Adsorbed Sediment in the Water and Bottom Layers 60 Hours After the Start of the Accidental Release 113

28. Velocity Vector Representation of the Flowfield 132 Hours After the Start of the Accidental Release 115

FIGURE PAGE

29. Logarithmic Iso-Concentration Contours of the Dissolved and Adsorbed Sediment in the Water and Bottom Layers 132 Hours After the Start of the Accidental Release 116

30. Velocity Vector Representation of the Flowfield 144 Hours After the Start of the Accidental Release 117

31. Logarithmic Iso-Concentration Contours of the Dissolved and Adsorbed Sediment in the Water and Bottom Layers 144 Hours After the Start of the Accidental Release 118

1. INTRODUCTION

The present consumption of electric power has caused a need for the construction of larger power generating stations. The majority of electrical power has been generated by fossil fueled steam power plants, but due to present needs nuclear powered electrical generating stations are coming of age. Large megawatt nuclear power plants such as Indian Point: 2100 MWe, Browns Ferry: 3450 MWe, and San Onofre: 2800 MWe, consist of up to three nuclear units. Many of these plants are presently in operation with additional plants in the planning or construction stages. Along with the advent of nuclear powered electrical generating stations comes the concern of their impact on the environment.

The possibility of radionuclide releases from these plants is a real and present possibility that deserves study, both the cumulative effects from minute daily releases into the plants cooling system, and the chance of a large release due to an accident. These releases can be transported into the receiving water body by the plant's cooling system. In some cases, during low flow in rivers, a power generating station can use up to 30 percent of the total river flow for cooling purposes, presenting a real possibility for a large impact on the local eco-system.

The ultimate effect of radionuclide releases is dependent upon their pathway to humans. Through biological organisms, and sources of drinking water, these effects can be propagated through the food chain. In order to understand this pathway of radionuclides, it is essential

to first understand their transport in the environment under controlling physical phenomena.

Radionuclides from nuclear generating stations are released into a variety of receiving water bodies, including lakes, rivers, reservoirs, cooling ponds, and estuaries. The controlling factor in the transport of these radionuclides is the flow conditions that exist in the receiving body of water. Overall dispersion of the radionuclides is also affected by local turbulent phenomena and the design of the discharge structures.

Standards regulating the maximum allowable radionuclide releases from nuclear powered electrical generating stations are set by the Nuclear Regulatory Commission (NRC). These standards are contained in Section 20.106 of 10 CFR Part 20 [1] of the Nuclear Regulatory Commission's (NRC) regulations. Also contained in the NRC regulations are a set of guidelines [2] for use in predicting aquatic dispersion of radionuclide releases.

Previous to the NRC publications [1, 2], guidelines for radionuclide release were not well defined. It was assumed that the oceans could be used as limitless receiving water bodies for radionuclide releases from large nuclear power plants. Under tidal conditions this is not the case. Due to the long half-lives of many radionuclides, the problem of recirculation of the radionuclides will occur. The severity of this recirculation is dependent upon the design and location of the intake and discharge structures. In non-tidal rivers this problem should not occur.

In cases where more than one nuclear unit is in use, such as two power plants located in the same receiving water body region, interaction can take place between the two plant's cooling systems. For discharge into rivers, only the downstream plants will be affected, but under tidal conditions the interaction can cause all the plants or units to be affected.

Dispersion models exist that are excellent representations of the dispersion of matter and thermal energy under turbulent flow conditions, such as the pioneering work by Taylor [3]. A review of these models will not be contained in this study; if the reader desires further information, Eraslan [4] presents a good treatise on the subject. Heavy emphasis has been placed in the field of hydrothermal prediction over the past ten years. Policastro and Tokar [5] and Jirka, Abraham and Harleman [6] have published comprehensive reviews on these models; also, Dunn, Policastro and Paddock [7] have published an excellent state of the art review concerned with mathematical modeling techniques for thermal plumes.

Models for radionuclide dispersion prediction are not as plentiful as hydrothermal prediction models. Yousef, Kudo and Gloyna [8], and Fields [9] have developed one-dimensional mathematical models for radionuclide transport in streams. Yousef, Kudo and Gloyna [8] developed two models; a basic one-dimensional dispersed flow model and a "sorption-desorption" model. The sorption-desorption model attempted to take into account the non-equilibrium interaction between radionuclides and sediment in the aqueous and solid phases. Comparisons of results from the two models to experimental data show that the dispersed

flow model does not give satisfactory results, while the sorption-desorption model gives an excellent comparison. Sayre and Chang [10] studied radionuclide transport in streams by solving the convection-diffusion equation statistically.

Models for radionuclide transport analysis in non-tidal rivers, lakes, reservoirs, cooling ponds, estuaries and coastal situations are presented in Regulatory Guide 1.113 [2]. This guide gives an excellent overview of models that can be applied to assess the impact of radionuclides.

Presently, there is a need for models which can successfully simulate radionuclide transport in different receiving water bodies. The model should be fast transient, within tidal cycle, as averaging over daily periods could not accurately represent accident conditions. It should be at least two-dimensional. In most cases, fully three-dimensional hydrodynamic models which solve the momentum equations require large core storage and a small time step to satisfy stability criteria, thus making them impractical for long environmental simulations.

Flow data can be obtained for environmental impact analysis. This flow data should be accurate and if made to meet conservation of mass equations should closely approximate physical conditions. Proper care in turbulence modeling will give an accurate representation of the velocity gradient with respect to depth, thus negating the need for a three-dimensional model. Proper boundary conditions need to be assigned to represent solid shorelines and open end boundary conditions.

A simulation of radionuclide transport is not complete without an accompanying sediment transport representation. The ability of suspended and bottom sediments to absorb and adsorb radionuclides will greatly influence the overall transport of radionuclides.

This study will present a transient, two-dimensional, discrete-element, far-field model for transport of radionuclide effluents from nuclear powered electric generating stations. It includes the development of the model, by using the fluid in discrete element (FLIDE) method as presented by Eraslan [4], and its application to the San Onofre Nuclear Generating station. Conservation of water mass is solved to insure a proper velocity field by checking the variation of surface heights. Radionuclide mass is conserved by taking into account a first order decay rate and the uptake of dissolved radionuclides into the bottom sediment. This is accomplished by using a simplistic sediment transport model, since a comprehensive sediment transport model is not within the scope of this study.

2. MATHEMATICAL FORMULATION OF THE GOVERNING EQUATIONS

2.1 General Discussion of Numerical Simulation Model

The present formulation is based on a control volume approach which highlights a direct numerical simulation process without necessitating continuum limit differential equations for the conservation principles. This method is best exemplified by the two well-known computer codes developed at Los Alamos Scientific Laboratory by Evans and Harlow [11] for particle-in-cell (PIC), and by Gentry, Martin, and Daly [12] for fluid-in-cell (FLIC) formulations for transient fluid flow problems. Details of these formulations are available in reports by Harlow [13], Harlow and Amsden [14, 15], and an excellent text in computational fluid mechanics by Roache [16].

Both the PIC and FLIC methods directly formulate the necessary computational system of equations by applying the macroscopic forms of mass, momentum and energy principles for a cell of rectangular enclosure surfaces by assuming uniform values over the surface areas. The flow region is divided into a sufficient number of cells which span the flow region, and the computation procedure is based on approximate satisfaction of the conservation equations for each cell at every time step.

A high degree of resolution is required in the assessment of the radionuclide transport problem. Equal cell division would not be computationally practical when spanning a large flow region. In assessing the transport of radionuclides, the two critical areas are located at the immediate vicinity of the discharge, and possibly, the shallow

water regions near the shore. Any model must maintain a high degree of resolution in these areas. Concurrently, it must span a large enough region to assess the total ecological impact of possible radionuclide releases from large nuclear powered electric generating stations. Equal cell division models could only cover both of these areas by employing an excessive number of computational cells, requiring both large amounts of computer time and storage. If the number of cells was reduced, the desired degree of resolution would be lost.

The "segment" or "box" water-quality models suggested by Thoman [17] and Connor [18] are based on the simple application of constituent mass conservation principles to the "segments" or "boxes" representing various parts of coastal bays or estuaries. These "segment" or "box" models are conceptually similar to the FLIC method, and are extremely efficient from computational considerations, but they employ simplistic formulations of the turbulent transport fluxes and lack rigorous mathematical consideration of the stability and accuracy of their solutions.

In the present formulation first developed by Eraslan [4], the fundamental concepts of the FLIC method and "segment" or "box" models are combined to develop a computationally efficient and mathematically rigorous numerical simulation model for the fast-transient analysis of radionuclide transport in coastal regions, estuaries, non-tidal rivers and lakes. The formulation is based on the relaxation of the conditions of the FLIC method in its application of the macroscopic, integral forms of the conservation principles to the equal-sized computational cells. The two necessary modifications are the following:

1. The flow region should be divided into arbitrarily sized discrete elements, preferably with rectangular enclosure surfaces except at the boundaries, such that a finite number of discrete elements completely spans the region.

2. Integral forms of the physical conservation laws should be applied to each discrete element without assuming uniform values for flow properties over the surface areas; integrate the necessary volume and surface integrals in formulating the governing equations.

2.2 Integral Forms of Conservation Principles

The mathematical formulation of the two-dimensional fast-transient radionuclide transport model will be based on Eraslan's [4] discrete-element numerical simulation approach, in which the integral forms of the physical conservation principles are employed.

In the formulation, field data for depths and velocities are used, therefore, the momentum equations need not be solved. Hence, the equations for conservation of water mass and conservation of radionuclide mass in water and sediment are the necessary and sufficient physical principles for the formulation of the discrete-element system of equations for the transport of radionuclide mass.

The general integrated forms of the conservation equations for any arbitrary control volume enclosed by the enclosure surface A, can be represented as, conservation principle for water mass,

$$\frac{\partial}{\partial t}\iiint_{\forall} \rho_w \, d\forall + \iint_A \rho_w (\vec{V}\cdot\hat{n}) \, dA = 0, \qquad (1)$$

and the conservation principle for radionuclide mass in water,

$$\frac{\partial}{\partial t}\iiint_{\mathcal{V}} \rho_{r,w}\, d\mathcal{V} + \iint \rho_{r,w}\, \bar{V}\cdot\hat{n}\, dA = \iiint_{\mathcal{V}} \dot{\rho}_{r,w}\, d\mathcal{V} + \iint_A \bar{q}_{r,w}\cdot(-\hat{n})\, dA \,. \tag{2}$$

where:

ρ_w = constant mass density of water and suspended sediment mixture,

$\bar{V}$ = mass average velocity vector of the flow field,

$\rho_{r,w}$ = mass density of radionuclide in water,

$\dot{\rho}_{r,w}$ = rate of decay of mass concentration of radionuclide in water,

$\bar{q}_{r,w}$ = mass diffusion flux of radionuclide in water.

The suspended sediment concentration is assumed to be appreciably low such that the variations of the density of water due to settling and resuspension of the sediment in water does not affect the density appreciably. Hence, the conservation of mass equation for water can be approximated with,

$$\frac{\partial \mathcal{V}}{\partial t} + \iint_A \bar{V}\cdot\hat{n}\, dA = 0. \tag{3}$$

In considering the mass concentration of radionuclides in water in the dissolved state, and adsorbed state for suspended sediment, it is sometimes more practical to consider a dimensionless concentration $C_{r,w}$. The concentration can be non-dimensionalized based on a

reference density ρ_{ref}. Hence, in the formulation of the discrete-element equations, the dimensionless form will be employed as,

$$C_{r,w} = \rho_{r,w} / \rho_{ref} \quad . \tag{4}$$

The formulation will actually represent actual mass concentration on a volumetric basis for the reference density ρ_{ref} specified as unity. Hence, in the subsequent system of equations, the integral form of the conservation principle for radionuclide mass in water can be represented as,

$$\frac{\partial}{\partial t} \iiint_{\mathcal{V}} C_{r,w} \, d\mathcal{V} + \iint_A C_{r,w} \, \bar{V} \cdot \hat{n} \, dA =$$

$$\iiint_{\mathcal{V}} \dot{C}_{r,w} \, d\mathcal{V} + \iint_A \bar{g}_{m,r,w} \cdot (-\hat{n}) \, dA \quad , \tag{5}$$

where all the terms in Equation (5) are the dimensionless forms of the terms in Equation (2), i.e.,

$\dot{C}_{r,w}$ = dimensionless rate of decay of radionuclide concentration in water,

$\bar{g}_{m,r,w}$ = dimensionless molecular diffusion transport flux of radionuclide in water.

Since the vertical component of velocity due to periodic tidal elevations is negligible as compared to the horizontal components, the flow field can be taken as two dimensional,

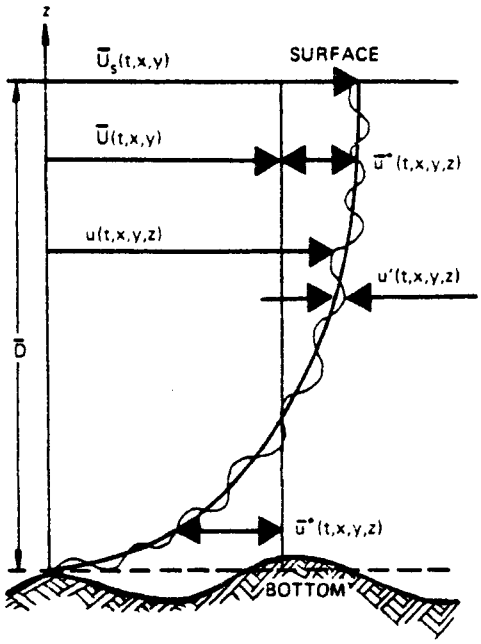
$$\vec{V} = \vec{V}(t,x,y,z) = u(t,x,y,z)\,\hat{i} + v(t,x,y,z)\,\hat{j}. \quad (6)$$

Flow situations in any large body of water such as oceans or rivers are predominantly turbulent. The velocity vector $\vec{V}$ and the radionuclide mass concentration in water are taken as instantaneous quantities which include the contributions of random turbulent fluctuations. Furthermore, since the model is two-dimensional, the velocity components and radionuclide mass concentrations must be vertically averaged over the depth by integrating over the appropriate surface or volume integrals in Equations (2) and (3). Hence, there will be two averaging processes associated with the system. The first is the mean time averaging of the flow properties to separate the turbulent fluctuations; and the second is the spatial depth averaging to reduce the mathematical system into two dimensions.

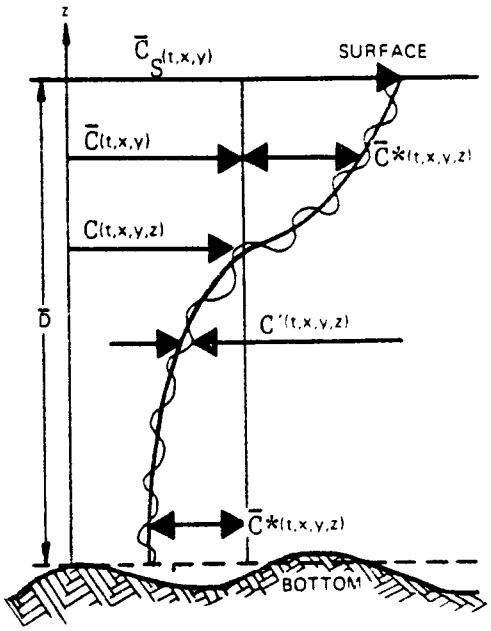
Considering that two averaging processes are to be employed for the mathematical system, each flow property will be divided into three parts, as shown in Figure 1,

where:

$\left.\begin{array}{l} \bar{U}(t,x,y) \\ \bar{V}(t,x,y) \\ \bar{C}_{r,w}(t,x,y) \end{array}\right\}$ = mean time averaged and depth averaged principal variables of the formulation,



a.) Turbulent Velocity Profile



b.) Turbulent Radionuclide Concentration Profile

Figure 1. Schematic Representation of the Parts of the Flow Variables in the X Direction.

$\bar{u}^*(t,x,y,z)$
$\bar{v}^*(t,x,y,z)$
$\bar{C}^*_{r,w}(t,x,y,z)$
} = differences between mean time averaged vertical distributions and depth averaged values of principal variables,

$u'(t,x,y,z)$
$v'(t,x,y,z)$
$C'_{r,w}(t,x,y,z)$
} = contributions of random turbulent fluctuations.

Hence, the principal variables of the formulation can be represented as the sum of the three parts as,

$$U(t,x,y,z) = \bar{U}(t,x,y) + \bar{u}^*(t,x,y,z) + u'(t,x,y,z),$$

$$V(t,x,y,z) = \bar{V}(t,x,y) + \bar{v}^*(t,x,y,z) + v'(t,x,y,z), \qquad (7)$$

$$C_{r,w}(t,x,y,z) = \bar{C}_{r,w}(t,x,y) + \bar{c}^*(t,x,y,z) + c'(t,x,y,z).$$

The definition of the terms in Equation (7) do not differ conceptually from the commonly employed forms. The first two terms consist of the mean time averaged and depth averaged principal variables, and the difference between the mean time averaged vertical distribution and depth averaged value. These two terms, when combined, are the classical

form of the mean time averaged quantity. Hence, the present formulation is equivalent to the classical form used in turbulent analysis.

The definitions of the turbulent fluctuations in Equation (7) result in the following constraint equations when they are time averaged,

$$\overline{u(t,x,y,z)} = \bar{U}(t,x,y) + \bar{u}^*(t,x,y,z),$$

$$\overline{u'(t,x,y,z)} = 0,$$

$$\overline{v(t,x,y,z)} = \bar{V}(t,x,y) + \bar{v}^*(t,x,y,z),$$

(8)

$$\overline{v'(t,x,y,z)} = 0,$$

$$\overline{C_{r,w}(t,x,y,z)} = \bar{C}_{r,w}(t,x,y) + \bar{C}^*_{r,w}(t,x,y,z),$$

$$\overline{C'_{r,w}(t,x,y,z)} = 0.$$

Applying depth averaging to the second part of Equation (8) results in

$$\int_0^{\bar{D}} \bar{u}^*(t,x,y,z)\,dz = 0,$$

$$\int_0^{\bar{D}} \bar{v}^*(t,x,y,z)\,dz = 0, \qquad (9)$$

$$\int_0^{\bar{D}} \bar{C}^*_{r,w}(t,x,y,z)\,dz = 0.$$

where the depth $\bar{D}$ is independent of turbulent fluctuations in the flow field, since the spatial scale of the fluctuations are definitely negligible in comparison to the dimensions of the water region.

Since the development of the model will be based on mean time averaged variables, it is more practical to employ the conservation principles in their mean time averaged forms. Hence, taking the mean time average of Equations (3) and (5),

$$\frac{\partial \mathcal{V}}{\partial t} + \overline{\iint_A \bar{V} \cdot \hat{n} \, dA} = 0 , \tag{10}$$

$$\frac{\partial}{\partial t} \overline{\iiint_{\mathcal{V}} C_{r,w} \, d\mathcal{V}} + \overline{\iint_A C_{r,w} (\bar{V} \cdot \hat{n}) \, dA} =$$

$$\overline{\iiint_{\mathcal{V}} \dot{C}_{r,w} \, d\mathcal{V}} + \overline{\iint_A \bar{g}_{m,r,w} \, dA} . \tag{11}$$

In Equation (11), the time derivative is taken out of the mean time averaging, because of the fundamental assumption about the comparison of the large time scales of the mean time averaged phenomena and the small time scales of random turbulent fluctuations.

The subsequent formulation of the discrete element model will be based on the final mean time averaged forms of the conservation principles, Equations (10) and (11).

2.3 Formulation of the Discrete-Element Equation for Conservation of Water Mass

The formulation of the FLIDE method is strictly Eulerian, therefore the horizontal dimensions of each discrete element remains constant. However, the depth of each element changes with time according to physical conservation principles for water mass.

In the FLIDE method, the elements are generally of unequal size, as shown in Figure 2. Along the shoreline boundary, they will usually be non-rectangular to approximate the shoreline geometry. Each discrete element maintains a constant cross-sectional area normal to the z direction with horizontal dimensions $\Delta x_{i,j}$ and $\Delta y_{i,j}$ along x and y respectively. Since non-rectangular discrete elements can occur adjacent to the shoreline boundaries, the locations of the elements are represented by the double subscripts i and j, along x and y respectively. Common boundaries for each element are represented by half-point subscripts, for example, (i + 1/2, j), for the common boundary between the two adjacent elements (i, j) and (i + 1, j). Fluid properties are assumed to be uniform over the boundary surfaces normal to the horizontal plane, while varying in the vertical direction according to vertical spatial distributions and turbulent fluctuations previously shown in Figure 1.

Considering the mean time averaged form of the conservation principles for water mass, Equation (10), for an arbitrary discrete element (i, j), and evaluating each integral term separately,

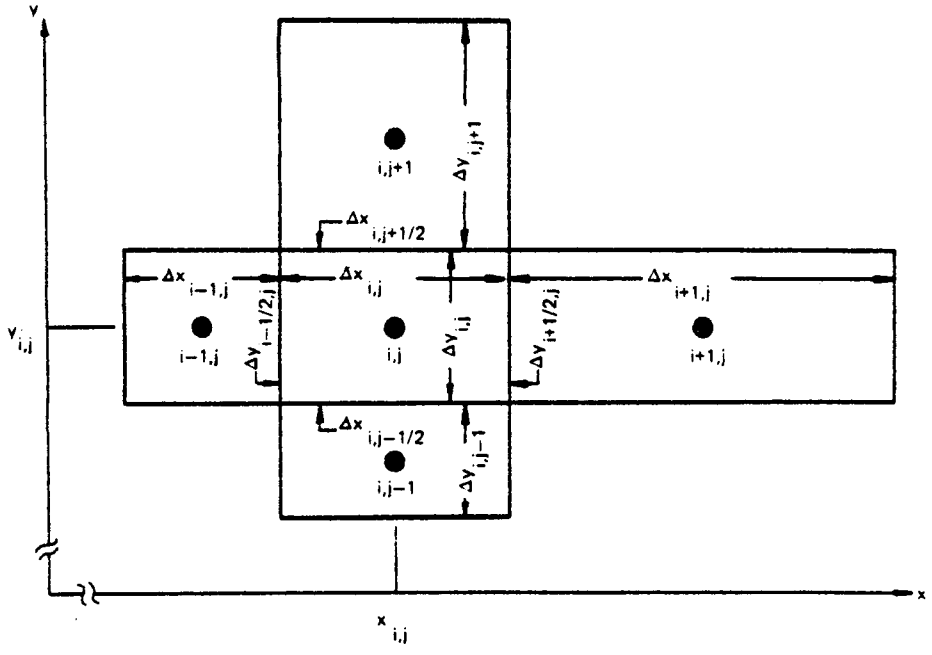


Figure 2. Geometrical Configuration of Discrete Elements for the FLIDE Method.

$$\frac{\partial \mathcal{H}}{\partial t} = \frac{\partial}{\partial t}\left[\Delta X_{i,j}\, \Delta Y_{i,j}\, \bar{D}_{i,j}\right],$$

$$= \Delta X_{i,j}\, \Delta Y_{i,j}\, \frac{\partial \bar{D}_{i,j}}{\partial t} \quad . \tag{12}$$

Considering the realistic assumption based on the comparison of dimensions of the control volumes and the turbulent fluctuations,

$$\iint_A \bar{V}\cdot\hat{n}\, dA = \iint_A \bar{V}\cdot\hat{n}\, dA,$$

$$= -\Delta Y_{i-1/2,j} \int_0^{\bar{D}_{i-1/2,j}} \bar{u}_{i-1/2,j}\, dz$$

$$+ \Delta Y_{i+1/2,j} \int_0^{\bar{D}_{i+1/2,j}} \bar{u}_{i+1/2,j}\, dz - \Delta X_{i,j-1/2} \int_0^{\bar{D}_{i,j-1/2}} \bar{V}_{i,j-1/2}\, dz$$

$$+\Delta X_{i,j+1/2} \int_0^{\bar{D}_{i,j+1/2}} \bar{V}_{i,j+1/2}\, dz - \Delta X_{i,j}\, \Delta Y_{i,j}\left(\bar{q}_{b;i,j} + \bar{q}_{s;i,j}\right)$$

$$-\bar{G}_{int,m}\, \delta_{int;m;i,j} - \bar{G}_{dis,m}\, \delta_{dis;m;i,j}, \tag{13}$$

where:

$\bar{G}_{int,m}$ = intake flow rate of the plant m,

$\bar{G}_{dis,m}$ = discharge flow rate of the plant m,

$\bar{g}_{s;i,j}$ = volumetric flux per unit area (velocity) of inflow from the surface,

$\bar{g}_{b;i,j}$ = volumetric flux per unit area (velocity) of inflow from the bottom,

and the Kronecker delta notation represents,

$$\delta_{int,m;i,j} = \begin{cases} 1: & \text{for intake of plant m in discrete element (i,j)} \\ 0: & \text{otherwise,} \end{cases}$$

$$\delta_{dis,m;i,j} = \begin{cases} 1: & \text{for discharge of plant m in discrete element (i,j)} \\ 0: & \text{otherwise.} \end{cases}$$

In order to evaluate the integrals over depth for the flow rates across the enclosure surfaces in Equation (13), the definitions of the components of the velocity vector, Equation (7), need to be substituted into Equation (13), resulting in Equations (14) and (15),

$$\int_0^{\bar{D}_{i\pm1/2,j}} \bar{u}_{i\pm1/2,j}\, dz = \int_0^{\bar{D}_{i\pm1/2,j}} [\bar{U}_{i\pm1/2,j} + \bar{u}^*_{i\pm1/2,j} + \bar{u}'_{i\pm1/2,j}]\, dz,$$

$$= \int_0^{\bar{D}_{i\pm1/2,j}} \bar{U}_{i\pm1/2,j}\, dz + \int_0^{\bar{D}_{i\pm1/2,j}} \bar{u}^*_{i\pm1/2,j}\, dz + \int_0^{\bar{D}_{i\pm1/2,j}} \bar{u}'_{i\pm1/2,j}\, dz, \tag{14}$$

$$\int_0^{\bar{D}_{i,j\pm1/2}} \bar{V}_{i,j\pm1/2}\, dz = \int_0^{\bar{D}_{i,j\pm1/2}} \left[\bar{V}_{i,j\pm1/2} + \bar{V}^*_{i,j\pm1/2} + \bar{V}'_{i,j\pm1/2}\right] dz,$$

$$= \int_0^{\bar{D}_{i,j\pm1/2}} \bar{V}_{i,j\pm1/2}\, dz + \int_0^{\bar{D}_{i,j\pm1/2}} \bar{V}^*_{i,j\pm1/2}\, dz + \int_0^{\bar{D}_{i,j\pm1/2}} \bar{V}'_{i,j\pm1/2}\, dz. \tag{15}$$

Considering the integral constraints associated with the definitions, the last two integrals in Equations (14) and (15) vanish; hence,

$$\int_0^{\bar{D}_{i\pm1/2,j}} \bar{u}_{i\pm1/2,j}\, dz = \bar{D}_{i\pm1/2,j}\ \bar{U}_{i\pm1/2,j}, \tag{16}$$

$$\int_0^{\bar{D}_{i,j\pm1/2}} \bar{V}_{i,j\pm1/2}\, dz = \bar{D}_{i,j\pm1/2}\ \bar{V}_{i,j\pm1/2}. \tag{17}$$

The surface integral for the flow over the enclosure surfaces of the discrete elements can be simplified by considering flow rates rather than velocities, defined as:

$$\bar{G}_{x;i\pm1/2,j} = \Delta y_{i\pm1/2,j}\ \bar{D}_{i\pm1/2,j}\ \bar{U}_{i\pm1/2,j},$$

$$\bar{G}_{y;i,j\pm1/2} = \Delta x_{i,j\pm1/2}\ \bar{D}_{i,j\pm1/2}\ \bar{V}_{i,j\pm1/2}. \tag{18}$$

where G_x represents the flow rate along the x direction across the $(i \pm 1/2)$ enclosure surface and G_y represents the flow rate along the y direction across the $(j \pm 1/2)$ enclosure surface. Substituting Equations (16) and (17) into Equation (13),

$$\iint_A \bar{V} \cdot \hat{n} \, dA =$$

$$-\Delta y_{i-1/2,j} \, \bar{D}_{i-1/2,j} \, \bar{U}_{i-1/2,j} + \Delta y_{i+1/2,j} \, \bar{D}_{i+1/2,j} \, \bar{U}_{i+1/2,j}$$

$$-\Delta x_{i,j-1/2} \, \bar{D}_{i,j-1/2} \, \bar{V}_{i,j-1/2} + \Delta x_{i,j+1/2} \, \bar{D}_{i,j+1/2} \, \bar{V}_{i,j+1/2}$$

$$-\Delta x_{i,j} \, \Delta y_{i,j} \, (\bar{q}_{s;i,j} + \bar{q}_{b;i,j}) - \bar{G}_{int,m} \, \delta_{int,m;i,j} - \bar{G}_{dis,m} \, \delta_{dis,m;i,j} \, . \tag{19}$$

Redefining Equation (19) in terms of flow rates by substituting Equation (18) into Equation (19), the surface integral for the flow over the enclosure surfaces becomes,

$$\iint_A \bar{V} \cdot \hat{n} \, dA = -\bar{G}_{x;i-1/2,j} + \bar{G}_{x;i+1/2,j}$$

$$- \bar{G}_{y;i,j-1/2} + \bar{G}_{y;i,j+1/2}$$

$$- \Delta x_{i,j} \, \Delta y_{i,j} \, (\bar{q}_{s;i,j} + \bar{q}_{b;i,j}) \tag{20}$$

$$- \bar{G}_{int,m} \, \delta_{int,m;i,j} - \bar{G}_{dis,m} \, \delta_{dis,m;i,j} \, .$$

Hence, the discrete-element equation for the conservation principle for water mass can be obtained by substituting Equations (12) and (20) into Equation (10) and rearranging,

$$\frac{\partial \bar{D}_{i,j}}{\partial t} =$$

$$\frac{1}{\Delta X_{i,j}\, \Delta Y_{i,j}} \left(G_{X;\, i-\frac{1}{2},j} - G_{X;\, i+\frac{1}{2},j} + G_{Y;\, i,j-\frac{1}{2}} - G_{Y;\, i,j+\frac{1}{2}} \right) \tag{21}$$

$$+ \frac{1}{\Delta X_{i,j}\, \Delta Y_{i,j}} \left(\bar{G}_{int,m}\, \delta_{int,m;\, i,j} + \bar{G}_{dis,m}\, \delta_{dis,m;\, i,j} \right) + \bar{q}_{s;\, i,j} + \bar{q}_{b;\, i,j} .$$

The change in surface height can be found by subtracting the mean water level from the instantaneous depth,

$$\bar{D}_{i,j} = \bar{H}_{MWL} + H_{i,j} \tag{22}$$

where $\bar{H}_{MWL}$ is the mean water level, and $H_{i,j}$ is the change in surface height. The final form of the conservation principle for water mass can be represented by Equation (21).

2.4 Formulation of the Discrete-Element Equation for Conservation of Radionuclide Mass in Water

It is now necessary to formulate the equation for conservation of radionuclide mass in water, in the discrete-element form. Considering the conservation equation for radionuclide mass, Equation (11),

for the arbitrary discrete element (i, j), and evaluating the terms in the equation,

$$\frac{\partial}{\partial t}\overline{\iiint_{\forall} C_{r,w}\, d\forall} = \frac{\partial}{\partial t}\left[\Delta X_{i,j}\,\Delta Y_{i,j}\int_{0}^{\bar{D}_{i,j}} C_{r,w;i,j}\, dz\right]. \tag{23}$$

Substituting the appropriate turbulent distributions from Equation (7) and employing the distributive property of mean time averaging with constraints from Equations (8) and (9), Equation (23) becomes,

$$\int_{0}^{\bar{D}_{i,j}} C_{r,w;i,j}\, dz = \int_{0}^{\bar{D}_{i,j}}\left[\overline{\bar{C}}_{r,w;i,j} + \overline{\bar{C}^{*}}_{r,w;i,j} + \bar{C}'_{r,w;i,j}\right] dz \tag{24}$$

$$= \bar{D}_{i,j}\;\bar{C}_{r,w;i,j}\,.$$

Substituting Equation (24) into Equation (23) results in,

$$\frac{\partial}{\partial t}\left[\Delta X_{i,j}\,\Delta Y_{i,j}\,\bar{D}_{i,j}\,\bar{C}_{r,w;i,j}\right] =$$

$$\Delta X_{i,j}\,\Delta Y_{i,j}\,\frac{\partial}{\partial t}\left[\bar{D}_{i,j}\,\bar{C}_{r,w;i,j}\right], \tag{25}$$

$$= \Delta X_{i,j}\,\Delta Y_{i,j}\left[\bar{D}_{i,j}\,\frac{\partial \bar{C}_{r,w;i,j}}{\partial t} + \bar{C}_{r,w;i,j}\,\frac{\partial \bar{D}_{i,j}}{\partial t}\right].$$

Continuing for the next term in Equation (11),

$$\overline{\iint_A C_{r,w}\,(\bar{V}\cdot\hat{n})\,dA} = \iint_A \overline{C_{r,w}\,\bar{V}}\cdot\hat{n}\,dA\ ,$$

$$= -\Delta y_{i-1/2,j} \int_0^{\bar{\delta}_{i-1/2,j}} \overline{C_{r,w;\,i-1/2,j}\;u_{i-1/2,j}}\;dz$$

$$+\Delta y_{i+1/2,j} \int_0^{\bar{\delta}_{i+1/2,j}} \overline{C_{r,w;\,i+1/2,j}\;u_{i+1/2,j}}\;dz$$

$$-\Delta x_{i,j-1/2} \int_0^{\bar{\delta}_{i,j-1/2}} \overline{C_{r,w;\,i,j-1/2}\;V_{i,j-1/2}}\;dz$$

$$+\Delta x_{i,j+1/2} \int_0^{\bar{\delta}_{i,j+1/2}} \overline{C_{r,w;\,i,j+1/2}\;V_{i,j+1/2}}\;dz$$

$$-\Delta x_{i,j}\,\Delta y_{i,j}\,(\bar{q}_{b;\,i,j}\,C^*_{b;\,i,j} + \bar{q}_{s;\,i,j}\,C^*_{s;\,i,j})$$

$$-G_{int,m}\,\delta_{int,m;\,i,j}\,C_{int,m;\,i,j} - \bar{G}_{dis,m}\,\delta_{dis,m;\,i,j}\,C_{dis,m;\,i,j}\ , \qquad (26)$$

where:

$C^*_{b;i,j}$ = mass concentration of radionuclides in fluid inflow from bottom,

$C^*_{s;i,j}$ = mass concentration of radionuclides in fluid inflow from surface (e.g. atmospheric radiation),

$C_{int,m;i,j}$ = mass concentration of radionuclides in intake flow,

$C_{dis,m;i,j}$ = mass concentration of radionuclides in discharge flow.

Since the integrands in Equation (26) contain product forms of instantaneous quantities, the evaluation of the integrals must be handled with care. The time averaging must be carried out over the entire integrand. Substituting the turbulent distributions along the vertical direction from Equation (7), the integrals in Equation (26) become,

$$\int_0^{\bar{D}_{i\pm1/2,j}} \overline{C_{r,w;i\pm1/2,j}\, u_{i\pm1/2,j}}\, dz =$$

$$\int_0^{\bar{D}_{i\pm1/2,j}} \overline{\left[\bar{C}_{r,w;i\pm1/2,j} + \bar{C}^*_{r,w;i\pm1/2,j} + C'_{r,w;i\pm1/2,j}\right] \cdot \left[\bar{U}_{i\pm1/2,j} + \bar{u}^*_{i\pm1/2,j} + u'_{i\pm1/2,j}\right]}\, dz,$$

$$\int_0^{\bar{D}_{i,j\pm1/2}} \overline{C_{r,w;i,j\pm1/2}\, V_{i,j\pm1/2}}\, dz = \tag{27}$$

$$\int_0^{\bar{D}_{i,j\pm1/2}} \overline{\left[\bar{C}_{r,w;i,j\pm1/2} + \bar{C}^*_{r,w;i,j\pm1/2} + C'_{r,w;i,j\pm1/2}\right] \cdot \left[\bar{V}_{i,j\pm1/2} + \bar{V}^*_{i,j\pm1/2} + V'_{i,j\pm1/2}\right]}\, dz .$$

Expanding the integrand in Equation (27) and employing the distributive property of mean time averaging,

$$\int_0^{\bar{D}_{i\pm1/2,j}} \overline{C_{r,w;i\pm1/2,j}\, u_{i\pm1/2,j}}\, dz = \int_0^{\bar{D}_{i\pm1/2,j}} \overline{C}_{r,w;i\pm1/2,j}\, \overline{U}_{i\pm1/2,j}\, dz$$

$$+ \int_0^{D_{i\pm1/2,j}} \overline{C}_{r,w;j\pm1/2,j}\, \overline{u}^{*}_{i\pm1/2,j}\, dz + \int_0^{\bar{D}_{i\pm1/2,j}} \overline{C}_{r,w;i\pm1/2,j}\, u'_{i\pm1/2,j}\, dz$$

$$+ \int_0^{\bar{D}_{i\pm1/2,j}} \overline{C}^{*}_{r,w;i\pm1/2,j}\, \overline{U}_{i\pm1/2,j}\, dz + \int_0^{\bar{D}_{i\pm1/2,j}} \overline{C}^{*}_{r,w;i\pm1/2,j}\, \overline{u}^{*}_{i\pm1/2,j}\, dz$$

$$+ \int_0^{\bar{D}_{i\pm1/2,j}} \overline{C}^{*}_{r,w;i\pm1/2,j}\, u'_{i\pm1/2,j}\, dz + \int_0^{\bar{D}_{i\pm1/2,j}} \overline{C}'_{r,w;i\pm1/2,j}\, \overline{U}_{i\pm1/2,j}\, dz$$

$$+ \int_0^{\bar{D}_{i\pm1/2,j}} \overline{C}'_{r,w;i\pm1/2,j}\, \overline{u}^{*}_{i\pm1/2,j}\, dz + \int_0^{\bar{D}_{i\pm1/2,j}} \overline{C'_{r,w;i\pm1/2,j}\, u'_{i\pm1/2,j}}\, dz \,. \tag{28}$$

Rearranging the terms and taking the mean time averaged term outside the integral since it is a constant results in the following:

$$\int_0^{\bar{D}_{i\pm1/2,j}} \overline{C_{r,w;i\pm1/2,j}\, u_{i\pm1/2,j}}\, dz = \bar{D}_{i\pm1/2,j}\; \overline{C}_{r,w;i\pm1/2,j}\; \overline{U}_{i\pm1/2,j} +$$

$$\overline{C}_{r,w;i\pm1/2,j} \int_0^{\bar{D}_{i\pm1/2,j}} \overline{u}^{*}_{i\pm1/2,j}\, dz + \overline{C}_{r,w;i\pm1/2,j} \int_0^{\bar{D}_{i\pm1/2,j}} \overline{u'_{i\pm1/2,j}}\, dz$$

$$+ \bar{U}_{i\pm1/2,j} \int_0^{\bar{D}i\pm1/2,j} \overline{C^*_{r,w;i\pm1/2,j}}\, dz + \int_0^{\bar{D}i\pm1/2,j} \overline{C^*_{r,w;i\pm1/2,j}}\, \bar{u}^*_{i\pm1/2,j}\, dz$$

$$+ \int_0^{\bar{D}i\pm1/2,j} \overline{C^*_{r,w;i\pm1/2,j}}\, \overline{u'_{i\pm1/2,j}}\, dz + \bar{U}_{i\pm1/2,j} \int_0^{\bar{D}i\pm1/2,j} \overline{C'_{r,w;i\pm1/2,j}}\, dz$$

$$+ \int_0^{\bar{D}i\pm1/2,j} \overline{C'_{r,w;i\pm1/2,j}}\, \bar{u}^*_{i\pm1/2,j}\, dz + \int_0^{\bar{D}i\pm1/2,j} \overline{C'_{r,w;i\pm1/2,j}\, u'_{i\pm1/2,j}}\, dz. \tag{29}$$

Employing the constraint conditions of Equations (8) and (9), six of the integrals in Equation (29) are found to vanish; hence,

$$\int_0^{\bar{D}i\pm1/2,j} \overline{C_{r,w;i\pm1/2,j}\, u_{i\pm1/2,j}}\, dz = \bar{D}_{i\pm1/2,j}\, \bar{C}_{r,w;i\pm1/2,j}\, \bar{U}_{i\pm1/2,j}$$

$$+ \int_0^{\bar{D}i\pm1/2,j} \overline{C^*_{r,w;i\pm1/2,j}}\, \bar{u}^*_{i\pm1/2,j}\, dz + \int_0^{\bar{D}i\pm1/2,j} \overline{C'_{r,w;i\pm1/2,j}\, u'_{i\pm1/2,j}}\, dz. \tag{30}$$

Applying the same procedure to the second part of Equation (27), the last two integrals become,

$$\int_0^{D_{i,j\pm1/2}} \overline{C_{n,w;i,j\pm1/2}\, V_{-i,j\pm1/2}}\, dz =$$

$$\overline{D}_{i,j\pm1/2}\, \overline{C}_{n,w;i,j\pm1/2}\, \overline{V}_{-i,j\pm1/2} + \int_0^{D_{i,j\pm1/2}} \overline{C}^{*}_{n,w;i,j\pm1/2}\, \overline{V}^{*}_{i,j\pm1/2}\, dz$$

$$+ \int_0^{D_{i,j\pm1/2}} \overline{C'_{n,w;i,j\pm1/2}\, V'_{i,j\pm1/2}}\, dz \,. \qquad (31)$$

The integrals in Equations (30) and (31) are of extreme importance since they represent the overall convective transport of the mass concentration of the radionuclide across the enclosure surface of the discrete element. Dominant turbulent transport phenomena is included in the definitions of the integrals according to mean time averaged products of the random turbulent fluctuations.

The proper evaluation of these integrals requires a knowledge of how velocity and mass concentration of radionuclides varies with depth. Development of the non-convective turbulent transport for mass concentration of radionuclides will be presented in a later section.

At this point, the integrals are represented as transport flux terms;

$$\overline{G'^{*}_{w,x;i\pm1/2,j}} =$$

$$\frac{1}{\bar{D}_{i\pm 1/2,j}}\left[\int_0^{D_{i\pm 1/2,j}} \bar{C}^{*}_{r,w;i\pm 1/2,j}\ \bar{u}^{*}_{i\pm 1/2,j}\,dz \int_0^{\bar{D}_{i\pm 1/2,j}} \overline{C'_{r,w;i\pm 1/2,j}\ u'_{i\pm 1/2,j}}\,dz\right]$$

$$\bar{G}'^{*}_{w;y;i,j\pm 1/2} =$$

$$\frac{1}{\bar{D}_{i,j\pm 1/2}}\left[\int_0^{D_{i,j\pm 1/2}} \bar{C}^{*}_{r,w;i,j\pm 1/2}\ \bar{V}^{*}_{i,j\pm 1/2}\,dz + \int_0^{D_{i,j\pm 1/2}} \overline{C'_{r,w;i,j\pm 1/2}\ V'_{i,j\pm 1/2}}\,dz\right]dz. \tag{32}$$

Substituting Equation (32) into Equations (30) and (31),

$$\int_0^{\bar{D}_{i\pm 1/2,j}} \overline{C_{r,w;i\pm 1/2,j}\ u_{i\pm 1/2,j}}\,dz =$$

$$\bar{D}_{i\pm 1/2,j}\ \bar{C}_{r,w;i\pm 1/2,j}\ \bar{U}_{i\pm 1/2,j} + \bar{D}_{i\pm 1/2,j}\ \bar{G}'^{*}_{w,x;i\pm 1/2,j}\ ) \tag{33}$$

$$\int_0^{\bar{D}_{i,j\pm 1/2}} \overline{C_{r,w;i,j\pm 1/2}\ u_{i,j\pm 1/2}} =$$

$$\bar{D}_{i,j\pm 1/2}\ \bar{C}_{r,w;i,j\pm 1/2} + \bar{D}_{i,j\pm 1/2}\ \bar{G}'^{*}_{w;y;i,j\pm 1/2}\ .$$

Substituting Equation (33) into Equations (31) and (32), and the resulting equation into Equation (26),

$$\iint_A \overline{C_{r,w}(\bar{v}\cdot\hat{n})}\,dA = -G_{x;i-1/2,j}\,\bar{C}_{r,w;i-1/2,j}$$

$$+\bar{G}_{x;i+1/2,j}\,\bar{C}_{r,w;i+1/2,j} - G_{y;i,j-1/2}\,\bar{C}_{r,w;i,j-1/2}$$

$$+\bar{G}_{y;i,j+1/2}\,\bar{C}_{w;i,j+1/2} - \Delta y_{i-1/2,j}\,\bar{D}_{i-1/2,j}\,\bar{G}'^{*}_{w;x;i-1/2,j} \qquad (34)$$

$$+\Delta x_{i+1/2,j}\,\bar{D}_{i+1/2,j}\,\bar{G}'^{*}_{w;x;i+1/2,j} - \Delta x_{i,j-1/2}\,\bar{D}_{i,j-1/2}\,\bar{G}'^{*}_{w;y;i,j-1/2}$$

$$+\Delta x_{i,j+1/2}\,\bar{D}_{i,j+1/2}\,\bar{G}'^{*}_{w;y;i,j+1/2} - \Delta x_{i,j}\,\Delta y_{i,j}\,(\bar{q}_{b;i,j}\,\bar{C}^{*}_{b;i,j} + \bar{q}_{s;i,j}\,\bar{C}^{*}_{s;i,j})$$

$$-\bar{G}_{int,m}\,\delta_{int,m;i,j}\,C_{int,m;i,j} - \bar{G}_{dis,m}\,\delta_{dis,m;i,j}\,C_{dis,m;i,j}\,.$$

Evaluating the integrals on the right hand side of Equation (11), the first term is the molecular diffusion rate of radionuclides. It depends linearly on the concentration gradients in the horizontal planes, surface and bottom radionuclide transport effects. Hence, it can be represented as,

$$\iint_A \bar{G} \cdot (-\hat{n})\, dA =$$

$$\Delta y_{i-1/2,j}\, \bar{D}_{i-1/2,j}\, \bar{G}_{w,m,x;i-1/2,j} - \Delta y_{i+1/2,j}\, \bar{D}_{i+1/2,j}\, \bar{G}_{w,m,x;i+1/2,j}$$

$$+\Delta x_{i,j-1/2}\, \bar{D}_{i,j-1/2}\, \bar{G}_{w,m,y;i,j-1/2} - \Delta x_{i,j+1/2}\, \bar{D}_{i,j+1/2}\, \bar{G}_{w,m,y;i,j+1/2}$$

$$-\Delta x_{i,j}\, \Delta y_{i,j}\, (\bar{q}_{b,m;i,j} + \bar{q}_{s,m;i,j}) . \qquad (35)$$

where:

$\bar{G}_{w,m,x;,i\pm1/2,j}$ = molecular diffusion transport flux for radionuclides in water along x,

$\bar{G}_{w,m,y;i,j\pm1/2}$ = molecular diffusion transport flux for radionuclides in water along y,

$\bar{g}_{b,m;i,j}$ = volumetric flux per unit area through the bottom due to molecular diffusion,

$\bar{g}_{s,m;i,j}$ = volumetric flux per unit area through the surface due to molecular diffusion.

The last term in Equation (11) is a volumetric decay of radionuclide mass. It can be approximated by a first order decay form,

$$\iiint_{\forall} \dot{C}\, d\forall = \Delta x_{i,y}\, \Delta y_{i,j}\, \bar{D}_{i,j}\, \dot{C}_{i,j} . \qquad (36)$$

where $\dot{C}$ is the volumetric decay term. Substituting Equations (24), (34), (35) and (36) into Equation (11) and rearranging,

$$\frac{\partial \bar{C}_{r,w,i,j}}{\partial t} + \frac{\partial \bar{C}_{r,w,i,j}}{\bar{D}_{i,j}}\left[\frac{\partial \bar{D}_{i,j}}{\partial t}\right] = \frac{1}{\Delta X_{i,j}\,\Delta Y_{i,j}\,\bar{D}_{i,j}}$$

$$\Big\{(\bar{G}_{x,j,i-1/2,j}\,\bar{C}_{r,w,j,i-1/2,j} - \bar{G}_{x,j,i+1/2,j}\,\bar{C}_{r,w,j,i+1/2,j})$$

$$+(\bar{G}_{y,j,i,j-1/2}\,\bar{C}_{r,w,j,i,j-1/2} - \bar{G}_{y,j,i,j+1/2}\,\bar{C}_{r,w,j,i,j+1/2})$$

$$+\ \Delta Y_{i-1/2,j}\,\bar{D}_{i-1/2,j}\left[\bar{G}_{w,m,x,j,i-1/2,j} + \bar{G}'^{*}_{w,x,j,i-1/2,j}\right]$$

$$-\Delta Y_{i+1/2,j}\ \bar{D}_{i+1/2,j}\left[\bar{G}_{w,m,x,j,i+1/2,j} + \bar{G}'^{*}_{w,x,j,i+1/2,j}\right]$$

$$+\Delta X_{i,j-1/2}\ \bar{D}_{i,j-1/2}\left[\bar{G}_{w,m,y,j,i,j-1/2} + \bar{G}'^{*}_{w,y,j,i,j-1/2}\right]$$

$$-\Delta X_{i,j+1/2}\,\bar{D}_{i,j+1/2}\left[\bar{G}_{w,m,y,j,i,j+1/2} + \bar{G}'^{*}_{w,y,j,i,j+1/2}\right]$$

$$+\bar{G}_{int,m}\,\delta_{int,m,j,i,j}\,C_{int,m,j,i,j} + \bar{G}_{dis,m}\,\delta_{dis,m,j,i,j}\,C_{dis,m,j,i,j}\Big\} + \dot{C}_{i,j}$$

$$+\frac{1}{\bar{D}_{i,j}}\left[\bar{q}_{b,j,i,j}\,C^{*}_{b,j,i,j} + \bar{q}_{s,j,i,j}\,C^{*}_{s,j,i,j}\right] + \frac{1}{\bar{D}_{i,j}}\left[\bar{q}_{b,m,j,i,j} + \bar{q}_{s,m,j,i,j}\right]. \tag{37}$$

Molecular and turbulent diffusion fluxes can be combined as:

$$\bar{G}_{w,x;i\pm 1/2,j} = \bar{G}_{w,m,x;i\pm 1/2,j} + \bar{G}'^{*}_{w,x;i\pm 1/2,j} \,,$$

$$\bar{G}_{w,y;i,j\pm 1/2} = \bar{G}_{w,m,y;i,j\pm 1/2} + \bar{G}'^{*}_{w,y;i,j\pm 1/2} \,. \tag{38}$$

To eliminate the time derivative of depth from the radionuclide mass conservation equation, (37), the equation for time rate of change of depth, (21), is used. Hence, substituting Equation (21) in Equation (37), the final form of the conservation principle for radionuclide mass becomes,

$$\frac{\partial \bar{C}_{r,w;i,j}}{\partial t} = \frac{1}{\Delta x_{i,j}\,\Delta y_{i,j}\,\bar{D}_{i,j}} \Big\{ \big(\bar{G}_{x;i-1/2,j}\,[\bar{C}_{r,w;i-1/2,j} - \bar{C}_{r,w;i,j}]$$

$$- \bar{G}_{x;i+1/2,j}\,[\bar{C}_{r,w;i+1/2,j} - \bar{C}_{r,w;i,j}]\big) + \big(\bar{G}_{y;i,j-1/2}\,[\bar{C}_{r,w;i,j-1/2} - \bar{C}_{r,w;i,j}]$$

$$+ \bar{G}_{y;i,j+1/2}\,[\bar{C}_{r,w;i,j+1/2} - \bar{C}_{r,w;i,j}]\big)\Big\}$$

$$+ \frac{1}{\Delta x_{i,j}\,\Delta y_{i,j}\,\bar{D}_{i,j}} \Big\{ [\Delta y_{i-1/2,j}\,\bar{D}_{i-1/2,j}\,\bar{G}_{w,x;i-1/2,j} - \Delta y_{i+1/2,j}\,\bar{D}_{i+1/2,j}\,\bar{G}_{w,x;i+1/2,j}]$$

$$+ [\Delta x_{i,j-1/2}\,\bar{D}_{i,j-1/2}\,\bar{G}_{w,y;i,j-1/2} - \Delta x_{i,j+1/2}\,\bar{D}_{i,j+1/2}\,\bar{G}_{w,y;i,j-1/2}]\Big\}$$

$$+ \frac{1}{\Delta X_{i,j}\,\Delta Y_{i,j}\,\bar{D}_{i,j}} \left\{ \bar{\epsilon}_{int,m}\,\delta_{int,m;i,j}\left[C_{int,m;i,j} - \bar{C}_{r,w;i,j} \right] \right.$$

$$\left. + \bar{\epsilon}_{dis,m}\,\delta_{dis,m;i,j}\left[C_{dis,m;i,j} - \bar{C}_{r,w;i,j} \right] \right\}$$

$$+ \dot{C}_{i,j} + \frac{1}{\bar{D}_{i,j}} \left\{ \bar{q}_{b;i,j}\left[\bar{C}^{*}_{b;i,j} - \bar{C}_{r,w;i,j} \right] \right.$$

$$\left. + \bar{q}_{s;i,j}\left[C^{*}_{s;i,j} - \bar{C}_{r,w;i,j} \right] + \bar{q}_{b,m;i,j} + \bar{q}_{s,m;i,j} \right\} . \qquad (39)$$

Equation (39) represents the final form of the conservation principle for radionuclide mass for an arbitrary discrete element. The mathematical terms on the right-hand side of the equation can be grouped into four parts representing the four fundamental types of physical phenomena which control the time rate of change of the mass concentration of radionuclides in a discrete element.

Convection Effect of Mean Time and Depth Average Flow Field

$$(\bar{F}_c)_{i,j} = \frac{1}{\Delta X_{i,j}\,\Delta Y_{i,j}\,\bar{D}_{i,j}} \left(\left\{ \bar{G}_{x;i-1/2,j}\left[\bar{C}_{r,w;i-1/2,j} - \bar{C}_{r,w;i,j} \right] \right. \right.$$

$$\left. - \bar{G}_{x;i+1/2,j}\left[\bar{C}_{r,w;i+1/2,j} - \bar{C}_{r,w;i,j} \right] \right\} + \left\{ \bar{G}_{y;i,j-1/2}\left[\bar{C}_{r,w;i,j-1/2} - \bar{C}_{r,w;i,j} \right] \right.$$

$$\left. \left. - \bar{G}_{y;i,j+1/2}\left[\bar{C}_{r,w;i,j+1/2} - \bar{C}_{r,w;i,j} \right] \right\} \right) \qquad (40)$$

It should be noted that the convective terms in Equation (40) are arranged in a special form based on radionuclide concentration differences between the half-point values, which represent the location of the enclosure surfaces, and the radionuclide concentrations in the discrete element. This slightly unconventional form has a distinct computational property which minimizes the effect of possible errors in the specified flow field. The present form of the FLIDE model, unlike Eraslan's [4] original version, utilizes the mass conservation equation to solve for depth changes during the tidal cycle. Yet, the model does not solve the momentum equations. This method could cause artificial radionuclide concentration variations if the standard forms for convective terms based on half-point values of radionuclide concentrations were utilized. These errors would result from flow field errors starting from equal radionuclide conditions throughout the flow region. The particular forms of the convective terms in Equation (40) avoid this computational problem, since equal radionuclide concentrations automatically eliminate convective effects regardless of the velocity values at the half-point surfaces.

Overall Diffusion Effect of Depth Averaged Molecular and Turbulent Transport Phenomena

$$(\bar{F}_D)_{i,j} = \frac{1}{\Delta X_{i,j}\, \Delta Y_{i,j}\, \bar{D}_{i,j}}$$

$$\left\{ \left[\Delta Y_{i-1/2,j}\, \bar{D}_{i-1/2,j}\, \bar{G}_{w,x;\, i-1/2,j} - \Delta Y_{i+1/2,j}\, \bar{D}_{i+1/2,j}\, \bar{G}_{w,x;\, i-1/2,j} \right] \right.$$

$$\left. + \left[\Delta X_{i,j-1/2}\, \bar{D}_{i,j-1/2}\, \bar{G}_{w,y;\, i,j-1/2} - \Delta X_{i,j+1/2}\, \bar{D}_{i,j+1/2}\, \bar{G}_{w,y;\, i,j+1/2} \right] \right\} \qquad (41)$$

The formulation of the non-convective transport terms and the molecular diffusion rate will be discussed in the next chapter.

Radionuclide Effect of Power Plant Intakes and Discharges

$$(\bar{F}_p)_{i,j} = \frac{1}{\Delta x_{i,j} \Delta y_{i,j} \bar{D}_{i,j}} \left\{ \bar{G}_{int,m} \delta_{int,m;i,j} \left[C_{int,m;i,j} - \bar{C}_{r,w;i,j} \right] \right. \tag{42}$$

$$\left. + \bar{G}_{dis,m} \delta_{dis,m;i,j} \left[C_{dis,m;i,j} - \bar{C}_{r,w;i,j} \right] \right\}$$

In this formulation, it is important to note that the radionuclide release by the power plants into the flow is not represented as radionuclide source terms. It is more realistic to employ the form of Equation (42), which considers the radionuclide input effects based on the flow rates and radionuclide concentrations at the intakes and discharges. For discharge radionuclide concentration, $C_{dis,m;i,j}$ equal to the local concentration $\bar{C}_{r,w;i,j}$, according to the present formulation, the radionuclide input of the discharge completely vanishes, which is correct from physical considerations.

Under normal operating conditions, particularly in shallow regions, it is realistic to assume that the intake concentration is equal to the local mean radionuclide concentration $C_{r,w;i,j}$. This assumption will take into account recirculation effects caused by interaction between the intakes and discharges. In certain flow regions, a certain severe stratification condition may exist, where the intake

concentration can realistically be assumed to be equal to the ambient radionuclide concentration. Considering the present form, Equation (42), and since the intake flow rate $\bar{G}_{int,m}$ is negative, this assumption immediately produces a concentrating effect in the intake discrete element. This result is definitely correct from physical considerations, since the assumption forces the intake to eliminate the water with a lower mass concentration of radionuclides. Consequently, the stratified layer which remains in the element causes the unavoidable effect of increasing the local mean radionuclide concentration of the water in the discrete element.

Hence, in the application of the present mathematical model to the assessment of radionuclide impact of a power plant, it is more realistic to assume the intake concentration to be the local mean radionuclide concentration of the discrete element in which the intake is located. If stratification effects are to be imposed on the intake conditions, extreme care should be taken to make sure that all the physical conditions have been considered.

Overall Effects of Surface and Bottom Conditions and Radionuclide Decay

$$(\bar{F}_s)_{i,j} = \dot{C}_{i,j} + \frac{1}{\bar{D}_{i,j}} \left\{ \left[\bar{q}_{b,m;i,j} + \bar{q}_{s,m;i,j} \right] \right.$$

$$\left. + (\bar{q}_{b;i,j}) \left[C^*_{b;i,j} - \bar{C}_{n,w;i,j} \right] + (\bar{q}_{s;i,j}) \left[C^*_{s;i,j} - \bar{C}_{n,w;i,j} \right] \right\} \qquad (43)$$

The radionuclide decay term $\dot{C}_{i,j}$ is retained in the formulation to simulate radioactive decay of the radionuclides. It will be used as a first order decay rate.

The terms representing the radionuclide flux $\bar{g}_{b;m;i,j}$ and inflow $\bar{g}_{b;i,j}$ from the bottom can be neglected in usual applications which consider the total depth. However, for special situations in deep regions where stratification is present, these terms can be employed to approximately incorporate the vertical entrainment and radionuclide transfer from the lower stratified region.

The surface radionuclide flux $\bar{g}_{s;m;i,j}$ and inflow $\bar{g}_{s;i,j}$ depend on the atmospheric conditions. The main source of surface fluxes is from fallout produced by the power plant and any neighboring plants.

Substituting the mathematical forms of the above discussed physical effects, Equations (40), (41), (42), (43) into Equation (39), the final simulation form of the conservation principle for radionuclide mass in water can be expressed as,

$$\frac{\partial C_{r,w;i,j}}{\partial t} = \overline{F}_{i,j} = (\overline{F}_c)_{i,j} + (\overline{F}_D)_{i,j} + (\overline{F}_P)_{i,j} + (\overline{F}_s)_{i,j} \quad , \tag{44}$$

which represents a first-order, ordinary differential equation for the unknown mean radionuclide concentration $\bar{C}_{r,w;i,j}$ in discrete element (i,j). Hence, provided the terms in the right-hand side of Equation (44) can be formulated in terms of the principal unknown variable, the mean radionuclide concentration $\bar{C}_{r,w;i,j}$, the mathematical system of the Discrete-Element method consists of a system of coupled,

first-order, ordinary differential equations which can be integrated from a given set of initial conditions.

3. CLOSURE OF MATHEMATICAL SYSTEM OF EQUATIONS

3.1 Formulation of Half-Point Values on Discrete-Element Surfaces

The first necessary step to keep the governing system of equations of the Discrete-Element method consistent, Equation (39), is to eliminate the half-point values for velocity components $\bar{U}_{i \pm 1/2,\, j}$, $\bar{V}_{i,\, j \pm 1/2}$ and radionuclide concentrations $\bar{C}_{r,w;\, i \pm 1/2,\, j}$, $\bar{C}_{r,w;\, i,\, j + 1/2}$ in terms of their mean values in the discrete elements. From the solution point of view, this is a very crucial problem, since the stability of the numerical methods, particularly the explicit ones, critically depends upon the forms of the convective terms.

The most successful form, from the computational point of view, for eliminating the half-point values in terms of the principal unknown values, is the "second upwind differencing" or "donor cell" method, which was first presented by Gentry, Martin, and Daly [12] with the formulation of the FLIC method; see Roache [16] for further discussion.

The standard "second upwind differencing" or "donor cell" forms of the FLIC method must be slightly modified to incorporate the unequal dimensions of the discrete elements utilized in the FLIDE method in evaluating the half-point values of depth, $\bar{D}_{i \pm 1/2,\, j}$, $\bar{D}_{i,\, j \pm 1/2}$, and velocity components $\bar{U}_{i \pm 1/2,\, j}$, $\bar{V}_{i,\, j \pm 1/2}$. Hence, the modified forms based on linear averaging become,

$$\bar{D}_{i\pm 1/2,j} = \frac{[\Delta X_{i,j}\bar{D}_{i\pm 1,j} + \Delta X_{i\pm 1,j}\bar{D}_{i,j}]}{[\Delta X_{i,j} + \Delta X_{i\pm 1,j}]} ,$$

$$\bar{D}_{i,j\pm 1/2} = \frac{[\Delta y_{i,j}\bar{D}_{i,j\pm 1} + \Delta y_{i,j\pm 1}\bar{D}_{i,j}]}{[\Delta y_{i,j} + \Delta y_{i,j\pm 1}]} ,$$

$$\bar{U}_{i\pm 1/2,j} = \frac{[\Delta y_{i,j}\bar{U}_{i\pm 1,j} + \Delta y_{i\pm 1,j}\bar{U}_{i,j}]}{[\Delta y_{i,j} + \Delta y_{i\pm 1,j}]} ,$$

$$\bar{V}_{i,j\pm 1/2} = \frac{[\Delta x_{i,j}\bar{V}_{i,j\pm 1} + \Delta x_{i,j\pm 1}\bar{V}_{i,j}]}{[\Delta x_{i,j} + \Delta x_{i,j\pm 1}]} . \qquad (45)$$

The standard forms of the FLIC method for the transported property of the fluid, represented by the radionuclide concentration $C_{r,w}$, are retained in the Discrete-Element method as:

$$\bar{C}_{r,w;i-1/2,j} = \begin{cases} \bar{C}_{r,w;i,j} , \text{ for } \bar{U}_{i-1/2,j} < 0 , \\ \bar{C}_{r,w;i-1,j} , \text{ for } \bar{U}_{i-1/2,j} > 0 , \end{cases}$$

$$\bar{C}_{r,w;i+1/2,j} = \begin{cases} \bar{C}_{r,w;i+1,j} , \text{ for } \bar{U}_{i+1/2,j} < 0 , \\ \bar{C}_{r,w;i,j} , \text{ for } \bar{U}_{i+1/2,j} > 0 , \end{cases}$$

$$\bar{C}_{r,w;i,j-1/2} = \begin{cases} \bar{C}_{r,w;i,j} , \text{ for } \bar{V}_{i,j-1/2} < 0 , \\ \bar{C}_{r,w;i,j-1} , \text{ for } \bar{V}_{i,j-1/2} > 0 , \end{cases}$$

$$\bar{C}_{r,w;i,j+1/2} = \begin{cases} \bar{C}_{r,w;i,j+1} , \text{ for } \bar{V}_{i,j+1/2} < 0 , \\ \bar{C}_{r,w;i,j} , \text{ for } \bar{V}_{i,j+1/2} > 0 . \end{cases} \quad (46)$$

In Equation (46), the special case when the normal components of the velocity field identically vanish on the surfaces need not be

considered, since under these conditions, the convective transport terms also vanish regardless of the value of the radionuclide concentration on the element surfaces.

The evaluation of half-point values in Equation (46) is based on the flow direction; that is, as the fluid crosses an enclosure surface normal to its flow direction, it always has the radionuclide concentration of the discrete element upstream of the enclosure surface. The generalized mathematical expressions for this physically realistic argument are represented by Equation (46) for the evaluation of the half-point values on all enclosure surfaces of a discrete element.

It should be pointed out that this method of upwind differencing could cause errors in the Discrete-Element method due to the unequal dimensions of the adjacent elements. In constructing a grid for application of the Discrete-Element method, sizes of adjacent elements should not be excessively different. This will be discussed in detail in a later section.

3.2 Initial and Boundary Half-Point Conditions

Since the mathematical system of the FLIDE method, Equation (39) or Equation (44), represents a system of coupled, ordinary, first-order differential equations in time, the initial conditions are straight forward as specified values at any arbitrarily assigned time t_0 for all discrete elements at positions (i,j) that is,

$$\overline{C}_{n,w;i,j}(t_0) = [\overline{C}_0]_{i,j} \quad \text{for all } (i,j) . \tag{47}$$

These are necessary and sufficient initial conditions for the solution of the system.

Since the mathematical system of the Discrete-Element method is based on the integration of conservation laws, there are no boundary conditions in the sense of boundary value problems. The effects of the boundaries are imposed on the half-point surfaces of the discrete elements located on the physical or hypothetical boundaries of the flow region in the horizontal x,y plane.

There are three classes of boundary half-point conditions associated with the radionuclide problems in coastal and off shore regions. In the discussion of these conditions, the discrete elements which have common surfaces with the boundaries will be identified by I, J, K, L to distinguish them from interior elements.

Specified Boundary Half-Point Conditions

This class represents the conditions when velocity components and radionuclide concentrations are expressed as time-dependent values on the enclosure surfaces of the boundary discrete elements, for example, effects of a neighboring power plant or a large river with known flow and radionuclide concentration discharging into a coastal region. These general conditions can be expressed as

$$\bar{U}_{I\pm1/2,j} = \bar{U}_x(t), \quad \bar{V}_{I\pm1/2,j} = \bar{V}_x(t), \quad \bar{C}_{r,w;I\pm1/2,j} = \bar{C}_x(t),$$

$$\bar{U}_{i,J\pm1/2} = \bar{U}_y(t)\ ,\ \bar{V}_{i,J\pm1/2} = \bar{V}_y(t)\ ,\ \bar{C}_{n,w,i,J\pm1/2} = \bar{C}_y(t)\ . \tag{48}$$

where the subscripts x and y represent the axes which are parallel to the lines that terminate at the discrete element surfaces corresponding to the boundaries.

The velocity conditions in Equation (46) can be omitted since the velocity field is specified for the region, but they are included in the formulation for the sake of completeness.

This class of conditions can also be used to implement a flow field caused by effects of an intake or discharge on the shoreline; since the near-field conditions can appreciably influence the flow conditions in the vicinity of the discharges and intakes.

Shoreline Boundary Half-Point Conditions

One of the fundamental advantages of the Discrete-Element method is its flexibility in using discrete elements of arbitrary geometry. Although the formulation is based on a Cartesian index system (i,j), the method does not require the use of rectangular elements to specify the shoreline geometry.

The flow region in the immediate vicinity of the shoreline can be represented by discrete elements of trapezoidal shapes. Each boundary element consists of at least one enclosure surface that will closely

approximate the section of shoreline that is contained in a particular discrete element.

Since the shoreline is assumed to be impermeable, there is no mass transfer across the enclosure surface of the element which corresponds to that section of shoreline; that is,

$$\bar{U}_{I\pm 1/2,j} = 0, \; G_{I\pm 1/2,j} = 0 \Rightarrow \bar{C}_{r,w;I\pm 1/2,j} = \bar{C}_{r,w;i,j} \,,$$

$$\bar{V}_{i,J\pm 1/2} = 0, \; G_{i,J\pm 1/2} = 0 \Rightarrow \bar{C}_{r,w;J\pm 1/2} = \bar{C}_{r,w;i,j} \,. \tag{49}$$

It should be noted that detailed nonslip or tangential-slip velocity conditions need not be considered in the formulations of the boundary half-point conditions, since the FLIDE method only requires the macroscopic transport fluxes across the enclosure surfaces.

The radionuclide concentration conditions in Equation (49) are consequences of the velocity and radionuclide flux conditions; and they are not essential for the solution of the mathematical system of equations, Equations (39) or (44).

Open Region Boundary Half-Point Conditions

A mathematical radionuclide transport model for a coastal or offshore region must be capable of considering hypothetical boundaries

which separate the region from the rest of the ocean. Although this is not essential from mathematical consideration since all world oceans can be treated as a flow region with closed or matching boundaries, from practical computational considerations, it is essential. Hence, in the general formulation of the Discrete-Element model, it is necessary to develop the appropriate boundary half-point conditions for open regions.

In the case of analytical methods, the open boundary conditions are usually specified by the behavior of the solutions at infinity. Since the Discrete-Element method or any finite-difference type method cannot handle conditions at infinity without artificial straining of coordinates, it is necessary to consider other conditions which can be used on the open boundaries.

A seemingly obvious assumption would be to specify the radionuclide concentration on the boundary as being that of ambient, except that this assumption could cause unnaturally high gradients. Consequently, it could produce large concentration gradients at the open boundary. Furthermore, the solution becomes extremely sensitive to the dimensions of the region bounded by an imaginary boundary.

Another seemingly natural condition is to assume that there is no radionuclide diffusion across the imaginary boundary. This solution produces excessively high radionuclide concentrations. Furthermore, the solutions again become extremely sensitive to the dimensions of the region bounded by the imaginary boundary. Hence, from physical considerations of radionuclide diffusion phenomena, this condition is also unacceptable.

It becomes evident that the imaginary boundary must be sufficiently far from the immediate influence of the intakes and discharges. Hence, the area around the open boundary will only be affected by convection and diffusion phenomena, and any surface or bottom mass transfer if they exist. Since all of these effects will have almost the same influence around the open boundary, it is plausible to assume that the variations of radionuclide concentrations normal to the boundary will be approximately the same on both sides.

This assumption is schematically represented in Figure 3 in terms of a boundary element (i,j) in the flow region and an additional imaginary discrete element (i + 1, j) outside the hypothetical boundary.

From mathematical considerations, this assumption corresponds to a linear variation of radionuclide concentrations in the real element (i,j) and the additional imaginary element (i + 1, j) across the half-point boundary (i + 1/2, j). Hence, the value of the radionuclide concentration in the imaginary element (i + 1, j) can be expressed in terms of the radionuclide concentration values in the boundary element as

$$\frac{\bar{C}_{radnuc;i+1,j} - \bar{C}_{radnuc;i,j}}{\Delta X_{i,j}} = 2 \quad \frac{\bar{C}_{radnuc;i,j} - \bar{C}_{radnuc;i-1/2,j}}{\Delta X_{i,j}} \; . \tag{50}$$

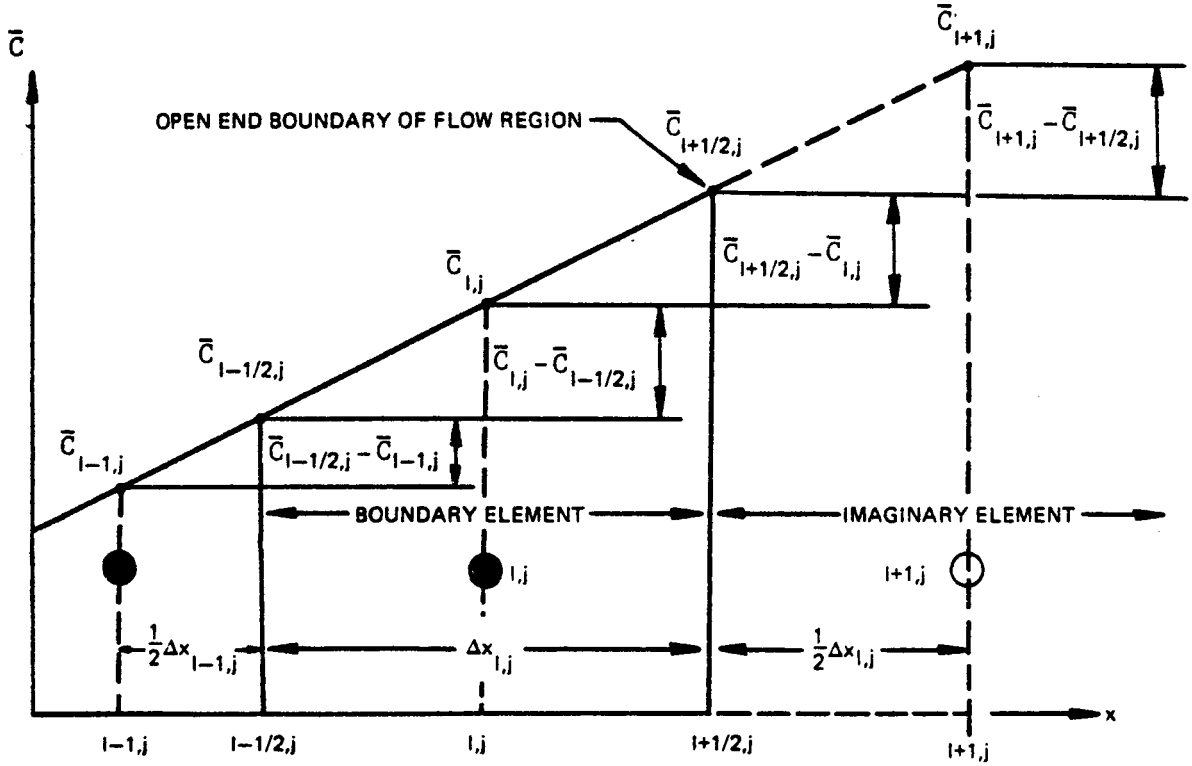


Figure 3. Schematic Representation of the Open-End Boundary Conditions.

Rearranging Equation (48),

$$\bar{C}_{r,w;i+1,j} = 3\bar{C}_{r,w;i,j} - 2\bar{C}_{r,w;i-\frac{1}{2},j} \,. \tag{51}$$

The half-point concentration can be eliminated by employing the linear averaging form of Equation (46), for internal discrete elements; that is,

$$\bar{C}_{r,w;i-\frac{1}{2},j} = \frac{[\Delta X_{i,j}\bar{C}_{r,w;i-\frac{1}{2},j} + \Delta X_{i-1,j}\bar{C}_{r,w;i,j}]}{[\Delta X_{i,j} + \Delta X_{i-1,j}]} \,. \tag{52}$$

Substituting Equation (52) into (51) and rearranging,

$$\bar{C}_{r,w;i+1,j} = \bar{C}_{r,w;i,j} + \frac{2\Delta X_{i,j}}{[\Delta X_{i,j} + \Delta X_{i-1,j}]}\,[\bar{C}_{r,w;i,j} - \bar{C}_{r,w;i-1,j}] \,, \tag{53}$$

which represents the value of the radionuclide concentration in the imaginary element.

Since the flow conditions are specified for the region, it is not necessary to compute velocity values for the imaginary elements. The velocities are specified in the imaginary elements, in the same manner as the internal elements of the region.

The conditions for the open boundaries normal to the y direction can be formulated in exactly the same manner as for the x direction, resulting in

$$\bar{C}_{r,w,j,i,j,j+1} = \bar{C}_{r,w,j,i,j,j} + \frac{2\Delta y_{i,j}}{[\Delta y_{i,j} + \Delta y_{i,j-1}]} [\bar{C}_{r,w,j,i,j,j} - \bar{C}_{r,w,j,i,j,j-1}] . \quad (54)$$

The previously formulated conditions for open boundary elements represent necessary and sufficient conditions for one solution of the Discrete-Element system of differential equations, Equations (39) and (44). The general half-point, second upwind differencing forms for the internal elements, Equations (45) and (46), can be directly applied to the real and imaginary elements. The formulation of the radionuclide concentration conditions, Equations (53) and (54), are equivalent to specifying the half-point values on element enclosure surfaces acting as the open boundary.

3.3 Formulation of Intake and Discharge Conditions

The volumetric flow rates for the intakes $\bar{G}_{int,m}$ and discharges $\bar{G}_{dis,m}$, used in Equations (39) and (44) are determined according to their locations in the discrete elements. If two intakes for one plant are located in the same discrete element, they are represented by a total intake flow rate for that discrete element. A large diffuser could span as many as five discrete elements, in which case the total flow rate would be broken into five parts, with a flow rate given for each discrete element. The flow rates are specified as time-dependent variations,

$$\bar{G}_{int,m} = \bar{G}_{int,m}(t), \quad \bar{G}_{dis,m} = \bar{G}_{dis,m}(t) , \tag{55}$$

based on the operational conditions of the power plants.

The intake radionuclide concentration represents the mass concentration of the water which enters the discrete element i(m), j(m) which contains the intake m. The intake concentration is dependent upon physical conditions that exist in the intake element. It may depend on the shape, orientation, depth, and velocity of the intake. Hence, the intake radionuclide concentration can be expressed as

$$C_{int,m;i,j} = \bar{C}_{nw;i,j} + (\Delta C_{in})_{i,j,m} , \tag{56}$$

where $(\Delta C_{in})_{i,j,m}$ represents the difference between the intake concentration and the local mean concentration $C_{r,w;i,j}$ in the discrete element of the intake m. Accurate determination of this difference will not be included, since it is most definitely outside the scope of this study. It would require a sophisticated near field analysis beyond the present state of the art in that area.

However, as discussed earlier, it is more plausible and realistic to assume the intake radionuclide concentration $C_{int,m;i,j}$ to be equal to the local mean concentration $\bar{C}_{r,w;\ i,j}$; that is

$$C_{int,m;i,j} \cong \bar{C}_{r,w;i,j}, \quad (C_{in})_{i,j,m} = 0 \tag{57}$$

This will provide a conservative assessment of the radionuclide impact of the power plant discharge, since it definitely takes into account the phenomena of recirculation. Hence, the near-field analysis of intake conditions can be neglected without introducing appreciable error.

The discharge concentration $C_{dis,m;i,j}$ also depends upon physical conditions in its respective discrete element. The radionuclide concentration is determined according to the input from the power plant. For a condenser with a multi-intake structure which spans more than one discrete element, the inlet concentration to the condenser $(\bar{C}_{in})_{CND}$ must be determined according to the flow rates $\bar{G}_{int,m}$ and the local intake concentrations $C_{int,m;i,j}$ in the discrete elements; that is,

$$(\bar{C}_{in}) = \frac{1}{\bar{G}_{CND}} = \sum_{m=1}^{M} \bar{G}_{int,m} C_{int,m;i,j} \dot{G}_{CND}$$

$$= \sum_{m=1}^{M} \bar{G}_{int,m} \quad . \tag{58}$$

The final discharge concentration C_n is a function of the plant contribution C_{CND} and the inlet concentration $(\bar{C}_{in})_{CND}$,

$$C_{dis,m;i,j} = (\bar{C}_{in})_{CND} + C_{CND} \quad . \tag{59}$$

3.4 Formulation of Radionuclide Flux Terms

At this point, it is necessary to eliminate the half-point values of the diffusion flux terms $\bar{G}^{*'}_{w;i \pm 1/2,\ j}$ and $\bar{G}^{*'}_{w;\ i,\ j \pm 1/2}$ in terms of the radionuclide concentration $\bar{C}_{r,w;i,j}$ in the discrete elements. This will require careful consideration of the turbulence phenomena that exists in the receiving water bodies. A detailed theoretical development of an accurate horizontal diffusion model will not be included in this study. The formulation of the radionuclide flux terms will be based on a cubic profile for spatial averaging of radionuclide concentration with respect to depth, and a Blasius [19] power law form for the velocity profile.

The molecular diffusion fluxes, $\bar{G}_{w,m,x;i \pm 1/2,\ j}$ and $\bar{G}_{w,m,y;i,\ j \pm 1/2}$ will be formulated according to the Fourier conduction law,

$$\bar{G}_{w,m,x,i\pm 1/2,j} = -K\left[\frac{\partial \bar{C}_{r,w}}{\partial x}\right]_{i\pm 1/2,j}$$

$$\bar{G}_{w,m,y,i,j+1/2} = -K\left[\frac{\partial \bar{C}_{r,w}}{\partial y}\right]_{i,j\pm 1/2}, \tag{60}$$

where K in this case represents the molecular diffusivity coefficient for the radionuclide under consideration.

Considering the dimensions of the adjacent discrete elements, the derivatives in Equation (60) can be approximated in their finite forms:

$$\bar{G}_{w,m,x,i-1/2,j} = -\frac{2K}{[\Delta x_{i,j} + \Delta x_{i-1,j}]}\left[\bar{C}_{r,w,i,j} - \bar{C}_{r,w,i-1,j}\right],$$

$$\bar{G}_{w,m,x,i+1/2,j} = -\frac{2K}{[\Delta x_{i,j} + \Delta x_{i+1,j}]}\left[\bar{C}_{r,w,i,j} - \bar{C}_{r,w,i+1,j}\right],$$

$$\bar{G}_{w,m,y,i,j-1/2} = -\frac{2K}{[\Delta y_{i,j} + \Delta y_{i,j-1}]}\left[\bar{C}_{r,w,i,j} - \bar{C}_{r,w,i,j-1}\right],$$

$$\bar{G}_{w,m,y,i,j+1/2} = -\frac{2K}{[\Delta y_{i,j} + \Delta y_{i,j+1}]}\left[\bar{C}_{r,w,i,j} - \bar{C}_{r,w,i,j+1}\right]. \tag{61}$$

The molecular diffusion coefficient has to be determined from experimental data. In general, it will not be important, since the magnitude of the molecular diffusion flux terms is small compared to the turbulent diffusion. Only in extreme slack conditions for tidal flow will its determination become important.

Since this study is considering a continuous discharge of radionuclide mass, it does not belong to the class of dispersion problems. The virtual coefficients of horizontal diffusion, derived by Taylor [3] and Elder [20] are based on strict mathematical assumptions for the integration of conservation of mass equation along the vertical direction. These assumptions are valid only for behavior of initial, instantaneous release types of concentrations in a Lagrangian frame of reference. For the present system, which is strictly Eulerian and considers a continuous discharge, the assumptions of the dispersion studies do not apply.

Also, since the present model considers fully transient tidal flow conditions in the convection terms, oceanic diffusion coefficients such as those considered by Wada [21], and Okubo [22] cannot be employed.

Considering the relatively shallow water conditions in oceans and rivers, it is physically realistic to assume that the fundamental mechanism of turbulent diffusion is based on the turbulent eddies associated with the vertical distributions of the turbulent velocity profile.

To simplify the following arithmetic operations, the subscripts and superscripts of Equation (32) will be discarded. The derivation for the radionuclide mass flux terms will be given only in the x

direction, since the derivation will be identical for the y direction,

$$\overline{G}'^{*}_{w,x} = \frac{1}{D}\int_0^{\bar{\delta}} \overline{C}^{*}_{r,w}\,\bar{u}^{*}\,dz + \frac{1}{D}\int_0^{\bar{D}} \overline{C'_{r,w}\,u'}\,dz \tag{62}$$

$$\overline{G}'^{*}_{w,y} = \frac{1}{D}\int_0^{\bar{D}} \overline{C}^{*}_{r,w}\,\bar{V}^{*}\,dz + \frac{1}{D}\int_0^{\bar{\delta}} \overline{C'_{r,w}\,V'}\,dz$$

Considering the terms separately for the x direction,

$$(\overline{G}'^{*}_{w,x})_1 = \frac{1}{D}\int_0^{\bar{D}} \overline{C}^{*}_{r,w}\,\bar{u}^{*}\,dz\ , \tag{63}$$

$$(\overline{G}'_{w,x})_2 = \frac{1}{D}\int_0^{\bar{D}} C'_{r,w}\,u'\,dz\ ,$$

such that

$$\overline{G}'^{*}_{w,x} = (\overline{G}'^{*}_{w,x})_1 + (\overline{G}'_{w,x})_2\ . \tag{64}$$

The mean time averaged velocity difference profile can be derived from the standard equation for turbulent pipe flow, from Goldstein [19],

$$\frac{U}{U_\tau} = C\left(\frac{y U_\tau}{\nu}\right)^m , \tag{65}$$

where C is a constant of proportionality.

Assuming the same form of the power law with respect to depth and replacing m with m = 1/n,

$$\frac{U}{U_\tau} = C\left(\frac{U_\tau}{\nu} z\right)^{1/n}, \tag{66}$$

at the surface z = D and U = U_s, hence substituting into Equation (66) results in;

$$\frac{U_s}{U_\tau} = C\left(\frac{U_\tau}{\nu} D\right)^{1/n}. \tag{67}$$

Dividing Equation (67) into Equation (66) results in Equation (68),

$$\frac{U}{U_s} = \left(\frac{z}{D}\right)^{1/n} , \tag{68}$$

which is the standard Blasius power law form.

Considering the mean velocity form,

$$\frac{U_m}{U_s} = \frac{1}{D}\int_0^D \left(\frac{z}{D}\right) dz = R\int_0^1 \eta^{1/n}\, d\eta = \frac{n}{n+1} , \tag{69}$$

and integrating Equation (69) results in,

$$U_m = \left(\frac{n}{n+1}\right) U_s \quad . \tag{70}$$

Substituting Equation (70) into Equation (68),

$$U = \left(\frac{n+1}{n}\right) U_m \left(\frac{Z}{D}\right)^{1/n}, \tag{71}$$

and letting $\eta = \frac{D-Z}{D}$,

$$U = \left(\frac{n+1}{n}\right) U_m \left(1-\eta\right)^{1/n} . \tag{72}$$

This expression can also be formed in terms of $\bar{U}$ and $\bar{u}^*$,

$$U = \bar{U} + \bar{u}^* = \bar{U} + \bar{U}\left[\left(\frac{n+1}{n}\right)\left(1-\eta\right)^{1/n} - 1\right], \tag{73}$$

such that

$$\bar{u}^* = \left[\left(\frac{n+1}{n}\right)\left(1-\eta\right)^{1/n} - 1\right] \bar{U} . \tag{74}$$

The variation of radionuclide mass with respect to depth will be represented as a cubic distribution with higher $\frac{\Delta C^*_{r,w}}{2}$ on the surface,

$$C_{r,w} = \bar{C}_{r,w} + \overline{\Delta C^*_{r,w}}\left[1 - 2\left(3\eta^2 - 2\eta^3\right)\right], \tag{75}$$

where the second term represents, $C^*_{r,W}$ as,

$$\bar{C}^*_{r,w} = \frac{\overline{\Delta C^*_{r,w}}}{2}\left[1-2(3\eta^2-2\eta^3)\right]. \tag{76}$$

Hence, the convection-defect transport rate of radionuclide mass $\bar{G}'^*_{W,X}$ across a surface normal to the x direction becomes,

$$\bar{G}'^*_{w,x} = \iint_A \bar{u}^* \bar{C}^*_{r,w}\, dA$$

$$= \Delta y \int_0^D \bar{U}\left[\left(\frac{n+1}{n}\right)(1-\eta)^{1/n}-1\right]\frac{\overline{\Delta C^*_{r,w}}}{2}\left[1-2(3\eta^2-2\eta^3)\right] dz. \tag{77}$$

Separating the integrals,

$$\bar{G}'^*_{w,x} = (\Delta y\, \bar{D}\, \frac{\overline{\Delta C^*_{r,w}}}{2}\, \bar{U})\left[\left(\frac{n+1}{n}\right)\int_0^1 (1-\eta)^{1/n}\, d\eta\right.$$

$$-2\left(\frac{n+1}{n}\right)\int_0^1 (1-\eta)^{1/n}(3\eta^2-2\eta^3)\, d\eta \tag{78}$$

$$\left.-\int_0^1 d\eta + 2\int_0^1 (3\eta^2-2\eta^3)\, d\eta\right].$$

Evaluating the integrals separately,

$$I_1 = \int_0 (1-\xi)^{1/n} \, d\xi = \left(\frac{n}{n+1}\right), \tag{79}$$

$$I_2 = \int_0^1 (1-\xi)^{1/n} (3\xi^2 - 2\xi^3) \, d\xi = \frac{6n^3}{(n+1)(3n+1)(4n+1)}, \tag{80}$$

$$I_3 = \int_0^1 d\xi = 1, \tag{81}$$

$$I_4 = \int_0^1 (3\xi^2 - 2\xi^3) \, d\xi = 1 - 1/2 = 1/2, \tag{82}$$

and substituting Equations (79) to (82) into Equation (78) results in,

$$\bar{G}'^{*}_{w,x} = (\Delta y \, \bar{D} \, \frac{\Delta \bar{C}^{*}_{r,w}}{2} \, \bar{U}) \tag{83}$$

$$\left[\left(\frac{n+1}{n}\right)\left(\frac{n}{n+1}\right) - 2\left(\frac{n+1}{n}\right)\frac{6n^3}{(n+1)(3n+1)(4n+1)} - 1 + 2(1/2)\right].$$

Cancelling the proper terms and rearranging results in the final form for the convection-defect transport rate of radionuclide mass perpendicular to the x direction,

$$\bar{G}'^{*}_{w,x} = 1/2\left[1 - \frac{12n^2}{(3n+1)(4n+1)}\right](\Delta y \, \bar{D} \, \Delta \bar{C}^{*}_{r,w} \, \bar{U}). \tag{84}$$

Employing the same procedure for the y direction results in,

$$\bar{G}'^{*}_{w,x} = \tfrac{1}{2}\left[1 - \frac{12n^2}{(3n+1)(4n+1)}\right](\Delta x \bar{D} \Delta \bar{C}^{*}_{r,w} \bar{V}) . \qquad (85)$$

The previous two equations for the convection-defect transport flux exhibit two very important properties:

a. Nonuniform radionuclide and velocity distributions in the vertical direction contribute to the horizontal transport fluxes. However, if sufficient vertical mixing exists in the region, the $\bar{C}^{*}_{r,w}$ term will approach zero, negating the contribution of the convection-defect.

b. The transport flux contribution of the vertically nonuniform radionuclide concentration profile cannot be considered as a truly diffusion type of phenomenon, since in general it does not conform to Fourier and Boussinesq type formulations.

The second part of Equation (64), $(\bar{G}'_{w,x})$ and $(\bar{G}'_{w,y})$, represent the true turbulent diffusion phenomenon due to micro-scale random turbulent eddies. Hence, they can be represented in Boussinesq forms as:

$$\overline{C'_{w,x} u'} = -\mathcal{E}_x \left(\frac{\partial \bar{C}_{r,w}}{\partial x} + \frac{\partial \bar{C}^{*}_{r,w}}{\partial x}\right),$$

$$\overline{C'_{w,y} V'} = -\mathcal{E}_y \left(\frac{\partial \bar{C}_{r,w}}{\partial y} + \frac{\partial \bar{C}^{*}_{r,w}}{\partial y}\right), \qquad (86)$$

where ε_x and ε_y represent the turbulent eddy diffusivities along the x and y directions respectively. Assuming that isotropic turbulence is valid for shallow regions,

$$\mathcal{E}_x = \mathcal{E}_y = \mathcal{E}_z = \mathcal{E} \quad , \tag{87}$$

where ε_z represents the vertical eddy diffusivity,

$$U_\tau = \left(\frac{1}{C}\right)^{\frac{n}{n+1}} \left(\frac{\nu}{D}\right)^{\frac{1}{n+1}} U_s^{\frac{n}{n+1}} \quad . \tag{88}$$

The friction velocity U_τ is defined in terms of the bottom shear stress as,

$$\tau_b = \rho U_\tau^2 \quad . \tag{89}$$

If the assumption is made that the shear stress varies linearly from the bottom to the surface, the shear stress can be represented by Equation (90),

$$\tau = \tau_b \left(1 - \frac{z}{D}\right) . \tag{90}$$

Substituting Equation (88) into Equation (89) and then substituting the resulting equation into Equation (90) results in,

$$\tau = \left(\frac{1}{C}\right)^{\frac{2n}{n+1}} \rho \left(\frac{\nu}{D}\right)^{\frac{2}{n+1}} U_s^{\frac{2n}{n+1}} \left(1 - \frac{z}{D}\right) . \tag{91}$$

Considering the Reynolds (23) analogy that the turbulent eddy diffusivities are identical for momentum as well as any constituent in

water, the particular diffusion transport is solely due to the turbulent eddy phenomenon,

$$\mathcal{E} = \frac{\tau}{\partial U/\partial Z} \quad . \tag{92}$$

From the standard power law form,

$$\frac{\partial U}{\partial Z} = \frac{1}{n} \frac{U_b}{D} \left(\frac{z}{D}\right)^{\frac{1-n}{n}} \quad . \tag{93}$$

Hence, substituting Equations (93) and (91) in Equation (92) and rearranging,

$$\mathcal{E} = n \left(\frac{1}{c}\right)^{\frac{2n}{n+1}} \nu^{\frac{2}{n+1}} D^{\frac{n-1}{n+1}} U_s^{\frac{n-1}{n+1}} \left(1 - \frac{z}{D}\right)\left(\frac{z}{D}\right)^{\frac{n-1}{n}} . \tag{94}$$

Letting the dimensionless variable η and the parameter β be defined as,

$$\eta = \frac{D-z}{D} \quad \text{and} \quad \beta = 1/c \,, \tag{95}$$

and substituting into Equation (94) results in the final form of the eddy diffusivity term,

$$\mathcal{E} = n \beta^{\frac{2n}{n+1}} \nu^{\frac{2}{n+1}} D^{\frac{n-1}{n+1}} U_s^{\frac{n-1}{n+1}} \eta (1-\eta)^{\frac{n-1}{n}} . \tag{96}$$

The cubic variation of radionuclides with respect to depth can again be represented by Equation (75) from the previous formulation. Taking the derivative of Equation (75) with respect to x results in,

$$\frac{\partial C_{r,w}}{\partial X} = \frac{\partial \bar{C}_{r,w}}{\partial X} + \frac{1}{2}\frac{\partial}{\partial X}\left(\Delta \bar{C}^{*}_{r,w}\right)\left[1-2\left(3\zeta^{2}-2\zeta^{3}\right)\right]$$

$$-\overline{\Delta C}^{*}_{r,w}\frac{\partial}{\partial X}\left(3\zeta^{2}-2\zeta^{3}\right). \qquad (97)$$

Rearranging the terms on the far right hand side of Equation (97) results in,

$$\frac{\partial C_{r,w}}{\partial X} = \frac{\partial \bar{C}_{r,w}}{\partial X} + \frac{1}{2}\frac{\partial}{\partial X}\left(\Delta \bar{C}^{*}_{r,w}\right)\left[1-2\left(3\zeta^{2}-2\zeta^{3}\right)\right]$$

$$+6\overline{\Delta C}^{*}_{r,w}\left(\zeta^{3}-\zeta^{2}\right)\frac{1}{D}\frac{\partial D}{\partial X}. \qquad (98)$$

The last term in Equation (99) represents the variation of the surface elevation with respect to depth, i.e.,

$$\frac{1}{D}\frac{\partial D}{\partial X} = \frac{1}{D}\frac{\partial h}{\partial X} \cong 0 \quad . \qquad (99)$$

For flow conditions in a region where the tidal wave is not extremely high, the last term in Equation (92) is negligible, particularly for coastal regions, hence,

$$\frac{\partial C_{r,w}}{\partial X} = \frac{\partial \bar{C}_{r,w}}{\partial X} + \frac{1}{2}\frac{\partial}{\partial X}(\Delta \bar{C}^{*}_{r,w})\left[1 - 2(3\eta^{2} - 2\eta^{3})\right] . \qquad (100)$$

Considering the turbulent transport rate across a surface normal to the x-direction,

$$\bar{G}'_{w,x} = -\iint_{A} \bar{q}'_{w,x}\, dA = \Delta y \int_{0}^{D} -\varepsilon \frac{\partial C_{r,w}}{\partial X}\, dz$$

(101)

$$= -\Delta y\, D \int_{0}^{1} \varepsilon \frac{\partial C_{r,w}}{\partial X}\, d\eta ,$$

Substituting Equations (96) and (100) into Equation (101) and integrating,

$$\bar{G}'_{w,x} = n\beta^{\frac{2n}{n+1}} \nu^{\frac{2}{n+1}} \Delta y\, D^{\frac{2n}{n+1}} U_{s}^{\frac{n-1}{n+1}}$$

(102)

$$\left[\frac{\partial \bar{C}_{r,w}}{\partial X} E_{1} + \frac{1}{2}\frac{\partial}{\partial X}(\Delta \bar{C}^{*}_{r,w})\, E_{2}\right] ,$$

where

$$E_{1} = \int_{0}^{1} \eta (1-\eta)^{\frac{n-1}{n}}\, d\eta , \qquad (103)$$

and

$$E_2 = \int_0^1 \eta (1-\eta)^{\frac{n-1}{n+1}} [1 - 2(3\eta^2 - 2\eta^3)] \, d\eta ,$$

$$E_2 = \int_0^1 \eta (1-\eta)^{\frac{n-1}{n+1}} d\eta - 2\int_0^1 \eta (1-\eta)^{\frac{n-1}{n+1}} (3\eta^2 - 2\eta^3) \, d\eta . \tag{104}$$

Integrating Equation (103),

$$E_1 = \frac{n^2}{(2n-1)(3n-1)} . \tag{105}$$

Hence, from Equation (102) and employing the results of Equation (105),

$$E_2 = E_1 - I_2 , \tag{106}$$

where,

$$I_2 = \int_0^1 \eta (1-\eta)^{\frac{n-1}{n+1}} (3\eta^2 - 2\eta^3) \, d\eta . \tag{107}$$

Integrating Equation (107),

$$I_2 = \frac{6n^4(10n-3)}{(2n-1)(3n-1)(4n-1)(5n-1)(6n-1)} . \tag{108}$$

Hence, substituting the results from Equations (108) and (105) into Equation (102), the turbulent transport rate $\bar{G}'_{W,X}$ becomes,

$$\bar{G}'_{w,x} = n\beta^{\frac{2n}{n+1}} \nu^{\frac{2}{n+1}} \Delta y D^{\frac{2n}{n+1}} U_s^{\frac{n-1}{n+1}}$$

(109)

$$\left[E_1 \frac{\partial \bar{C}_{r,w}}{\partial x} + \left(\frac{E_1}{2} - I_2\right) \frac{\partial}{\partial x} \left(\Delta \bar{C}^*_{r,w}\right)\right] .$$

For considering depth averaged flow rates, it is more practical to utilize the mean velocity in place of the surface velocity. Hence, substituting Equation (70) into Equation (109),

$$\bar{G}'_{w,x} = n\beta^{\frac{2n}{n+1}} \nu^{\frac{2}{n+1}} \Delta y D^{\frac{2n}{n+1}} \left(\frac{n+1}{n}\right)^{\frac{n-1}{n+1}} U_m^{\frac{n-1}{n+1}}$$

(110)

$$\left[E_1 \frac{\partial \bar{C}_{r,w}}{\partial x} + \left(\frac{E_1}{2} - I_2\right) \frac{\partial}{\partial x} \left(\Delta \bar{C}^*_{r,w}\right)\right] .$$

To make the derivation less cumbersome, the terms for the coefficients of the gradient terms will be combined by using Equations (105) and (108),

$$\bar{G}'_{w,x} = -\bar{E}'_1 \frac{\partial \bar{C}_{r,w}}{\partial x} - \bar{E}'_2 \frac{\partial}{\partial x} \left(\Delta \bar{C}^*_{r,w}\right) , \tag{111}$$

where

$$\bar{E}'_1 = \frac{n^3}{(2n-1)(3n-1)} \left(\frac{n+1}{n}\right)^{\frac{n-1}{n+1}}$$

(112)

$$\beta^{\frac{2n}{n+1}} \nu^{\frac{2}{n+1}} D^{\frac{n-1}{n+1}} U_m^{\frac{n-1}{n+1}} (\Delta y D) .$$

Rearranging the kinematic viscosity term in Equation (112),

$$\bar{E}_1' = \left[\frac{n^3}{(2n-1)(3n-1)} \left(\frac{n+1}{n}\right)^{\frac{n-1}{n+1}} \beta^{\frac{2n}{n+1}} \left(\frac{DU_m}{\nu}\right)^{\frac{n-1}{n+2}} \right] \tag{113}$$

$$(\nu \Delta y D),$$

and

$$\bar{E}_2' = n\beta^{\frac{2n}{n+1}} \nu^{\frac{2}{n+1}} \Delta y D^{\frac{2n}{n+1}} \left(\frac{n+1}{n}\right)^{\frac{n-1}{n+1}} U_m^{\frac{n-1}{n+2}} \tag{114}$$

$$\left[\frac{1}{2} \frac{n^2}{(2n-1)(3n-1)} - \frac{6n^4(10n-3)}{(2n-1)(3n-1)(4n-1)(5n-1)(6n-1)}\right],$$

$$\bar{E}_2' = \frac{n^3 \beta^{\frac{2n}{n+1}}}{2(2n-1)(3n-1)} \left(\frac{n+1}{n}\right)^{\frac{n-1}{n+1}} \left[1 - \frac{12n^2(10n-3)}{(4n-1)(5n-1)(6n-1)}\right] \tag{115}$$

$$\left(\frac{U_m \bar{D}}{\nu}\right)^{\frac{n-1}{n+1}} (\nu \Delta y \bar{D}),$$

the final form for the turbulent diffusion rate can be stated as,

$$\bar{G}_{w,x}' = -\bar{E}' \frac{\partial \bar{C}_{r,w}}{\partial x} - \bar{E}_2' \frac{\partial}{\partial x} (\Delta \bar{C}_{r,w}^*). \tag{116}$$

Substitute y for x into Equation (116) to obtain the turbulent diffusion rate in the y direction.

Substituting Equation (116) and Equations (84) and (85) into Equation (64), the combined net turbulent non-convective radionuclide mass transport rate becomes,

$$\bar{G}'^{*}_{w,x} = \tfrac{1}{2}\left[1 - \frac{12n^2}{(3n+1)(4n+1)}\right](\Delta y \bar{D}\, \Delta \bar{C}^{*}_{r,w}\, \bar{U}) \qquad (117)$$

$$-\bar{E}_1' \frac{\partial \bar{C}_{r,w}}{\partial x} - \bar{E}_2' \frac{\partial}{\partial x}(\Delta \bar{C}^{*}_{r,w}).$$

Defining the parts which contain the stratified radionuclide mass concentration difference $\bar{C}^{*}_{r,w}$ as the change in radionuclide concentration due to stratification effects,

$$G_{w,s,x} = \tfrac{1}{2}\left[1 - \frac{12n^2}{(3n+1)(4n+1)}\right](\Delta y \bar{D}\, \Delta \bar{C}^{*}_{r,w}\, \bar{U}) \qquad (118)$$

$$-\bar{E}_2' \frac{\partial}{\partial x}(\Delta \bar{C}^{*}_{r,w}).$$

Substituting Equation (118) into Equation (117),

$$\bar{G}'^{*}_{w,x} = -\bar{E}' \frac{\partial \bar{C}_{r,w}}{\partial x} + G_{w,s,x}. \qquad (119)$$

The last part of the formulation for the non-convective radionuclide mass transport rate, will show both the x and y components.

Evaluating the right-hand side of Equation (119) to obtain the half-point values according to Equation (38),

$$(\bar{G}'^{*}_{w,x})_{i\pm 1/2,j} = -[E'_1]_{i\pm 1/2,j}\left[\frac{\partial \bar{C}_{r,w}}{\partial X}\right]_{i\pm 1/2,j} + [G_{w,s}]_{i\pm 1/2,j}\,, \tag{120}$$

$$(\bar{G}'^{*}_{w,x})_{i,j\pm 1/2} = -[E'_1]_{i,j\pm 1/2}\left[\frac{\partial \bar{C}_{r,w}}{\partial Y}\right]_{i,j\pm 1/2} + [G_{w,s}]_{i,j\pm 1/2}\,.$$

Considering the dimensions of the adjacent discrete elements, the derivatives in Equation (120) can be approximated by their finite form as:

$$\bar{G}'^{*}_{w,x;i-1/2,j} = -2E'_{i,i-1/2,j}\left[\frac{[\bar{C}_{r,w;i,j} - \bar{C}_{r,w;i-1,j}]}{[\Delta X_{i,j} + \Delta X_{i-1,j}]}\right] + [G_{w,s}]_{i-1/2,j}\,,$$

$$\bar{G}'^{*}_{w,x;i+1/2,j} = -2E'_{i,i+1/2,j}\left[\frac{[\bar{C}_{r,w;i+1,j} - \bar{C}_{r,w;i,j}]}{[\Delta X_{i,j} + \Delta X_{i+1,j}]}\right] + [G_{w,s}]_{i+1/2,j}\,,$$

$$\bar{G}'^{*}_{w,y;i,j-1/2} = -2E'_{i,i,j-1/2}\left[\frac{[\bar{C}_{r,w;i,j} - \bar{C}_{r,w;i,j-1}]}{[\Delta Y_{i,j} + \Delta Y_{i,j-1}]}\right] + [G_{w,s}]_{i,j-1/2}\,,$$

$$\bar{G}^{\prime *}_{w_i x_j i_1 j+1/2} = -2 E'_{i_1 i_1 j+1/2} \frac{[\bar{C}_{r_1 w_j i_1 i+1} - \bar{C}_{r_1 w_j i_1 j}]}{[\Delta y_{i_1 j} + \Delta y_{i_1 j+1}]} + [G_{w_i s}]_{i_1 j+1/2} \cdot \quad (121)$$

The molecular and turbulent transport flux terms from Equations (61) and (121) can be combined according to Equation (38) in terms of equivalent diffusion coefficients $\bar{\varepsilon}_{i \pm 1/2,\, j}$ and $\bar{\varepsilon}_{i,\, j \pm 1/2}$ to obtain the net diffusion transport flux terms on the discrete element surfaces as:

$$\bar{G}_{w_i x_j i-1/2, j} = -2 \varepsilon_{i-1/2, j} \frac{[\bar{C}_{r_1 w_j i_1 j} - \bar{C}_{r_1 w_j i-1 j}]}{[\Delta x_{i_1 j} + \Delta x_{i-1 j}]} + [G_{w_i s}]_{i-1/2, j} \,,$$

$$\bar{G}_{w_i x_j i+1/2, j} = -2 \varepsilon_{i+1/2, j} \frac{[\bar{C}_{r_1 w_j i+1 j} - \bar{C}_{r_1 w_j i_1 j}]}{[\Delta x_{i_1 j} + \Delta x_{i+1 j}]} + [G_{w_i s}]_{i+1/2, j} \,,$$

$$\bar{G}_{w_i y_j i_1 j-1/2} = -2 \varepsilon_{i_1 j-1/2} \frac{[\bar{C}_{r_1 w_j i_1 j} - \bar{C}_{r_1 w_j i_1 j-1}]}{[\Delta y_{i_1 j} + \Delta y_{i_1 j-1}]} + [G_{w_i s}]_{i_1 j-1/2} \,,$$

$$\bar{G}_{w_i y_j i_1 j+1/2} = -2 \varepsilon_{i_1 j+1/2} \frac{[\bar{C}_{r_1 w_j i_1 j+1} - \bar{C}_{r_1 w_j i_1 j}]}{[\Delta y_{i_1 j} + \Delta y_{i_1 j+1}]} + [G_{w_i s}]_{i_1 j+1/2} \cdot \quad (122)$$

where the equivalent-diffusion coefficients are defined as:

$$\bar{\varepsilon}_{i\pm 1/2,j} = K + [E_1]_{i\pm 1/2,j} \quad ,$$

$$\bar{\varepsilon}_{i,j\pm 1/2} = K + [E_1]_{i,j\pm 1/2} \quad . \tag{123}$$

From mathematical considerations, Equations (122) and (123) complete the elimination of the half-point values of the diffusion flux terms $\bar{G}_{w,x;i \pm 1/2,\ j}$ and $\bar{G}_{w,y;\ i,\ j \pm 1/2}$ in terms of the principal unknown values of radionuclide mass concentration $C_{r,w;i \pm 1,\ j}$, $\bar{C}_{r,w;\ i,j}$, $\bar{C}_{r,w;\ i,\ j \pm 1}$ in the discrete elements. Hence, the Discrete-Element system of first-order differential equations, Equation (39) or (44), become consistent.

3.5 Approximate Formulation of the Exchange of Radionuclides Between the Water and Bottom Layers

To complete the mathematical simulation of radionuclide transport in the water and bottom layers, an approximate formulation of mass transport of radionuclides between the dissolved/adsorbed state in water and the adsorbed state in the bottom layer is included in the formulation. This mass transport is represented by the simple exchange model in Equation (124),

$$\bar{q}_{r,w,b} = -\gamma_j \bar{v}_j \bar{C}_{r,w} + \gamma_\tau \bar{v}_\tau \bar{C}_{r,b} + \gamma_\varepsilon \frac{\bar{\varepsilon}_b}{\bar{D}} (\bar{C}_{r,b} - \bar{C}_{r,w}) . \quad (124)$$

where:

γ_j = specified constant associated with the settling of the sediment,

$\bar{v}_j$ = specified fall velocity,

γ_τ = specified constant associated with re-suspension due to friction,

$\bar{v}_\tau$ = bottom friction velocity,

γ_ε = specified constant associated with the turbulent eddy transport effects in the vertical direction,

$\bar{\varepsilon}_b$ = mean turbulent eddy diffusivity over depth.

The mathematical terms on the right-hand side of Equation (124) can be grouped into three parts representing the two types of phenomena used to describe the mass transport of radionuclides between the dissolved/adsorbed state in water and the adsorbed state in the bottom layer.

Convection Effect of Vertical Fall Velocity on the Radionuclide Concentration in Water

$$F_{c,w} = -\gamma_j \bar{v}_j \bar{C}_{r,w} \quad (125)$$

The term $\bar{v}_j$ represents a specified fall velocity for the particular radionuclide being studied. This fall velocity is obtained from experimental data along with the constant γ_j.

Convection Effect of Resuspension of Radionuclides in the Adsorbed State in the Bottom Layer

$$F_{cb} = \gamma_{\tau} \bar{v}_{\tau,b} \bar{C}_{r,b} \tag{126}$$

The concentration of radionuclides in the adsorbed state in the bottom layer is represented in dimensionless concentration form as,

$$C_{r,b} = \frac{\rho_{r,b}}{\rho_{ref}} \quad . \tag{127}$$

The term γ_{τ} is an experimentally specified constant associated with resuspension due to friction. The bottom friction velocity, $\bar{v}_{\tau,b}$, can be derived from the shear stress at the bottom first shown in Equation (89). Substituting the form for the friction velocity shown in Equation (88) and employing Equation (95) results in the form for the shear stress at the bottom in Equation (128),

$$\tau_b = \rho \beta^{\frac{2n}{n+1}} \left(\frac{\nu}{D}\right)^{\frac{2}{n+1}} U_s^{\frac{2n}{n+1}} \quad . \tag{128}$$

Using the form of the mean velocity, Equation (70), and substituting into Equation (128),

$$\tilde{\tau}_b = \left(\frac{n+1}{n}\right)^{\frac{2n}{n+1}} \beta^{\frac{2n}{n+1}} \rho \left(\frac{\nu}{\bar{D}}\right)^{\frac{2}{n+1}} \bar{U}_m^{\frac{2n}{n+1}} . \tag{129}$$

Defining the bottom friction velocity as $v_{\tau,b} = \sqrt{\tau_b/\rho}$ and substituting Equation (129) the form for the bottom friction velocity is obtained,

$$v_{\tilde{\tau},b} = \left(\frac{n+1}{n}\right)^{\frac{2n}{n+1}} \beta \left(\frac{\nu}{\bar{D}}\right)^{\frac{2}{n+1}} \bar{U}_m^{\frac{2n}{n+1}} . \tag{130}$$

Factoring out $\nu/\bar{D}$ to make the expression dimensionally simpler, the final form of the bottom friction velocity is,

$$v_{\tilde{\tau},b} = \left[\left(\frac{n+1}{n}\right)^{\frac{n}{n+1}} \beta^{\frac{n}{n+1}}\right] R_e^{\frac{n}{n+1}} \left(\frac{\nu}{\bar{D}}\right) , \tag{131}$$

where R_e represents the Reynolds number based on the depth of the bottom layer.

Diffusion Effect of Depth Averaged Turbulent Transport Phenomena

$$F_{tb} = \gamma_\varepsilon \frac{\bar{\varepsilon}_b}{\bar{D}} \left(\bar{C}_{r,b} - \bar{C}_{r,w}\right) \tag{132}$$

where γ_ε represents an experimentally determined constant associated with the turbulent eddy transport effects in the vertical direction, and $\bar{\varepsilon}_b$ is the mean turbulent eddy diffusivity over depth. The

derivation of the eddy diffusivity term ε_b is similar to the derivation of the eddy diffusivity terms shown in Section 3.4, but the derivation will be shown for the sake of completeness assuming the form for the turbulent eddy diffusivity shown previously in Equation (96),

$$\mathcal{E}_b = n\beta^{\frac{2n}{n+1}} \nu^{\frac{2}{n+1}} D^{\frac{n-1}{n+1}} U_s^{\frac{n-1}{n+1}} \eta(1-\eta)^{\frac{n-1}{n}}, \tag{133}$$

and considering the integral from Equation (103) and integrating,

$$E_1 = \int_0^1 \eta(1-\eta)^{\frac{n-1}{n}} d\eta = \frac{n^2}{(2n-1)(3n-1)}. \tag{134}$$

Substituting Equation (134) and the form for the mean velocity, Equation (70), into Equation (133), the form for the mean turbulent eddy diffusivity over depth is,

$$\bar{\mathcal{E}}_b = \frac{n^3}{(2n-1)(3n-1)} \left(\frac{n+1}{n}\right)^{\frac{n-1}{n+1}} \beta^{\frac{2n}{n+1}} \nu^{\frac{2}{n+1}} \bar{D}^{\frac{n-1}{n+1}} \bar{U}_m^{\frac{n-1}{n+1}}. \tag{135}$$

Factoring out v to make the expression dimensionally simpler, and employing the Reynolds form results in the final form of the mean turbulent eddy diffusivity over depth, Equation (136),

$$\bar{\mathcal{E}}_b = \left[\frac{n^3 \beta^{\frac{2n}{n+1}}}{(2n-1)(3n-1)} \left(\frac{n+1}{n}\right)^{\frac{n-1}{n+1}}\right] R_e^{\frac{n-1}{n+1}}. \tag{136}$$

This completes the approximate formulation of the mass transport of radionuclides between the dissolved/adsorbed state in water and the adsorbed state in the bottom layer.

4. APPLICATION OF THE MATHEMATICAL RADIONUCLIDE TRANSPORT MODEL TO A SITE SPECIFIC CASE

4.1 Description of the Coastal Region and San Onofre Nuclear Generating Station

The San Onofre Nuclear Generating Station (SONGS) was selected as a test case because of its location in a typical tidal dominated open region. The flow conditions in the region and the set-up of the computational grid representation of the SONGS region are described.

Currents in the San Onofre region are influenced by three major factors; wind, tide and local topography. The major current in this area is the California current which is a continuation of the southeast flowing Aleutian current of the North Pacific. This current extends approximately 420 miles offshore and moves along the coast.

The dominant circulation pattern in the San Onofre region is up and down the coast, and fluctuates due to seasonal changes. Surface currents average 0.3 ft/sec or less, while subsurface currents, 15 feet or more, are usually less than 0.2 ft/sec. Average high tide elevation for this region is approximately 4.5 feet mean level low water, with a maximum tidal excursion, during a previous 17 year period, of 8.8 feet.

In simulating the currents in the San Onofre region, a general description of the flow phenomena is not sufficient. Regions such as San Onofre can have flow conditions which are unique to their location because of shoreline geometry and bottom conditions. At San Onofre, there is a very sharp drop in the depth of the region 9,000 feet from the shoreline. In a distance of 25,000 feet, the depth drops from

50 feet to 2000 feet. This extreme bottom slope can cause wave motions that will make the flow field unique to the region. Therefore, extreme care must be taken to properly model the flow field.

In modeling the flow field, the amplitude of the tidal height is used to determine the flow magnitudes. The average tidal excursion in the SONGS coastal region was determined to be six feet. This tidal amplitude is input into a small mass balancing computer model which utilizes the geometry from the FLIDE model. Using the tidal periods resulting from the influence of the sun and moon, and inputing a constant drift, a set of velocities is determined that will result in the proper tidal excursion. The y component and x component of velocity are determined separately and then combined to obtain the final flow field that is used in the Discrete-Element model.

The coastal region for the application of the FLIDE model in the SONGS region was represented as approximately 79,000 feet along the coast and 35,000 feet normal to the shoreline. This region is divided into 368 variable sized discrete elements as shown in Figure 4. The grid is set up as a 23 x 16 matrix with a fine mesh existing in the region of the intake and discharge. Of the 368 elements, 35 are external to the flow region and are not used in the solution, 72 of the elements are shoreline boundary or open region boundary and the remaining elements are internal.

The minimum dimensions of the discrete elements were determined according to the geometry of the shoreline and the distance between the intake and discharge of the plant; and the maximum dimensions were

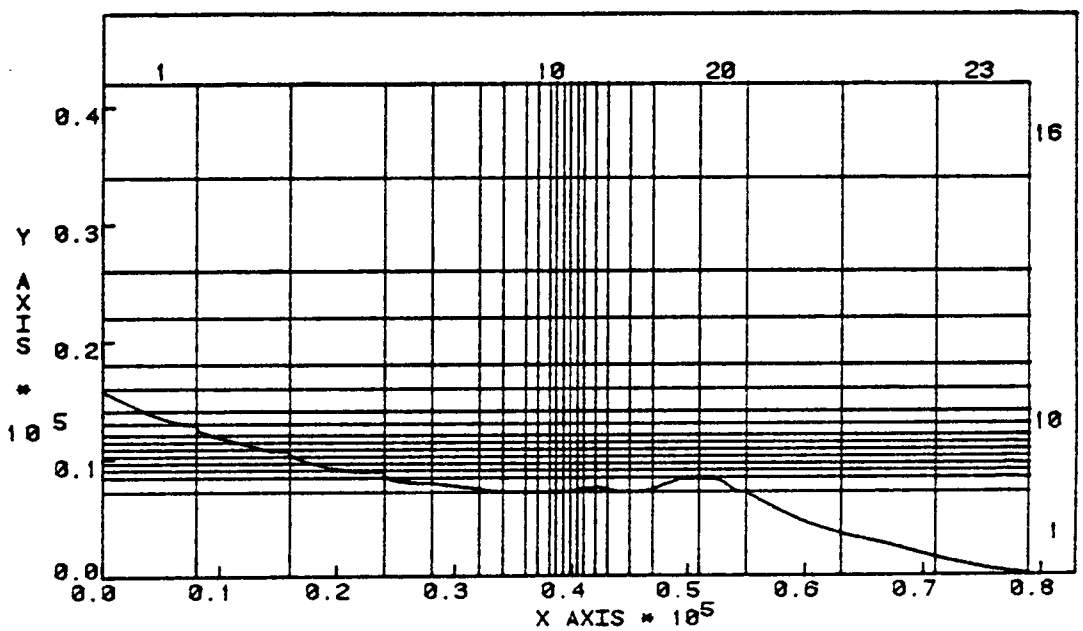


Figure 4. Discrete Element Geometry Representation of the San Onofre Coastal Region.

arbitrarily specified based on the overall dimensions of the modelled coastal region, as:

Δx_{min} = 500 ft, Δy_{min} = 500 ft,

Δx_{max} = 8000 ft, Δy_{max} = 8000 ft.

The depth geometry of the region as modelled in the RADTWO code, is shown in Figure 5. The maximum depth for the water layer is set at 100 feet. A discussion of this maximum depth selection is contained in Section 4.3.

The San Onofre Nuclear Generating Station consists of one 500-MW single nuclear unit with a once-through cooling system using submerged single-port intake and discharge structures.

The intake of the SONGS cooling system is located in the discrete element IX=12, JY=6, the depth in this discrete element at mean level low water (MLLW) is 17 feet. In the discharge discrete-element; IX=12, JY=5 the MLLW depth is 15 feet. The flow rates for the intake and discharge are 3.20×10^6 cubic feet per hour.

4.2 Description of the Accident

The RADTWO [23] computer model is used to simulate a hypothetical accident condition in the San Onofre coastal region. The accident is assumed to occur at 12:00 noon while the plant is operating under normal conditions. During the accident it is assumed that only one radionuclide is released into the coastal region. For the purposes of this accident simulation, the released radionuclide is Cesium 132, which has a half-life of 158.4 hours. The Cesium 132 is input into the accident situation at the plant discharge which is located in

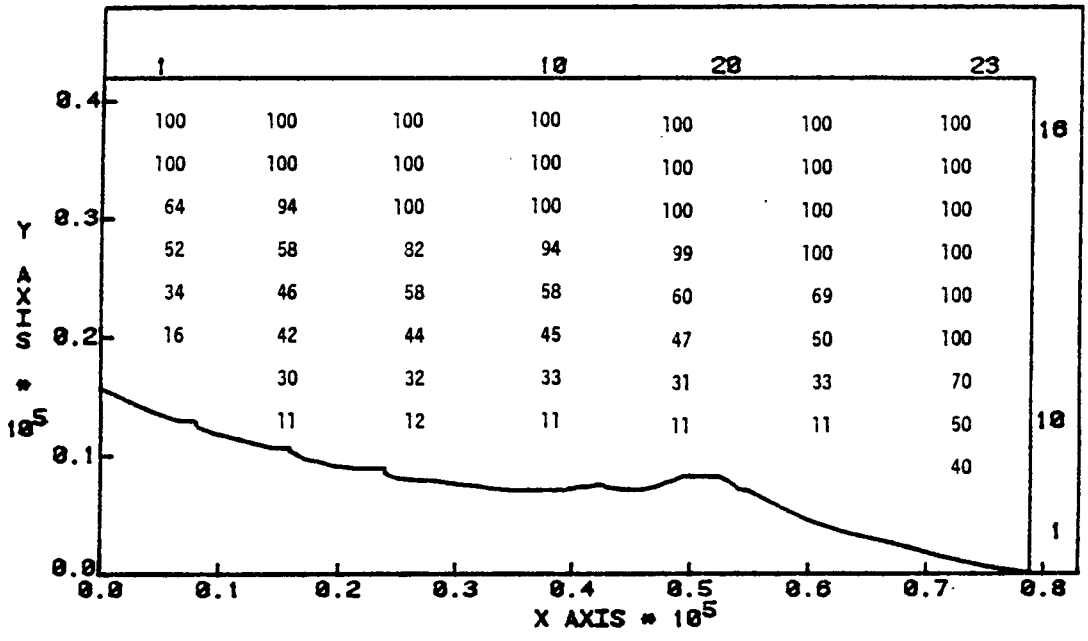


Figure 5. Depth Geometry of the San Onofre Coastal Region as Modeled in the RADTWO Computer Code, All Depths are in Feet.

discrete element IX=12, JY=5. The radionuclide release is formulated in terms of nondimensional units of radioactivity which are applicable to any active element release. During the accident, 100 units of Cesium 132 are released into the plant cooling flow.

The accident situation occurs for one hour before the plant is shut down and releases to the coastal region are stopped. During this time period the flow conditions in the coastal region are at ebb flow, which are the maximum flow velocities away from the shoreline.

4.3 Application of the Computer Model to the Accident Scenario at San Onofre

This section describes the set-up of the RADTWO model for the simulation of the transport of dissolved and adsorbed suspended sediment in the water layer, and dissolved and adsorbed resident sediment in the stationary bottom layer, in the SONGS region.

To accurately represent the impact of a radioactive release into a tidal dominated coastal flow region, the length of the model simulation has to be long enough to either reach equilibrium in the region for a constant release situation or as in the present application, till the combination of convective transport, molecular diffusion and radioactive half-life dilute and decay the radioactive concentration in the region to an insignificant amount. In the present simulation the accident occurs as an initial radioactive release for one hour only. For this case a 144 hour simulation, which represents approximately 12 tidal cycles, is sufficient.

In simulation of the accident condition it is assumed that the dissolved and adsorbed on suspended sediment water layer has a maximum depth of 100 feet. This assumption is particularly realistic and conservative in deep regions over 100 feet since full vertical mixing in depths over 100 feet would be unrealistic. The dissolved and adsorbed, on the resident sediment in the stationary bottom layer, is assumed to have a thickness of one foot.

Considering the shallow depth at the location of the intake, approximately 20 feet at mean level low water conditions, the elevation of the intake opening from the bottom, 10 feet, and the maximum tidal height, 8 feet, it is evident that full vertical mixing is realistic, hence the cooling water to the condensers will enter the intakes at the existing concentration of the dissolved and adsorbed on suspended sediment water layer of the intake discrete element.

The approximate time step size t for the numerical integration of the governing system of equations of the FLIDE model was determined according to already established stability criterion, as in Eraslan [4], based on the generalized form of the "Courant number", Roache [16], and numerical experimentation. The necessary terms for the stability criterion are approximately determined from the minimum size of the discrete elements in the flow region, oceanic flow conditions, and the maximum discharge flow rate.

The concentration distributions for the accident case were obtained from the associated computer code RADTWO of the general two dimensional fast transient FLIDE mathematical far-field radionuclide transport model for coastal regions, lakes and estuaries. The general

computer code was programmed on the PDP: DEC-10 computer system, but it is also compatible with IBM and CDC computer systems.

The numerical results for the transport of dissolved and adsorbed on suspended sediment concentrations in the water layer and dissolved and adsorbed on the resident sediment in the stationary bottom layer are presented as iso-concentration contour plots in figures to follow. Each of these figures is divided into three separate parts. Previous to each figure representing the dissolved and adsorbed on suspended sediment concentration in the water layer and the dissolved and adsorbed resident sediment in the stationary bottom layer, is a figure that represents the velocity field as a velocity vector plot for the given time step.

In figures for the iso-concentrations, the minimum concentration value at each time step corresponds to the outermost iso-concentration in the region. Since the contour values increase logarithmically, the next inner contour value is one order of magnitude greater than the adjacent contour. The subsequent discussion of the results for the assessment of the radionuclide impact of the San Onofre Generating Station during a hypothetical accident scenario will be based on the iso-concentration contour plots and the velocity vector plots.

4.4 Discussion of Computer Simulation Results

All the concentrations presented in this section, whether in the dissolved and adsorbed on suspended sediment in the water layer or the dissolved and adsorbed on the resident sediment in the stationary bottom layer are represented by contour plots. Each contour line,

both for water and bottom layer concentrations, is presented in logarithmic value contours. The innermost contour in each contour plot represents the highest concentration of dissolved and adsorbed sediment in the coastal region.

During the first hour of simulated plant operation the flow in the coastal region is at approximate ebb flow shown in Figure 6. At the end of the first hour, plant operation is halted and external input of radionuclides into the coastal flow region is halted. The dissolved and adsorbed on suspended sediment in the water layer shown in Figure 7(a) has spread in the direction of the flow field, down coast, 11000 feet from the discharge where a concentration of 0.10×10^{-9} units exists. The largest concentration, 0.10×10^{-5} units, is spread 3,000 feet from the discharge. Due to suspension caused by high flow conditions, the concentration of dissolved and adsorbed resident sediment in the stationary bottom layer is not as great as that in the water layer. The bottom layer concentration of 0.10×10^{-9} has spread 8,000 feet from the discharge, as shown in Figure 7(b).

Three hours after the start of the accident the flow condition is at approximate low water slack, Figure 8, concentrations of the dissolved and adsorbed on suspended sediment in the water layer have spread 19,000 feet, Figure 9(a) downcoast from the discharge, with the maximum concentration spreading to 5,000 feet. Due to very low velocities at slack conditions, the concentrations of the dissolved and adsorbed on the resident sediment in the stationary bottom layer has greatly increased- spreading to 18,000 feet. Here, the effect of the vertical exchange transport model in the RADTWO code can be seen, by

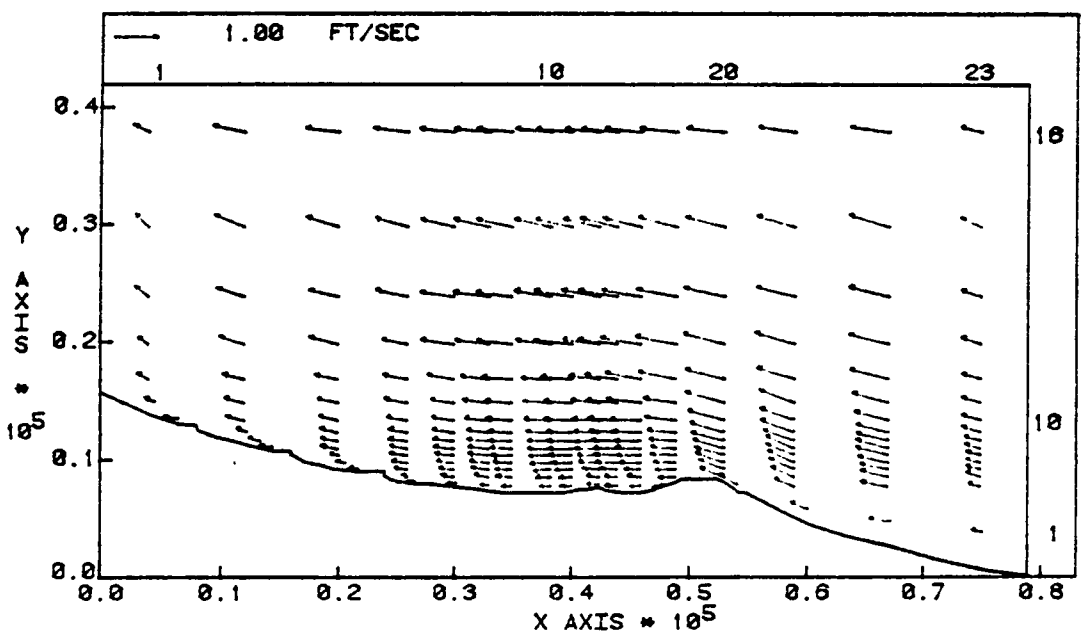
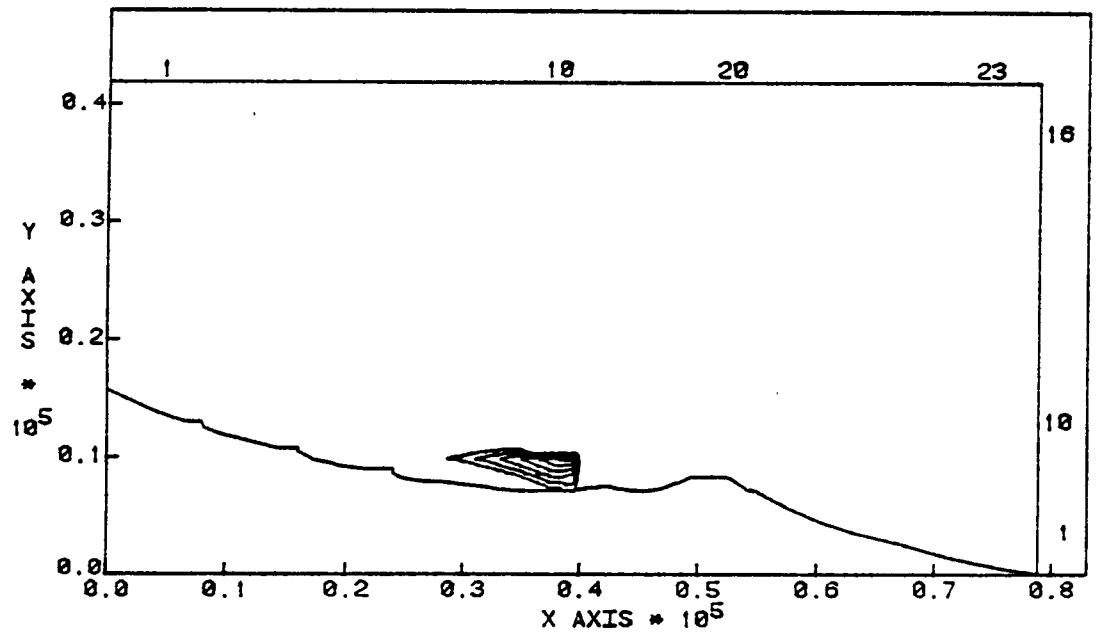
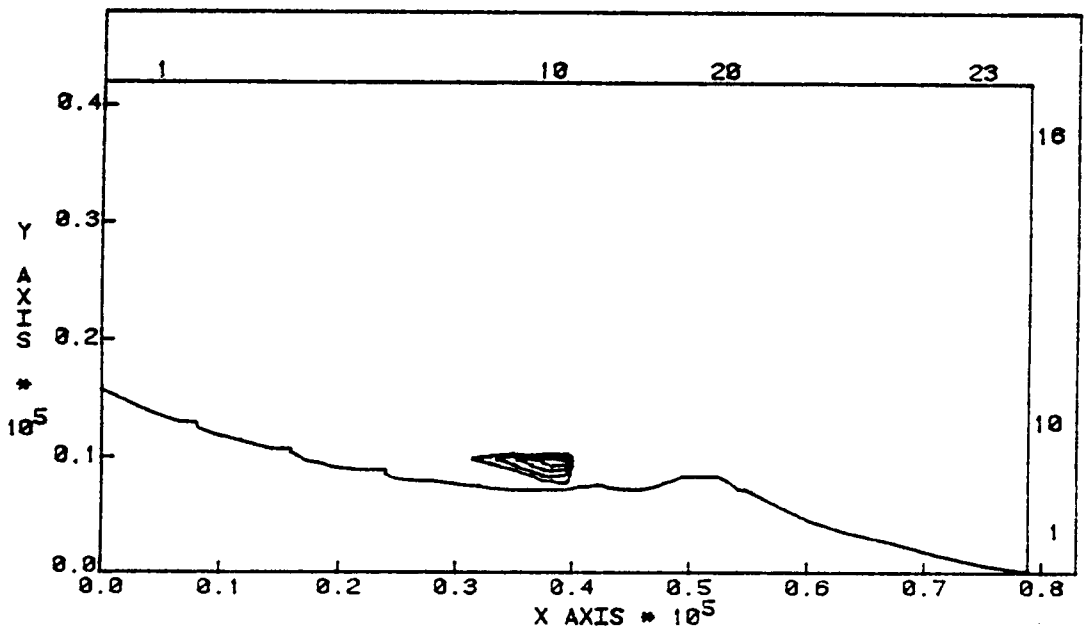


Figure 6. Velocity Vector Representation of the Flowfield 1 Hour After the Start of the Accidental Release.



a.) Water Layer



b.) Bottom Layer

Figure 7. Logarithmic Iso-Concentration Contours of the Dissolved and Adsorbed Sediment in the Water and Bottom Layers 1 Hour After the Start of the Accidental Release.

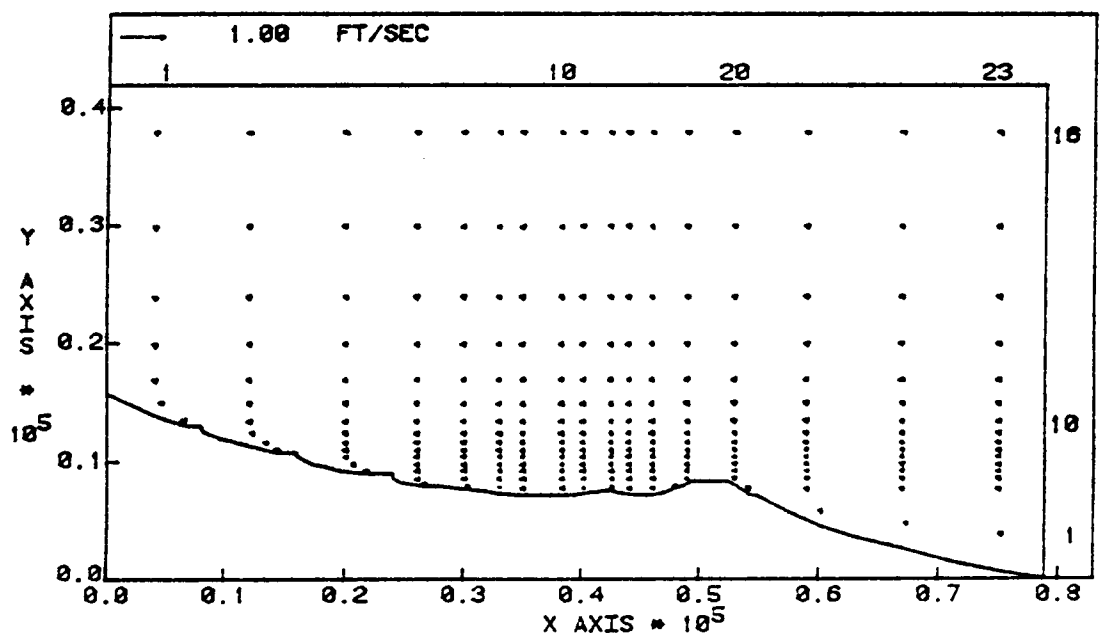
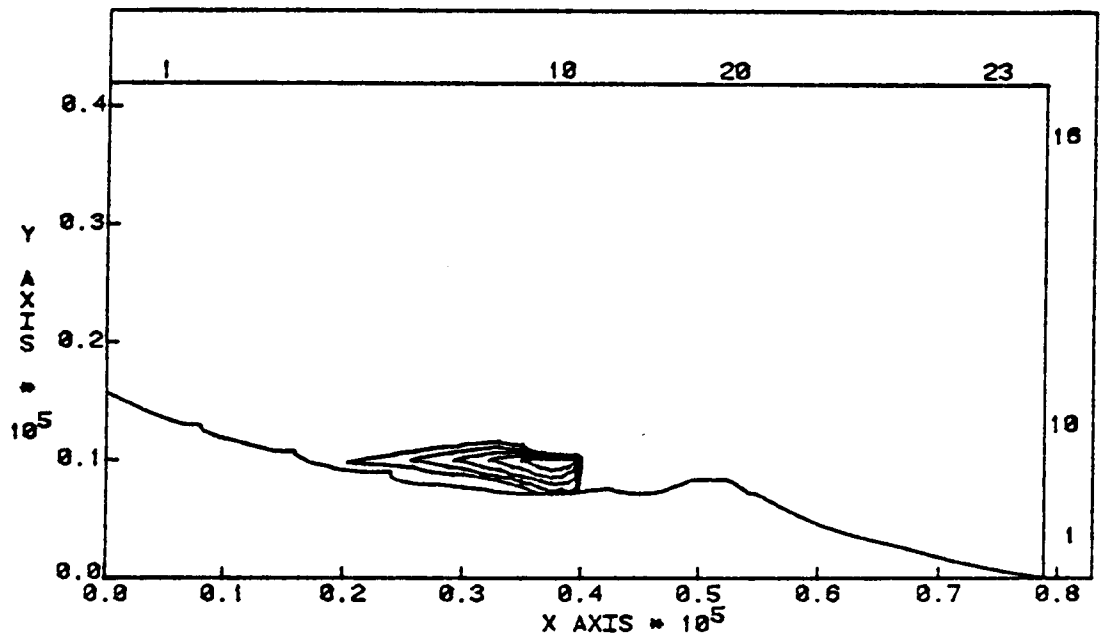
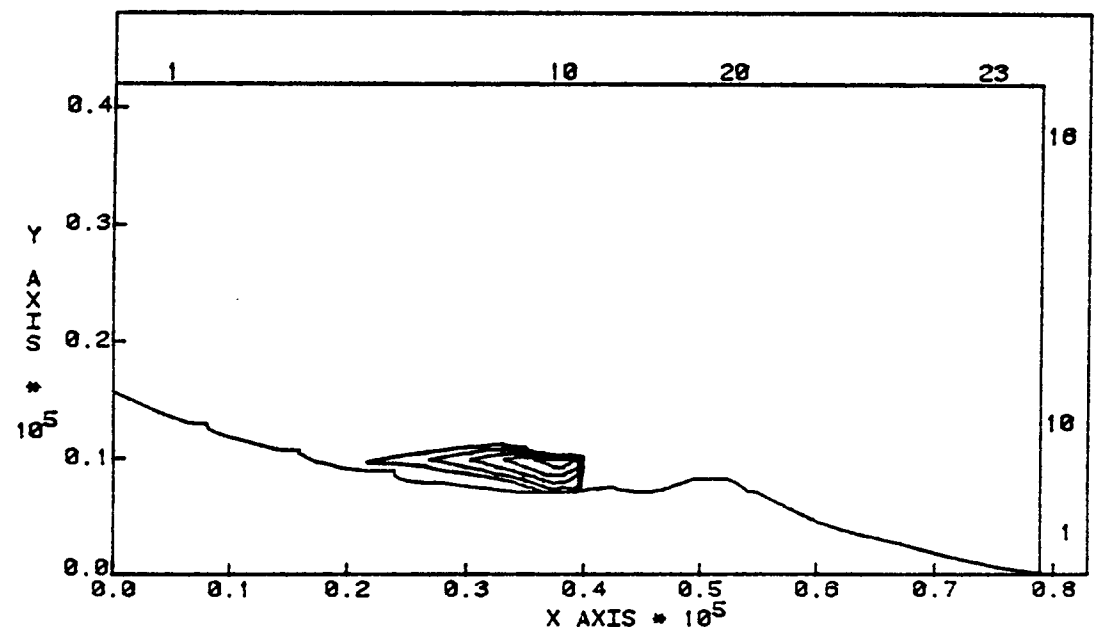


Figure 8. Velocity Vector Representation of the Flowfield 3 Hours After the Start of the Accidental Release.



a.) Water Layer



b.) Bottom Layer

Figure 9. Logarithmic Iso-Concentration Contours of the Dissolved and Adsorbed Sediment in the Water and Bottom Layers 3 Hours After the Start of the Accidental Release.

the settling of the dissolved and adsorbed sediment in the water layer, into the stationary bottom layer.

Since there is no transport in the bottom layer, spreading of the dissolved and adsorbed resident sediment in the stationary bottom layer is due to three phenomena occurring in the following order:

a. During high flow, the suspension of the dissolved and adsorbed resident sediment in the stationary bottom layer,
b. Movement of the dissolved and adsorbed suspended sediment with the flow in the water layer,
c. During low flow, settling of the dissolved and adsorbed suspended sediment into the stationary bottom layer.

Five hours after the start of the accident the flow direction has reversed, Figure 10, flowing upcoast, and is at approximate flood flow. Due to flood flow and convective transport phenomena the dissolved and adsorbed suspended sediment in the water layer is spreading upcoast about 6,000 feet, shown in Figure 11(a), while maintaining the previously shown concentrations downcoast. In the stationary bottom layer, Figure 11(b), the flood flow has caused a resuspension of part of the dissolved and adsorbed resident sediment in the stationary bottom layer, into the water layer. Due to local depth conditions in the region pockets of sediment concentrations remain in the stationary bottom layer. At higher flow conditions these pockets of resident sediment are resuspended.

Seven hours after the start of the accident an approximate flood flow is shown in Figure 12. The dissolved and adsorbed suspended

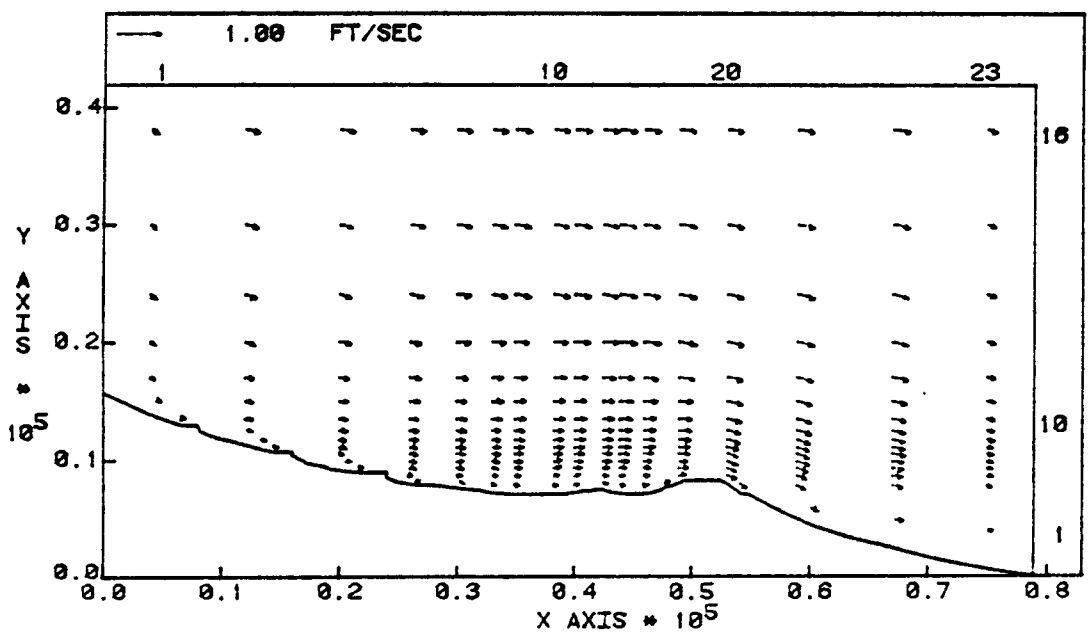
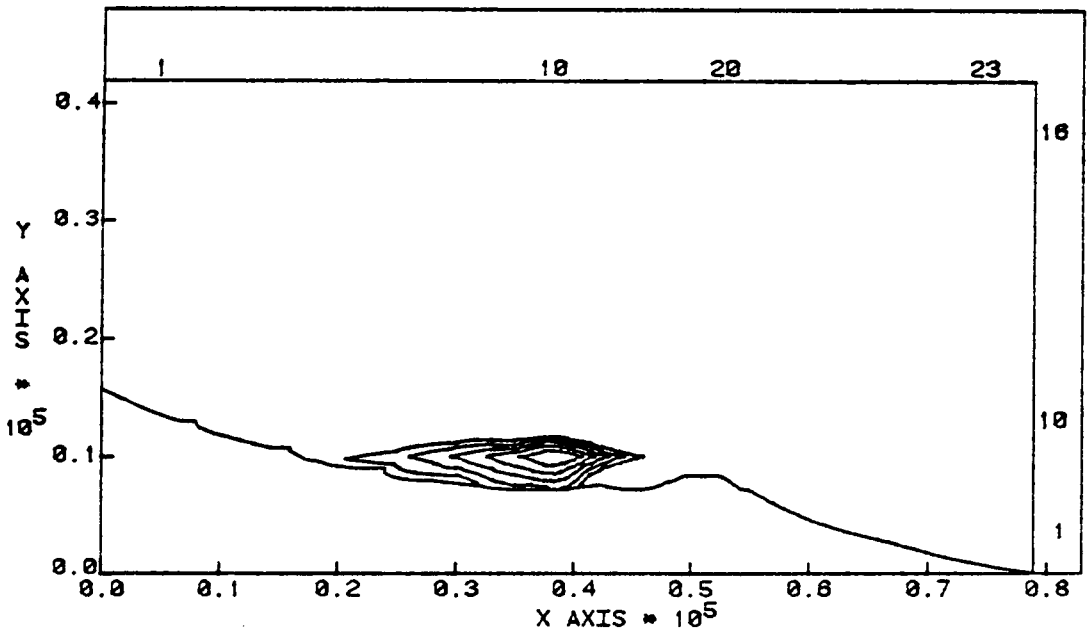
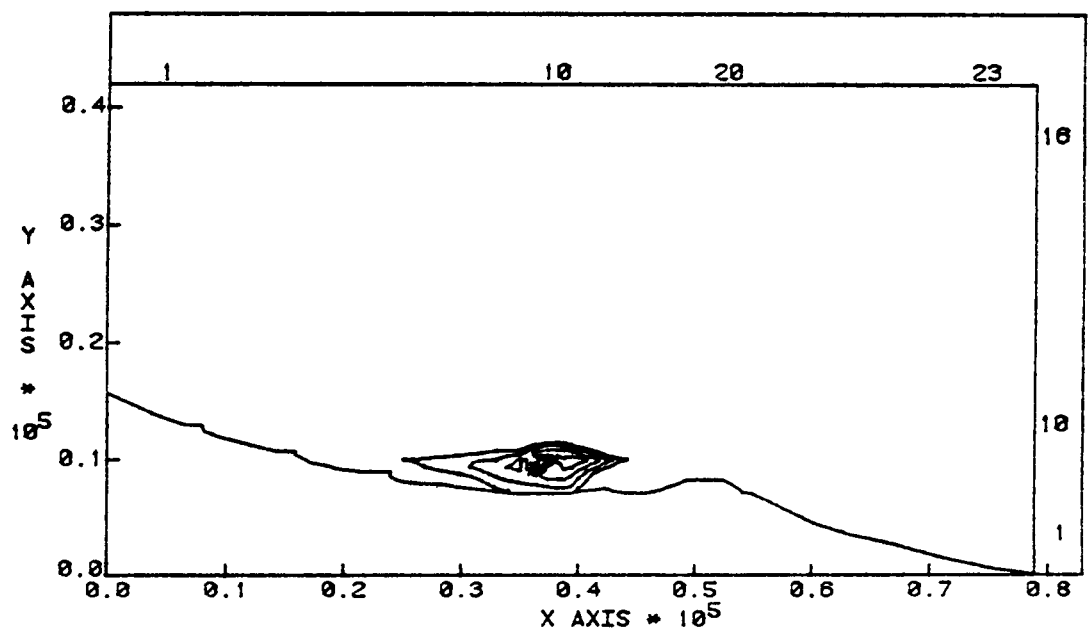


Figure 10. Velocity Vector Representation of the Flowfield 5 Hours After the Start of the Accidental Release.



a.) Water Layer



b.) Bottom Layer

Figure 11. Logarithmic Iso-Concentration Contours of the Dissolved and Adsorbed Sediment in the Water and Bottom Layers 5 Hours After the Start of the Accidental Release.

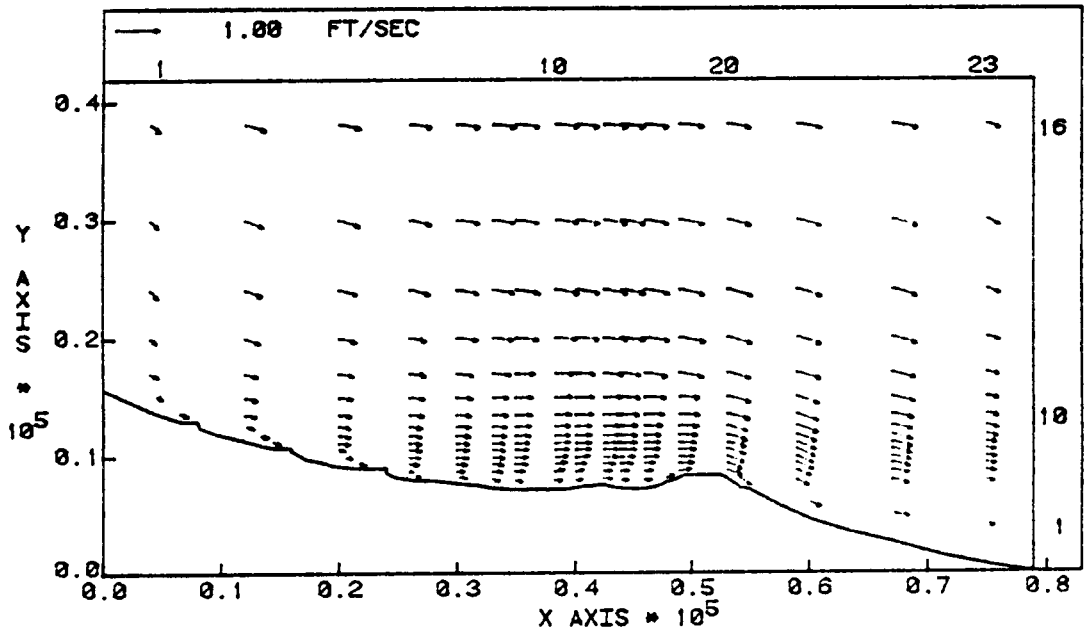
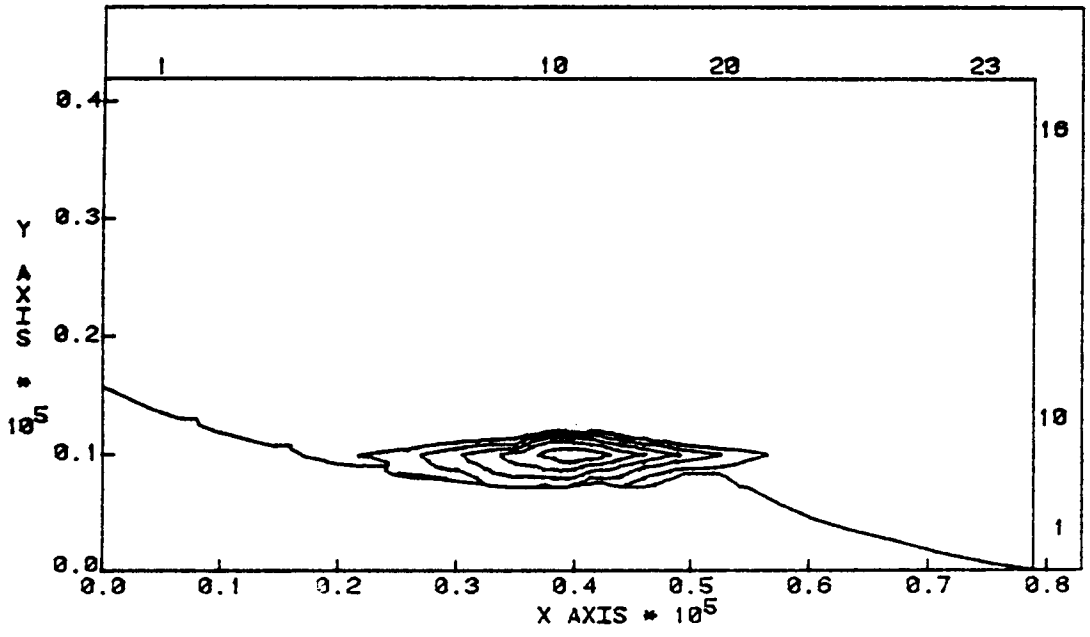


Figure 12. Velocity Vector Representation of the Flowfield 7 Hours After the Start of the Accidental Release.

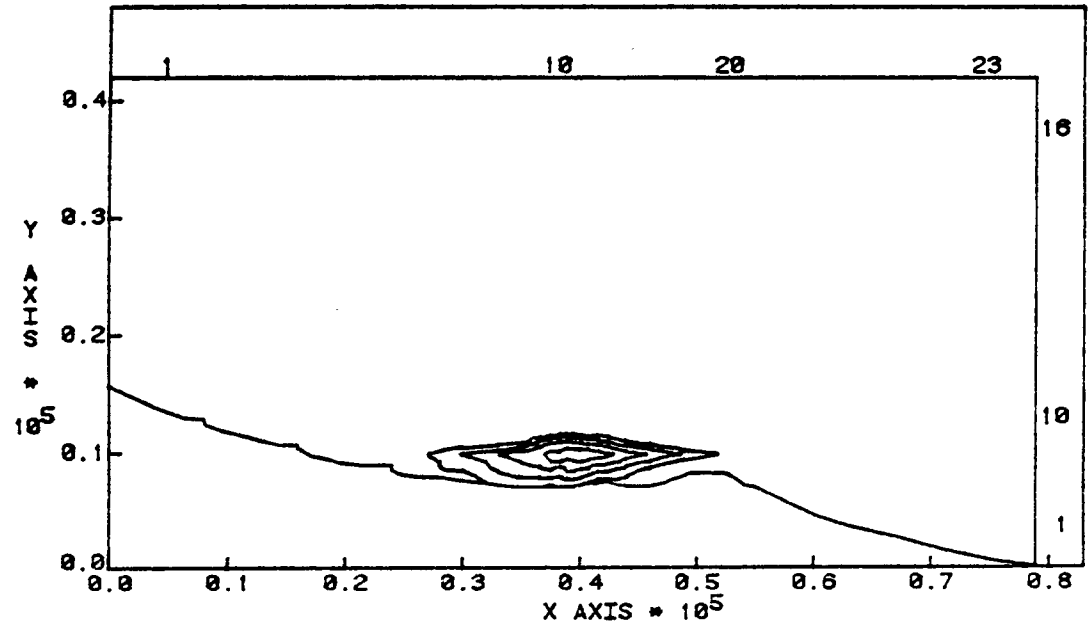
sediment layer has spread 16,000 feet up coast, shown in Figure 13(a), and 17,000 feet downcoast giving an almost symmetrical pattern of suspended sediment contours around the discharge. A maximum concentration of 0.10×10^{-5} still exists in the suspended sediment water layer, spread approximately 3,000 feet on each side of the discharge. The dissolved and adsorbed resident sediment in the bottom layer, Figure 13(b), is also spreading but due to high flow, suspension of sediment in the stationary bottom layer has resulted in lowering the highest concentration of resident sediment in the bottom layer to 0.10×10^{-6}.

Twelve hours after the start of the accident, a flood flow condition shown in Figure 14 still exists. The dissolved and adsorbed suspended sediment has moved upcoast out of the discrete element grid region, while down coast the position has remained relatively stationary. The maximum concentration value is still 0.10×10^{-5} but the location of the contour has moved approximately one mile up coast. In the resident sediment bottom layer the same levels of sediment concentration exist, Figure 15(b), as existed 7 hours after the start of the accident. The contours of the resident sediment concentrations in the stationary bottom layer have spread approximately 7 miles up coast. The maximum concentration of dissolved and adsorbed on resident sediment in the stationary bottom layer is one order of magnitude less than the maximum concentration of dissolved and adsorbed suspended sediment in the water layer. The two maximum concentrations in the water and bottom layers are located at the same position.

Since the transport phenomena of the dissolved and adsorbed sediment is not as short time dependent after the first 12 hours, the time increment for presentation of results is increased.



a.) Water Layer



b.) Bottom Layer

Figure 13. Logarithmic Iso-Concentration Contours of the Dissolved and Adsorbed Sediment in the Water and Bottom Layers 7 Hours After the Start of the Accidental Release.

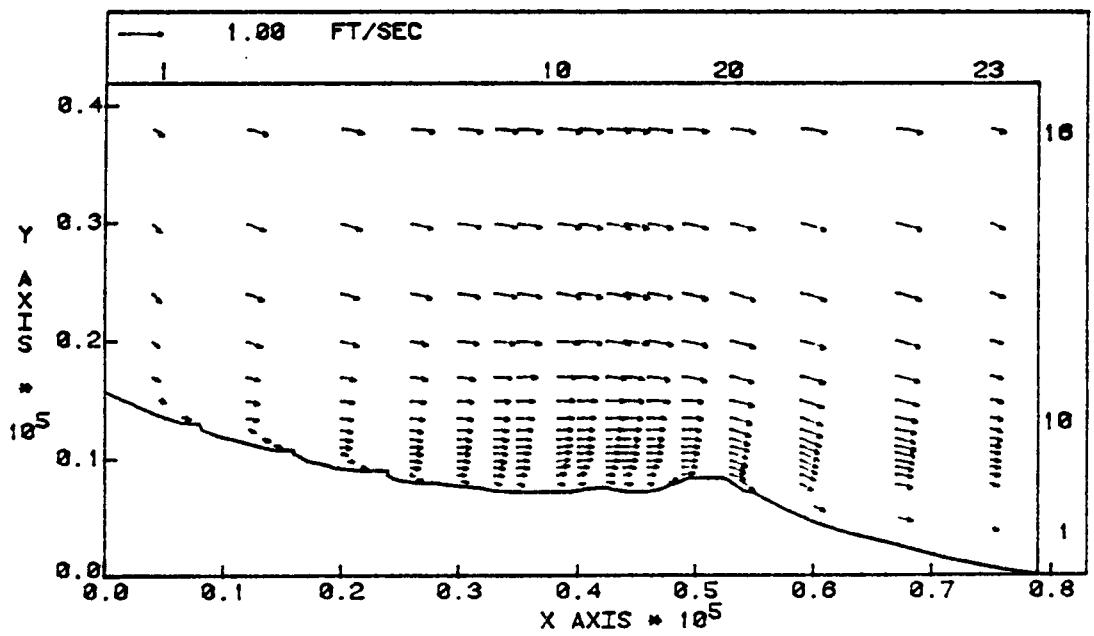
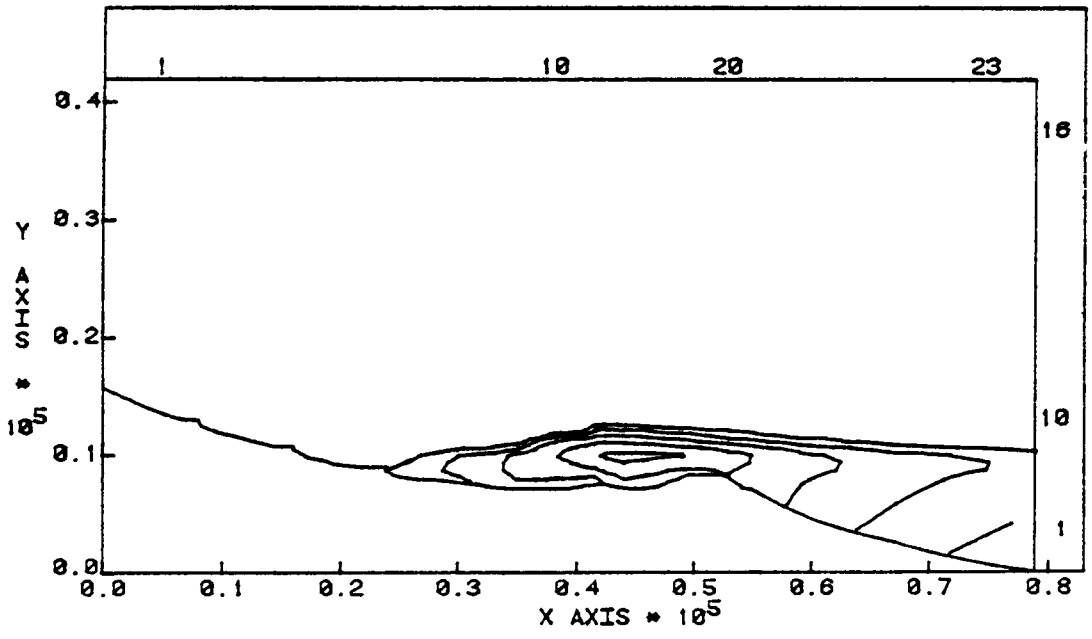
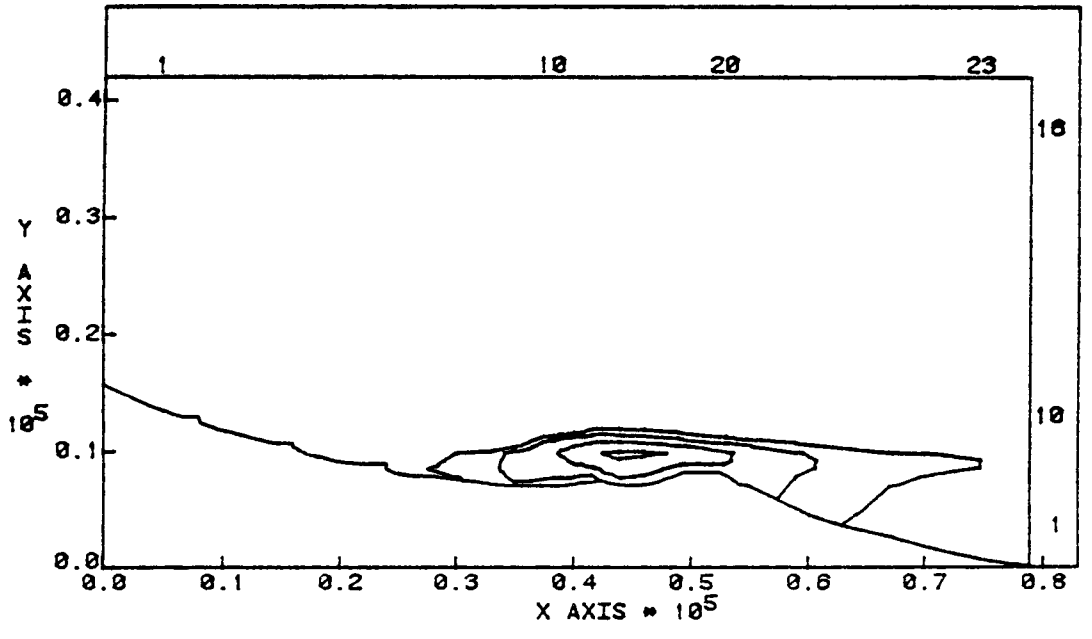


Figure 14. Velocity Vector Representation of the Flowfield 12 Hours After the Start of the Accidental Release.



a.) Water Layer



b.) Bottom Layer

Figure 15. Logarithmic Iso-Concentration Contours of the Dissolved and Adsorbed Sediment in the Water and Bottom Layers 12 Hours After the Start of the Accidental Release.

Twenty-four hours after the start of the accident an approximate ebb flow condition, Figure 16, exists. Concentration of the dissolved and adsorbed suspended sediment in the water layer is again spreading down coast approximately 6 miles from the discharge. The maximum concentration has been reduced since the 12 hour condition from 0.10×10^{-5} units to 0.10×10^{-6} units. This reduction in concentration is due to two phenomena, the dilution of the suspended sediment and the radioactive decay of the Cesium 132. The extent of the dissolved and adsorbed resident sediment in the stationary bottom layer, shown in Figure 17(b), has spread approximately five miles down coast of the discharge, and the maximum contour value of dissolved and adsorbed resident sediment in the bottom layer has dropped to 0.10×10^{-7}.

Thirty hours after the start of the accidental release the flow conditions have reversed to approximate flood flow, Figure 18. Concentrations of dissolved and adsorbed suspended sediment in the water layer, Figure 19(a), has spread to approximately 7 miles down coast. Up coast the dissolved and adsorbed suspended sediment in the water layer is spread over the boundary of the computational region. The dissolved and adsorbed resident sediment in the stationary bottom layer, shown in Figure 19(b), is being partially resuspended, again creating pockets of sediment concentrations in the bottom layer.

Forty-two hours after the start of the accidental release, an approximate high water slack flow condition, Figure 20, exists. The spread of dissolved and adsorbed suspended sediment in the water layer illustrated in Figure 21(a) has decreased due to settlement into the resident bottom layer, Figure 21(b). The dissolved and adsorbed

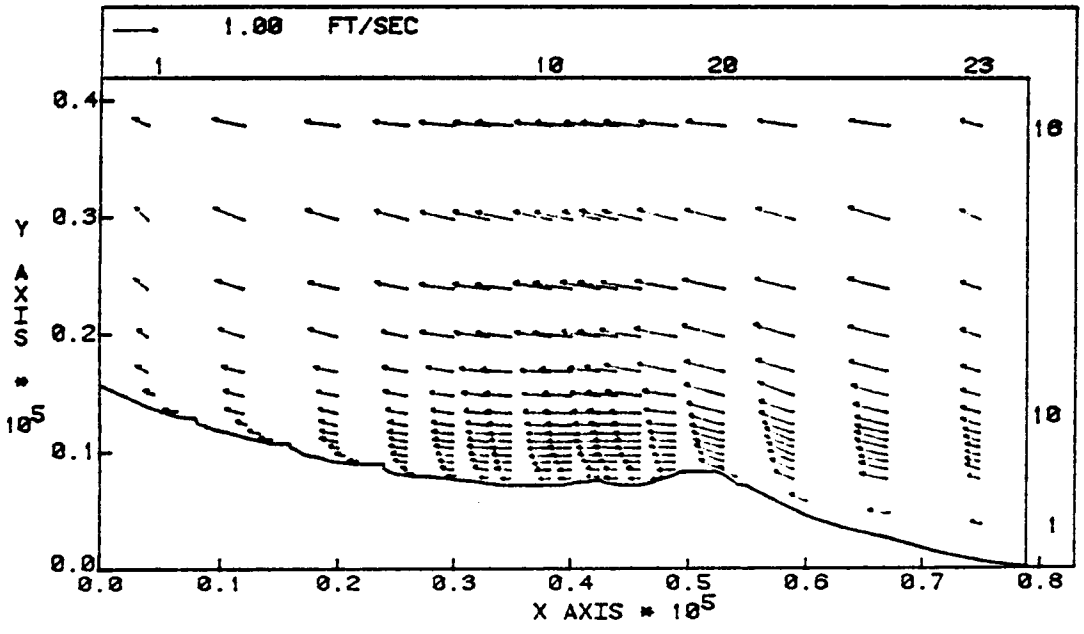
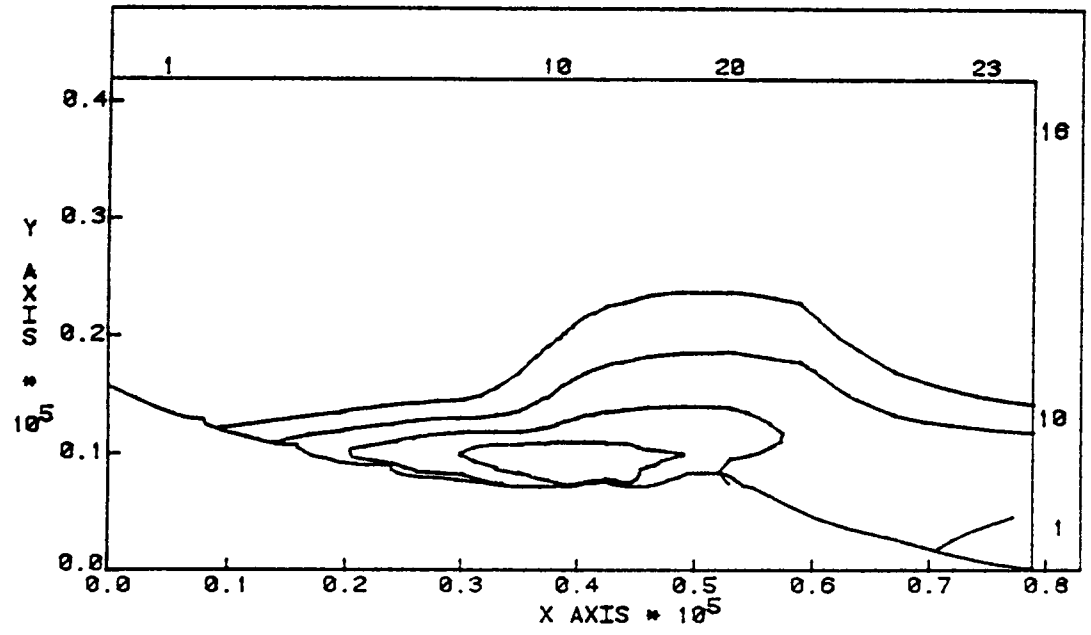
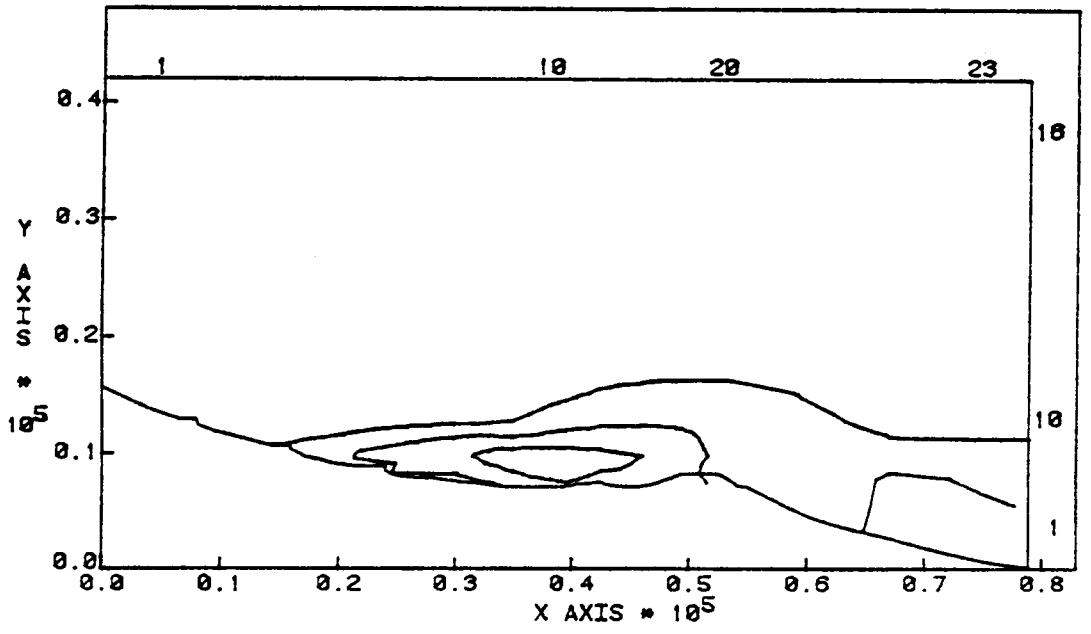


Figure 16. Velocity Vector Representation of the Flowfield 24 Hours After the Start of the Accidental Release.



a.) Water Layer



b.) Bottom Layer

Figure 17. Logarithmic Iso-Concentration Contours of the Dissolved and Adsorbed Sediment in the Water and Bottom Layers 24 Hours After the Start of the Accidental Release.

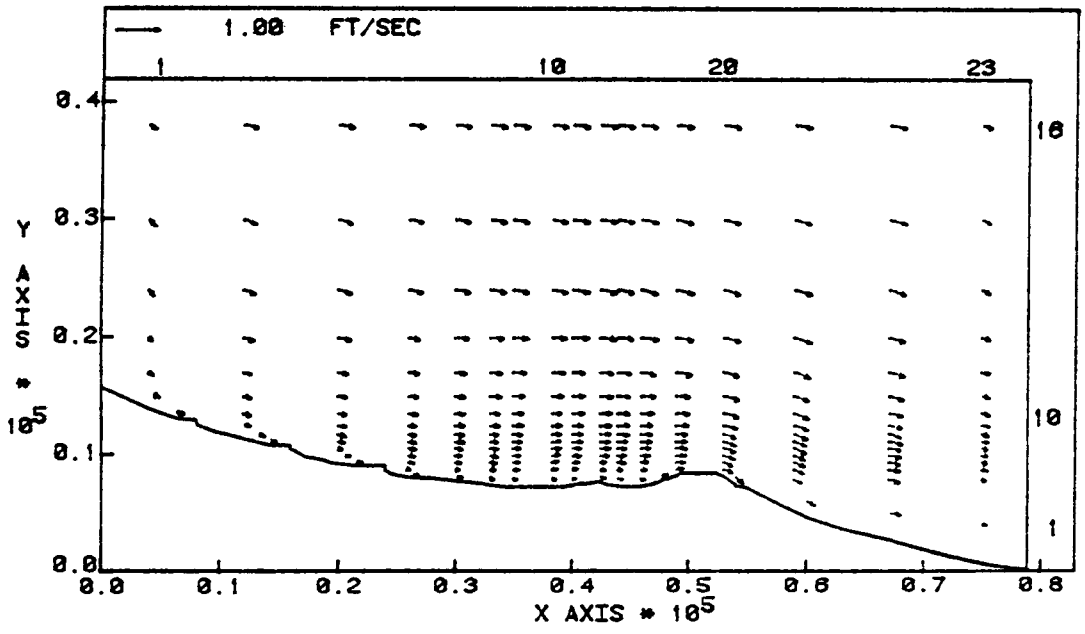
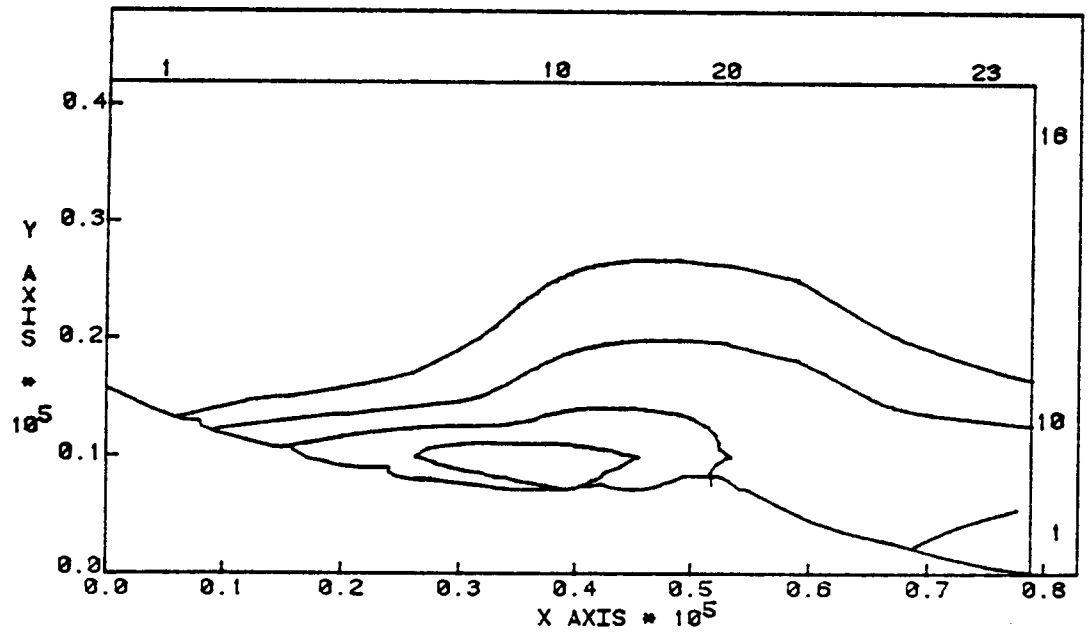
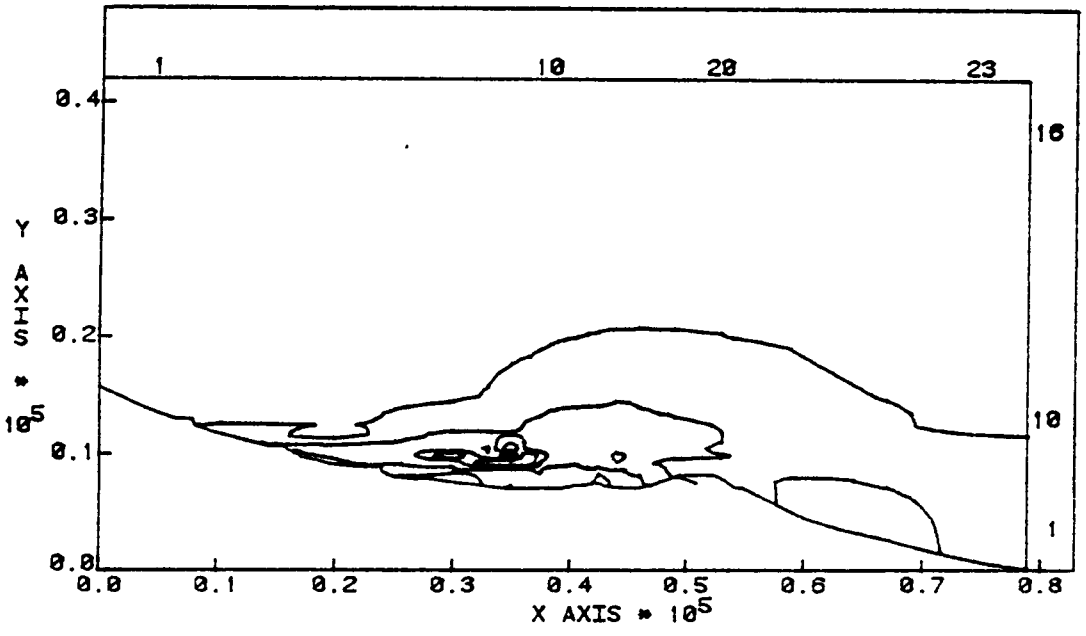


Figure 18. Velocity Vector Representation of the Flowfield 30 Hours After the Start of the Accidental Release.



a.) Water Layer



b.) Bottom Layer

Figure 19. Logarithmic Iso-Concentration Contours of the Dissolved and Adsorbed Sediment in the Water and Bottom Layers 30 Hours After the Start of the Accidental Release.

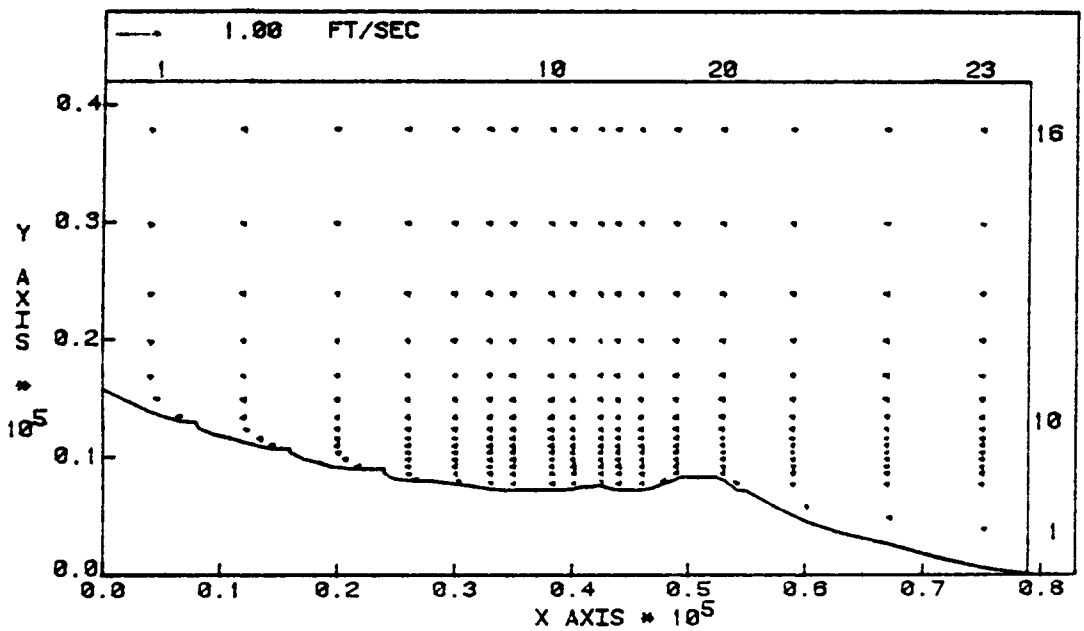
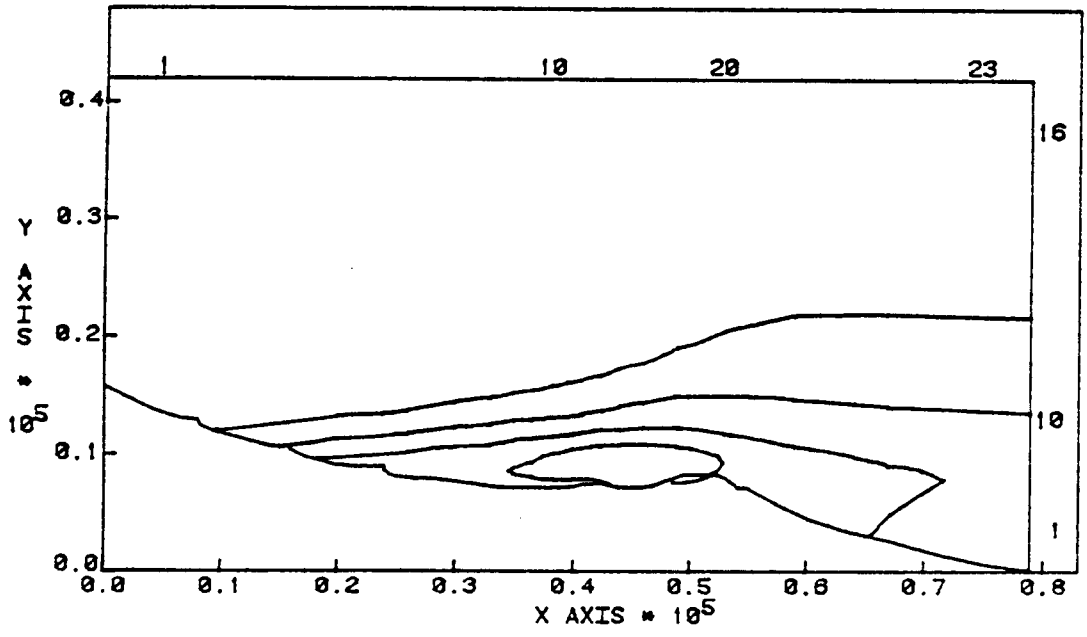
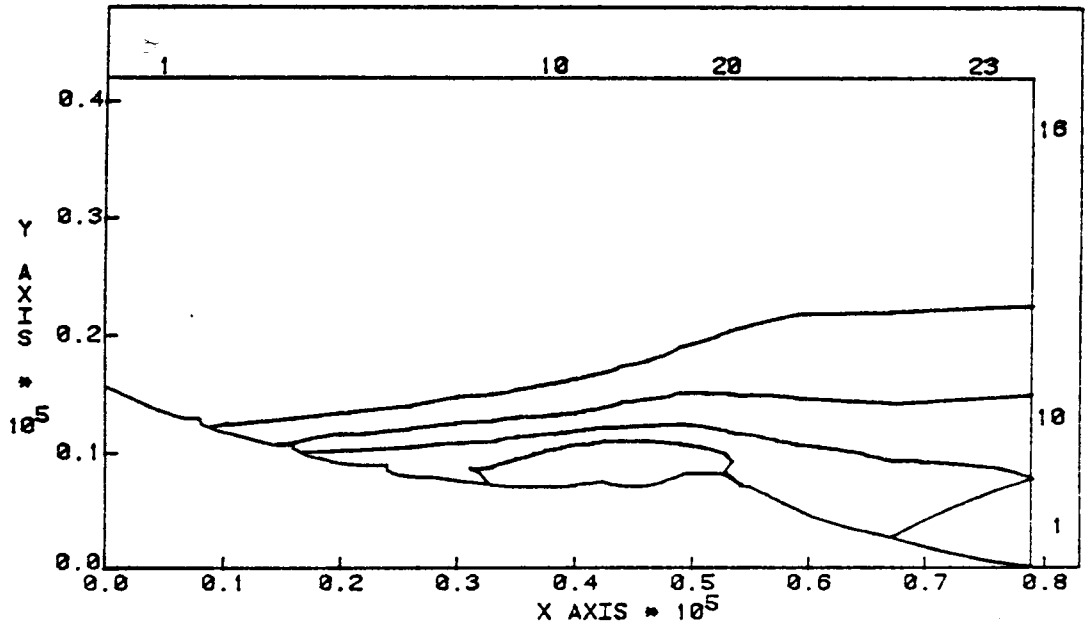


Figure 20. Velocity Vector Representation of the Flowfield 42 Hours After the Start of the Accidental Release.



a.) Water Layer



b.) Bottom Layer

Figure 21. Logarithmic Iso-Concentration Contours of the Dissolved and Adsorbed Sediment in the Water and Bottom Layers 42 Hours After the Start of the Accidental Release.

resident sediment in the stationary bottom layer has increased in both spread and concentration due to the settlement of the suspended sediment. At this high water slack condition the concentration contours between the two layers are almost exactly the same in size and magnitude. The maximum contour value is 0.10×10^{-6}.

Forty-eight hours after the start of the accidental release the flow conditions are at approximate ebb flow, Figure 22. The spread of the dissolved and adsorbed suspended sediment in the water layer, Figure 23(a), has increased due to resuspension of the dissolved and adsorbed resident sediment in the stationary bottom layer. The high flow has caused the maximum concentration to be reduced to 0.10×10^{-7}.

Fifty-four hours after the start of the accidental release, the flow conditions are at approximate flood flow, shown in Figure 24. A further spreading away from the shoreline of the dissolved and adsorbed suspended sediment, Figure 25(a), occurs. During the flow reversal to flood flow, settling of some of the suspended sediment occurs, spreading the concentrations of dissolved and adsorbed resident sediment in the stationary bottom layer, Figure 25(b).

Sixty hours after the start of the accidental release, the flow conditions are at flood flow, Figure 26. The spread of concentration of dissolved and adsorbed suspended sediment in the water layer, shown in Figure 27(a), has been slightly reduced due to decay of the Cesium 132. In the dissolved and adsorbed resident sediment in the stationary bottom layer, Figure 27(b), the spread of the concentrations have been reduced due to resuspension and radioactive decay.

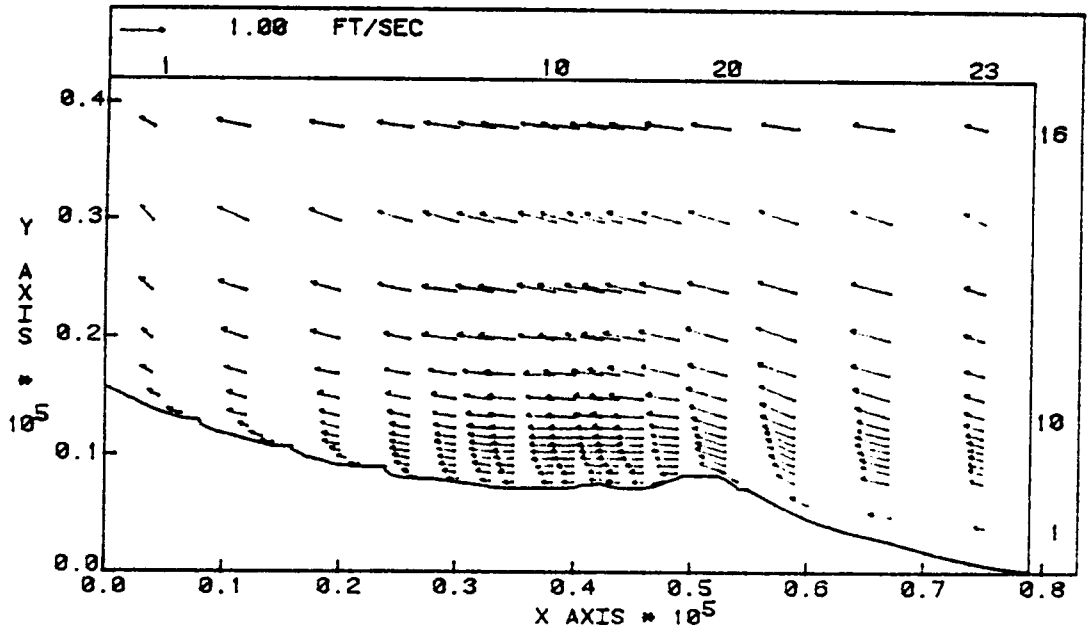
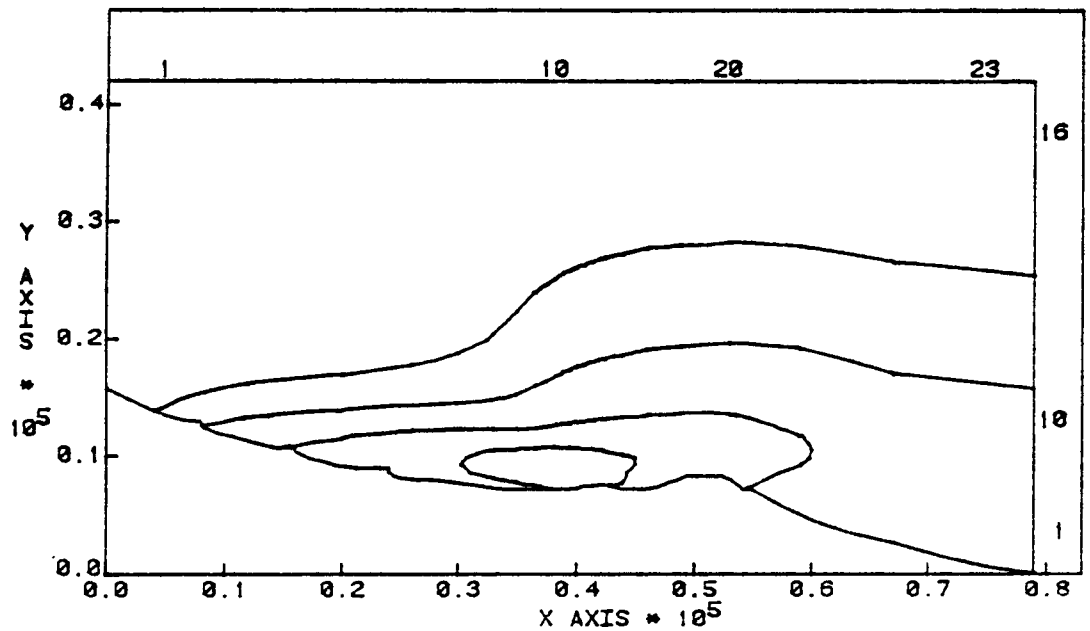
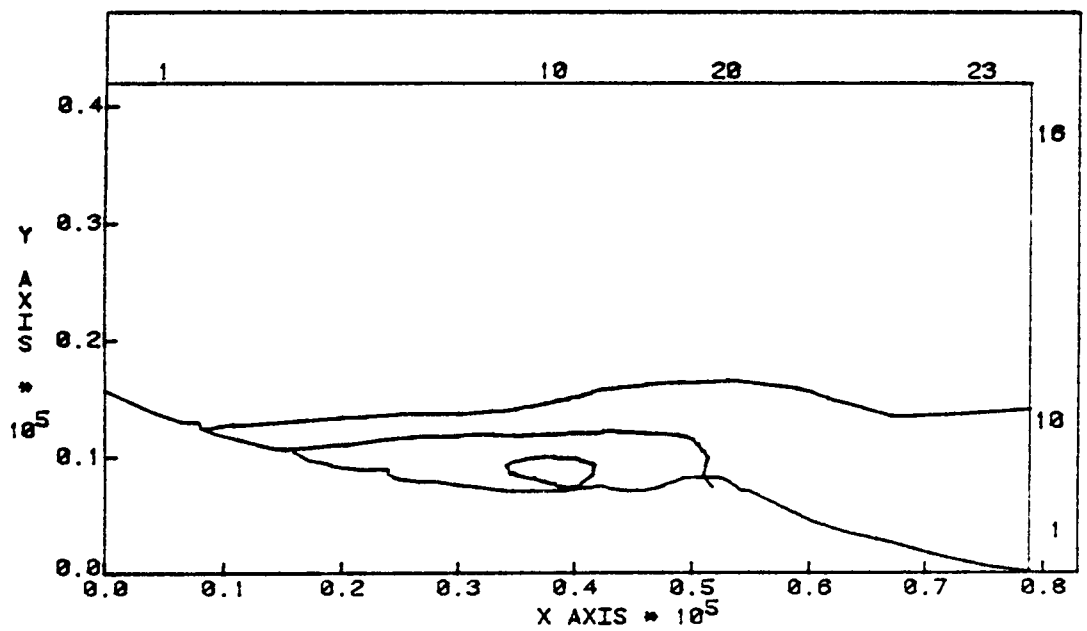


Figure 22. Velocity Vector Representation of the Flowfield 48 Hours After the Start of the Accidental Release.



a.) Water Layer



b.) Bottom Layer

Figure 23. Logarithmic Iso-Concentration Contours of the Dissolved and Adsorbed Sediment in the Water and Bottom Layers 48 Hours After the Start of the Accidental Release.

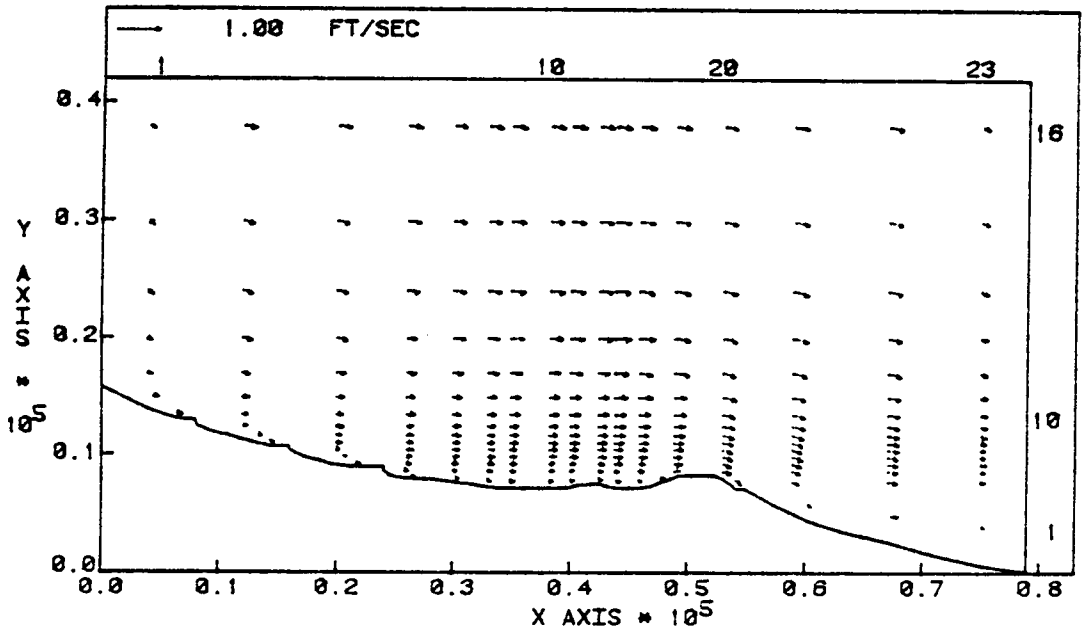
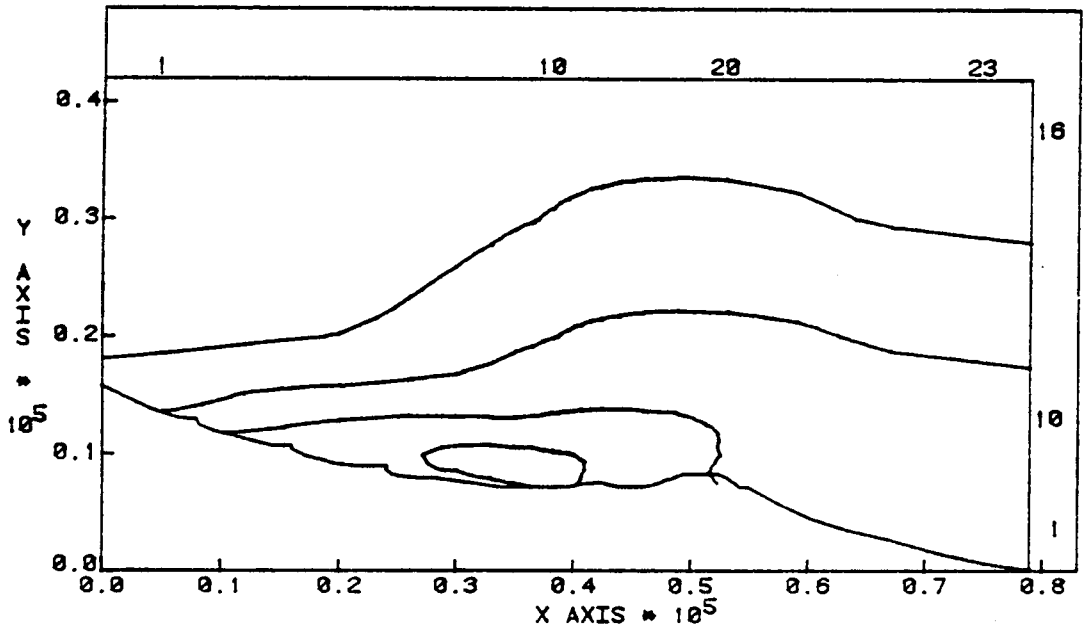
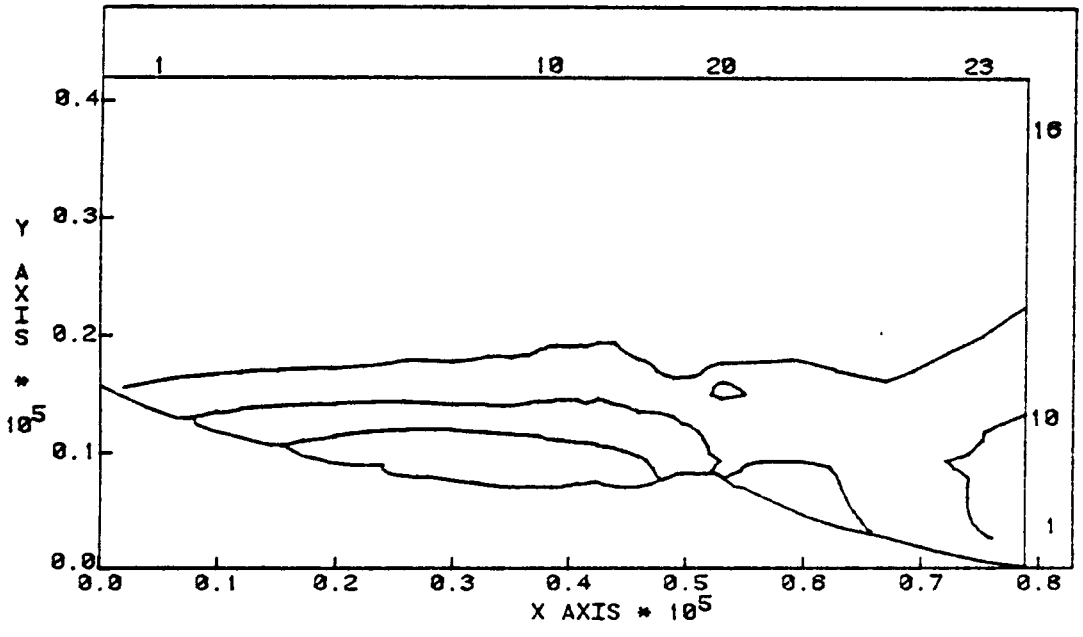


Figure 24. Velocity Vector Representation of the Flowfield 54 Hours After the Start of the Accidental Release.



a.) Water Layer



b.) Bottom Layer

Figure 25. Logarithmic Iso-Concentration Contours of the Dissolved and Adsorbed Sediment in the Water and Bottom Layers 54 Hours After the Start of the Accidental Release.

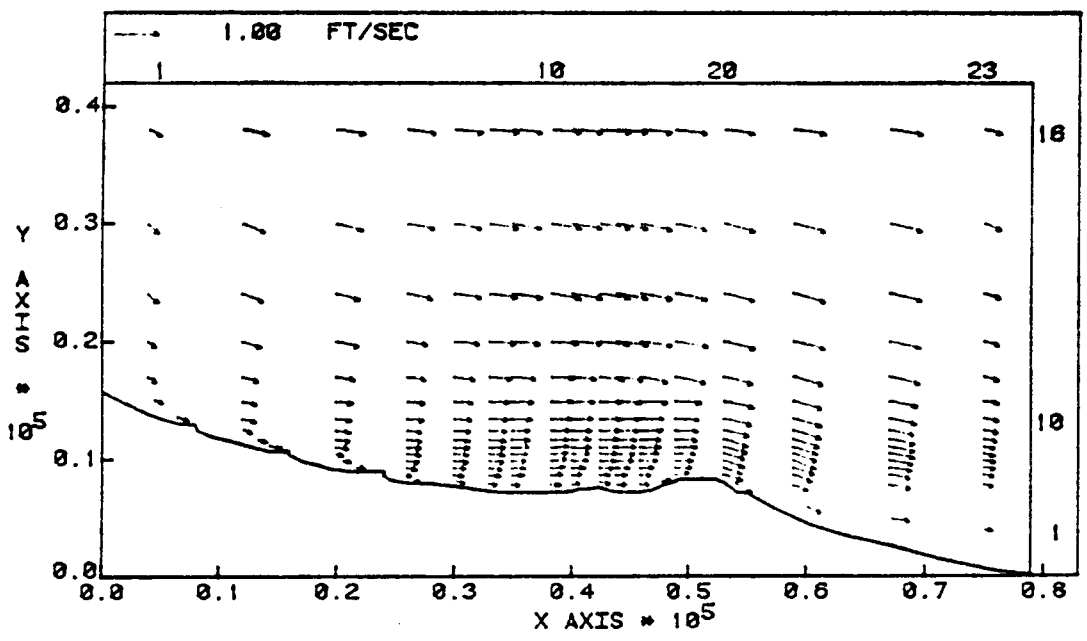
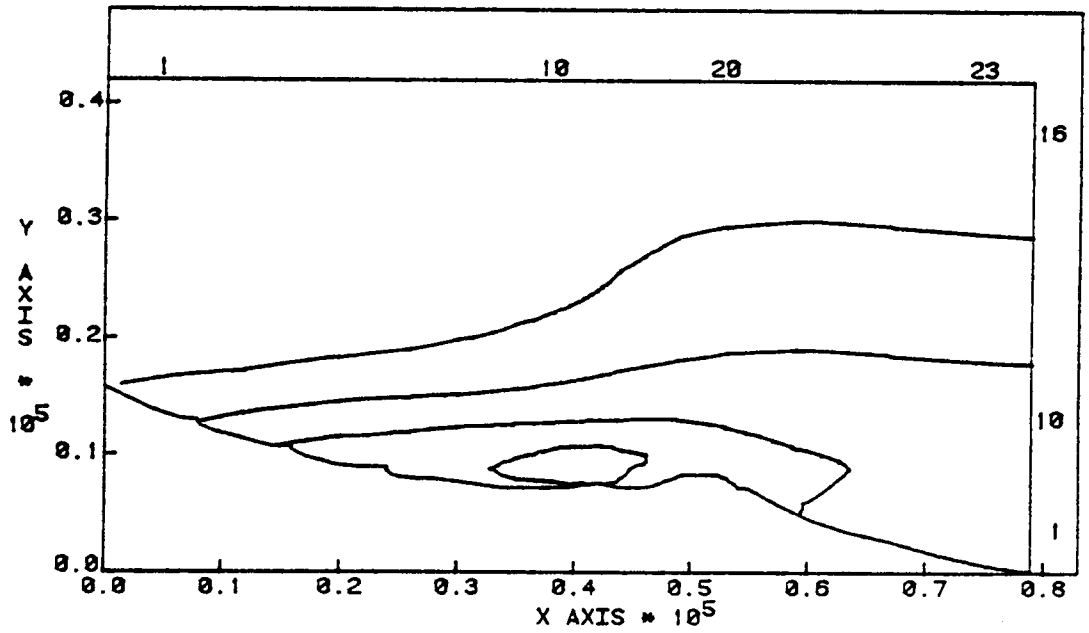
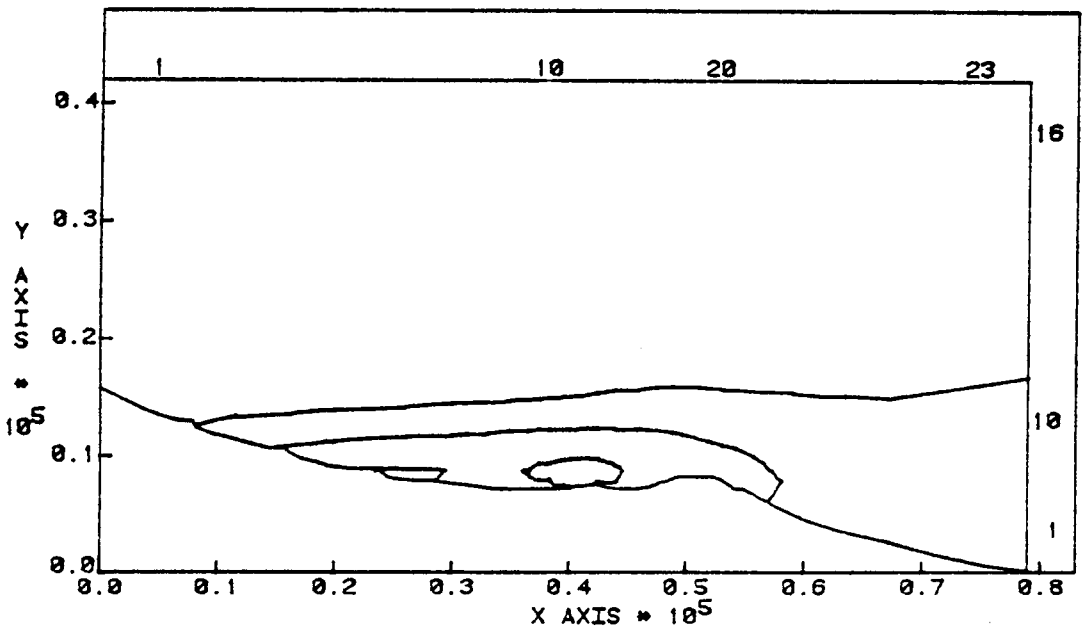


Figure 26. Velocity Vector Representation of the Flowfield 60 Hours After the Start of the Accidental Release.



a.) Water Layer



b.) Bottom Layer

Figure 27. Logarithmic Iso-Concentration Contours of the Dissolved and Adsorbed Sediment in the Water and Bottom Layers 60 Hours After the Start of the Accidental Release.

One hundred and thirty-two hours after the start of the accidental release the flow conditions are at flood flow, shown in Figure 28. The dissolved and adsorbed suspended sediment in the water layer contours, Figure 29(a), have spread completely over the flow region, but have been reduced one order of magnitude to a maximum concentration of 0.10×10^{-7} units. Since the half life of Cesium 132 is 158.4 hours, it is evident that radioactive decay has become the main factor in the deterioration of the concentrations. Due to the high flow condition and the decay, the maximum concentration of the dissolved and adsorbed resident sediment in the stationary bottom layer has dropped to 0.10×10^{-8}.

One hundred and forty-four hours after the start of the accidental release the flow conditions are at approximate ebb flow, Figure 30. The dissolved and adsorbed suspended sediment in the water layer (Figure 4.16.b) still has a maximum concentration value of 0.10×10^{-7} and is spread over the same region as the 132 hour case, i.e., Figure 29(a). The dissolved and adsorbed resident sediment in the stationary bottom layer, shown in Figure 31(b) is also spread over approximately the same region as the 132 hour case, i.e., Figure 29(b).

It is evident that at this point in the simulation the concentrations in both the water and stationary bottom layers are dominated by the half-life, 158.4 hours, of the released radionuclide, which in this case is Cesium 132. Since the time of the simulation is close to 158.4 hours after the end of the accident, the simulation of the flow region can be terminated.

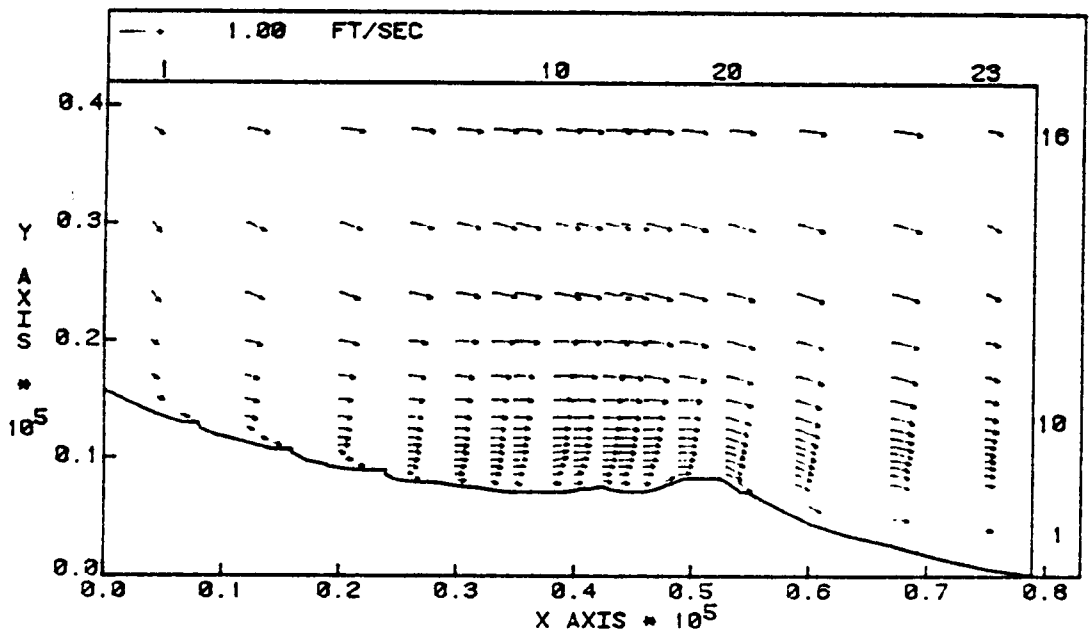
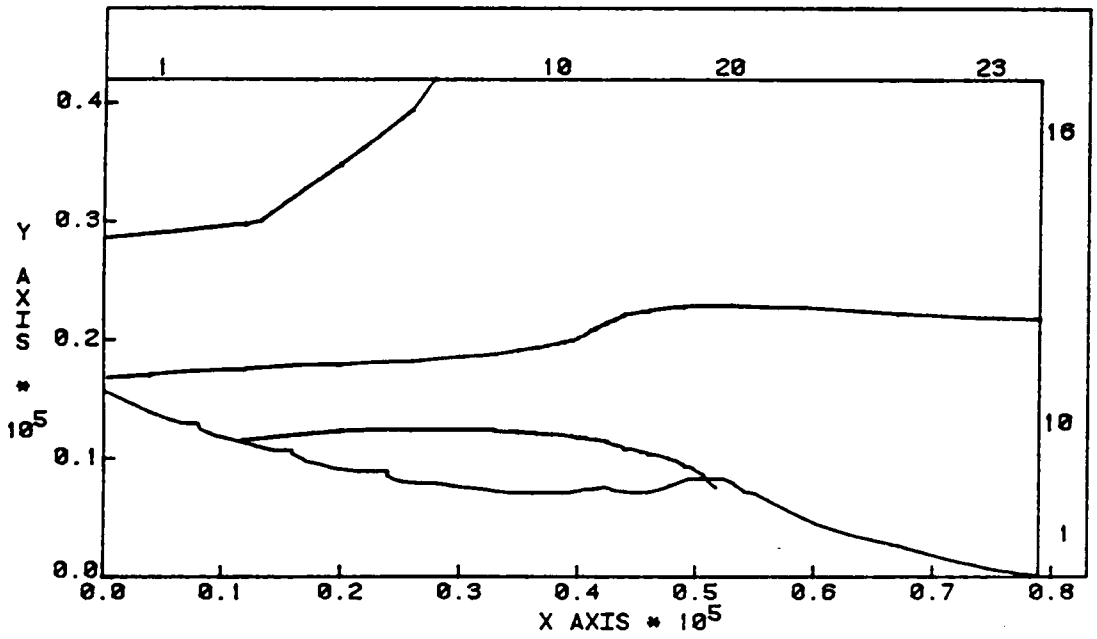
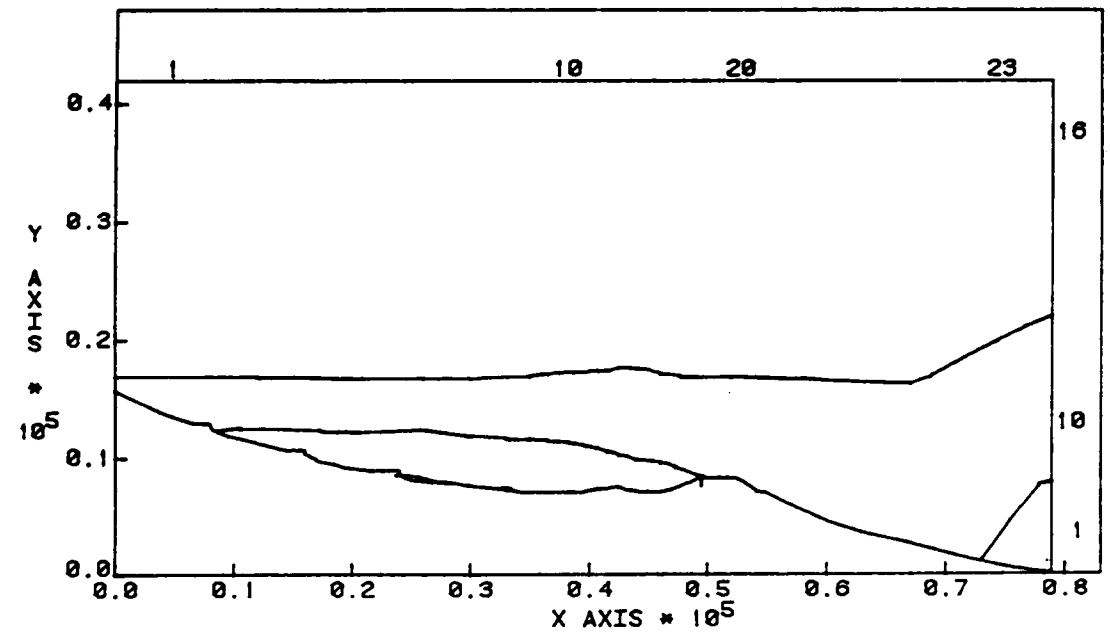


Figure 28. Velocity Vector Representation of the Flowfield 132 Hours After the Start of the Accidental Release.



a.) Water Layer



b.) Bottom Layer

Figure 29. Logarithmic Iso-Concentration Contours of the Dissolved and Adsorbed Sediment in the Water and Bottom Layers 132 Hours After the Start of the Accidental Release.

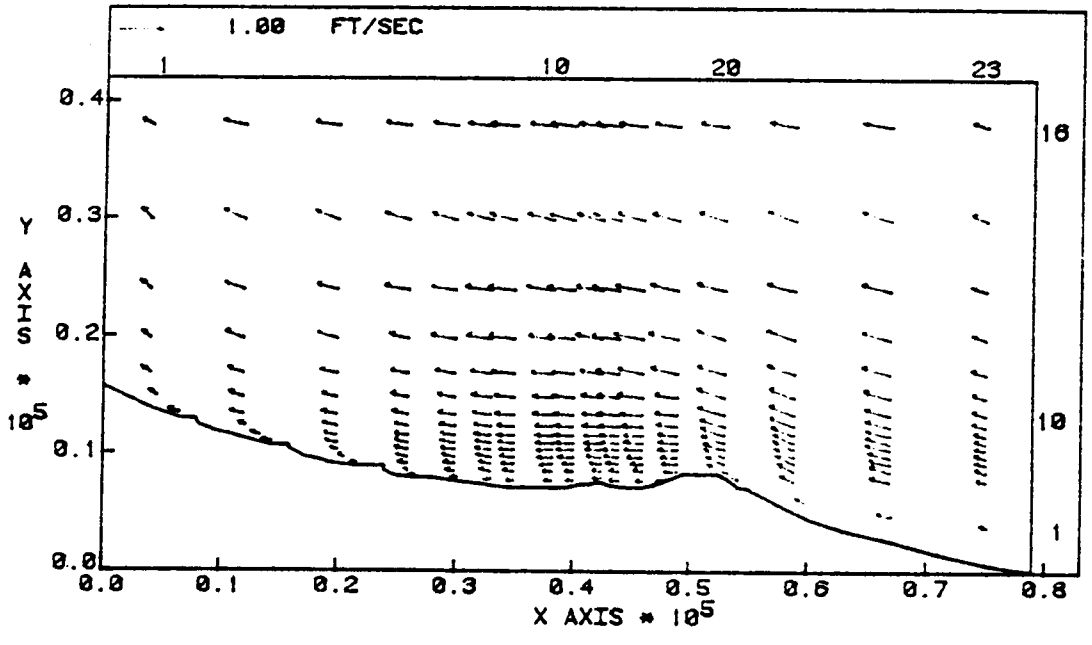
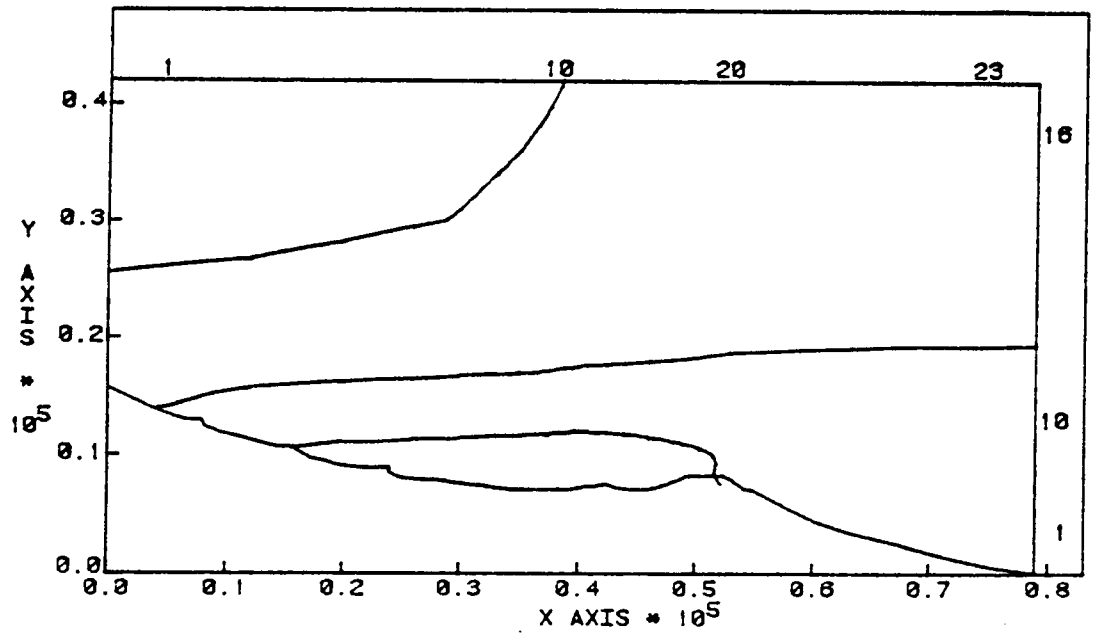
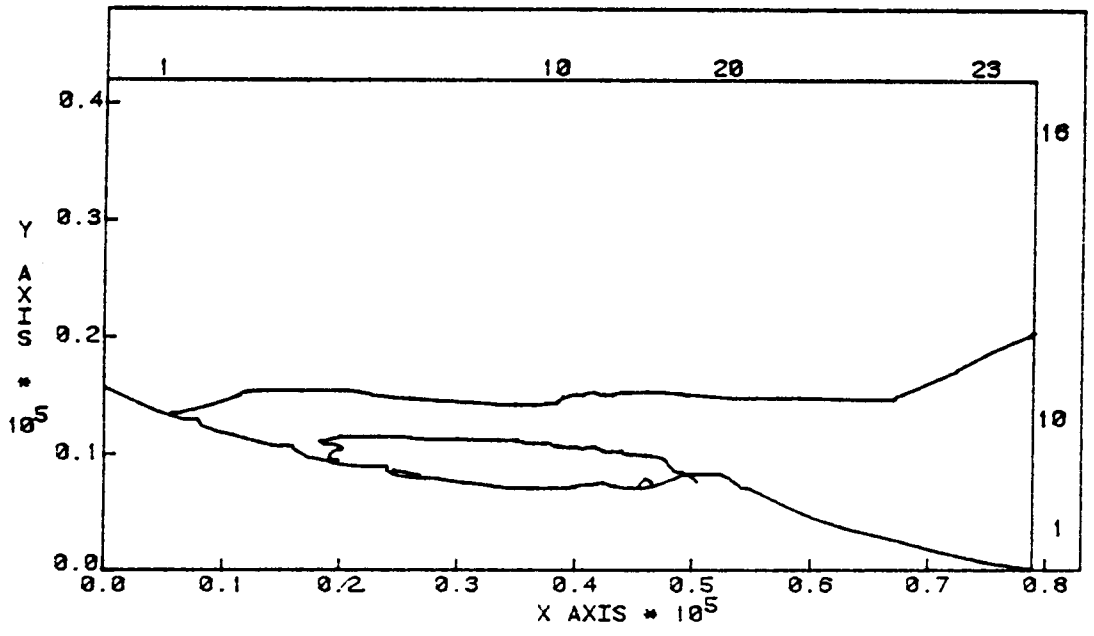


Figure 30. Velocity Vector Representation of the Flowfield 144 Hours After the Start of the Accidental Release.



a.) Water Layer



b.) Bottom Layer

Figure 31. Logarithmic Iso-Concentration Contours of the Dissolved and Adsorbed Sediment in the Water and Bottom Layers 144 Hours After the Start of the Accidental Release.

5. CONCLUSIONS AND RECOMMENDATIONS

5.1 Conclusions

A short time transient two-dimensional mathematical model for the transport of dissolved and adsorbed suspended sediment in the water layer and the dissolved and adsorbed on resident sediment in the stationary bottom layer, is presented for the assessment of the impact of radionuclide releases in large coastal regions, lakes and estuaries. The present model is based on the FLIDE (fluid-in-discrete-element) numerical method. The FLIDE method has previously been shown to be an extremely effective tool in modelling thermal transport, and transport of chemically reacting substances as shown in reports to be published under the Unified Transport Approach [23, 24, 25] being developed at Oak Ridge National Laboratory.

The RADTWO [23] computer code is a part of this study and is shown to be very efficient in solving the FLIDE method for long time durations. During the development of the computer model, many time saving methods were incorporated to assure the feasibility of a realistic simulation of the transport of dissolved and adsorbed sediment in both the water layer and in the stationary bottom layer.

During the simulation of a hypothetical accident condition at the San Onofre Generating Station the model showed that it readily takes into account the interaction of dissolved and adsorbed suspended sediment in the water layer and the dissolved and adsorbed resident sediment in the stationary bottom layer. Under high flow conditions, it showed the phenomena of the dissolved and adsorbed resident sediment

in the stationary bottom layer being resuspended into the water layer, presenting a realistic simulation of natural conditions. At low flow conditions the settling of the dissolved and adsorbed suspended sediment in the water layer into the stationary bottom layer was modelled, thus giving an effective simulation of the vertical exchange between the two layers. Decay of the radionuclide contaminant is effectively modelled using the basic exponential decay form based on the radionuclides' half-life. Although the contaminant in the bottom resident layer was not transported in the horizontal plane, computer results indicate that a realistic simulation is obtained by modeling the vertical interaction of the two layers, and only modelling horizontal plane transport in the water layer. All the results from the FLIDE model are fast-transient, no dispersion coefficients are used.

5.2 Recommendations

It is recommended that field experiments be undertaken to illustrate the validity of the RADTWO model. The values of all the parameters were selected based on plausible and realistic considerations, but experimental data was not employed. Further applications of the model to actual accident or routine release conditions are recommended using site specific conditions and experimental results as inputs for the model.

The model can be applied to any other radionuclide with a wide range of decay conditions by utilizing the appropriate half-life. If necessary, the model can be readily extended to consider releases of multiple concentrations.

Other applications for the model include lakes and estuaries. Since the model is fast-transient it is ideal for modeling release conditions in reservoirs or controlled rivers, such as Three Mile Island.

Hence, in conclusion, it can be stated that the RADTWO numerical simulation model of the present study is an effective method of modeling the impact of accident releases or normal releases of radionuclide contaminants into large receiving water bodies, such as coastal regions, lakes and estuaries. The computational efficiency and accuracy of the method and the associated computer code make it an ideal tool for environmental impact analysis.

LIST OF REFERENCES

LIST OF REFERENCES

1. Regulatory Standards, "Radioactivity in Effluents to Unrestricted Areas," Washington, D.C., REG/G-10CFR Part 20.106, 1978.

2. Nuclear Regulatory Guidelines 1.113, "Estimating Aquatic Dispersion of Effluents from Accidental and Routine Reactor Releases," U.S. Nuclear Regulatory Commission, Washington, D.C., REG/G-1.113, 1973.

3. G. I. Taylor, "The Dispersion of Matter in Turbulent Flow Through a Pipe," Proc. Roy. Soc. London A223, 446-68 (1954).

4. A. H. Eraslan, "Transient, Two-Dimensional, Discrete Element Far-Field Transport Model for Thermal Impact Analysis of Power Plant Discharges in Coastal and Offshore Regions. Part I" General Description of the Mathematical Model and the Results of an Application," United States Atomic Energy Commission Report ORNL-4940, Oak Ridge National Laboratory, Oak Ridge, Tennessee, 1975.

5. A. J. Policastro and J. V. Tokar, "Heated Effluent Dispersion in Large Lakes; State-of-the-Art of Analytical Modeling, Part 1: Critique of Model Formulations," United States Atomic Energy Commission Report ANL/ES-11, Center for Environmental Studies, Argonne National Laboratory, Argonne, Illinois, 1972.

6. G. H. Jirka, G. Abraham, and D.R.F. Harleman, "An Assessment of Techniques for Hydrothermal Prediction," Report No. 203, Ralph M. Parsons Laboratory for Water Resources and Hydrodynamics, Massachusetts Institute of Technology, Cambridge, Massachusetts, 1975.

7. W. E. Dunn, A. J. Policastro, and R. A. Paddock, "Surface Thermal Plumes: Evaluation of Mathematical Models for the Near and Complete Field," Energy and Environmental Systems Division, Report ANL/WR-75-3, Argonne National Laboratory, Argonne, Illinois, 1975.

8. Y. A. Yousef, A. Kudo, and E. F. Gloyna, "Radioactivity Transport in Water," TR-19, Center for Research in Water Resources, Austin, Texas, 1970.

9. D. E. Fields, "Modification of the Unified Transport Model to Allow for Sediment Transport and Chemical Exchange," Proceedings of the Second Annual NSF-RANN Trace Contaminants Conference, Asilomar, California, August 1974.

10. W. W. Sayre and F. M. Chang, "A Laboratory Investigation of Open Channel Dispersion Processes for Dissolved, Suspended, and Floating Dispersants," U.S. Geological Survey, Professional Paper 433-E, 1968.

11. M. E. Evans and F. H. Harlow, "The Particle-in-Cell Method for Hydrodynamic Calculations," Report No. LA-2139, Los Alamos Scientific Laboratory, Los Alamos, New Mexico, 1957.

12. R. A. Gentry, R. E. Martin, and B. J. Daly, "An Eulerian Differencing Method for Unsteady Compressible Flow Problems," Journal of Computational Physics, Vol. 1, pp. 87-118, 1966.

13. F. H. Harlow, "Numerical Methods for Fluid Dynamics: An Annotated Bibliography," Report No. LA-4281, Los Alamos Scientific Laboratory, Los Alamos, New Mexico, 1969.

14. F. H. Harlow and A. A. Amsden, "Fluid Dynamics," Report No. LA-4700, Los Alamos Scientific Laboratory, Los Alamos, New Mexico, 1971.

15. A. A. Amsden and F. H. Harlow, "The SMAC Method: A Numerical Technique for Calculating Incompressible Fluid Flows," LA-4370, Los Alamos, New Mexico, 1970.

16. P. J. Roache, Computational Fluid Dynamics, Hermosa Publishers, Albuquerque, New Mexico, 1972.

17. R. V. Thomann, "A Mathematical Model for Dissolved Oxygen," Proceedings of the American Society of Civil Engineers, Journal of Sanitary Engineering Division, Vol. 89, pp. 1-30, 1963.

18. D. J. O'Conner, "An Analysis of the Dissolved Oxygen Distribution in the East River," Journal of Water Pollution Control Federation, Vol. 38, No. 11, pp. 1813-1830, 1966.

19. Modern Developments in Fluid Dynamics, Ed. S. Goldstein, Vol. I, Dover Publications, New York, New York, 1965.

20. J. W. Elder, "The Dispersion of Marked Fluid in Turbulent Shear Flow," J. Fluid Mech. 5, 544-60, 1959.

21. A. Wada, "Numerical Analysis of Distribution of Flow and Thermal Diffusion Caused by Outfall of Cooling Water," Technical Report C:67004, Central Research Institute of Electric Power Industry, Abiko-cho, Japan, 1969.

22. A. Wada, "Study of Thermal Diffusion in a Two Layer Sea Caused by Outfall of Cooling Water," Proceedings of the International Symposium on Stratified Flows, International Association for Hydraulic Research, Novosibirsk, USSR, pp. 1-16, 1972.

23. A. H. Eraslan, H. Diament, et al, "RADTWO: A Computer Code for Simulating Fast-Transient, Two-Dimensional, Two-Layer Radionuclide Concentrations, Including Bottom Deposition and Release Effects, in Lakes, Estuaries and Coastal Regions Under Specified Natural and Plant-Induced Flow conditions," ORNL/NUREG, to be published.

24. A. H. Eraslan, K. H. Kim, et al, "ESTONE: A Computer Code for Simulating Fast-Transient, One-Dimensional Hydrodynamic, Thermal and Salinity Conditions in Controlled Rivers and Tidal Estuaries for the Assessment of the Impact of Multiple Power Plant Operations," ORNL/NUREG, to be published.

25. A. H. Eraslan, G. W. Zimmerman, et al, "CHMKIN: A General-Usage Computer Code for Systematic Analysis of Nonequilibrium Chemical Kinetics in Systems with Large Number of Chemical Species Undergoing Large Number of Moderately Fast Chemical Reactions," ORNL/NUREG, to be published.

VITA

Harry Diament was born in Memphis, Tennessee on March 12, 1952. He attended elementary and junior high schools in that city. In June 1970 he graduated from Germantown High School in Germantown, Tennessee. The following September he entered The University of Wisconsin, and in December 1974 he received a Bachelor of Science degree in Engineering Mechanics.

In January 1975 he accepted a research assistantship at the University of Tennessee, Knoxville. After completing his course work at the University of Tennessee in April 1977, he accepted a job at the McDonnell Aircraft Company in St. Louis, Missouri.